THEORETICAL MODELING OF THE TRANSIENT EFFECTS OF A TOWLINE USING THE METHOD OF CHARACTERISTICS

THESIS

Christopher A. Hill, Ensign, USN

AFIT/GAE/ENY/06-J06

DEPARTMENT OF THE AIR FORCE
AIR UNIVERSITY

AIR FORCE INSTITUTE OF TECHNOLOGY

Wright-Patterson Air Force Base, Ohio

APPROVED FOR PUBLIC RELEASE; DISTRIBUTION UNLIMITED

The views expressed in this thesis are those of the author and do not reflect the official policy or position of the United States Air Force, Department of Defense, or the United States Government.

AFIT/GAE/ENY/06-J06

THEORETICAL MODELING OF THE TRANSIENT EFFECTS OF A TOWLINE USING THE METHOD OF CHARACTERISTICS

THESIS

Presented to the Faculty

Department of Aeronautics and Astronautics

Graduate School of Engineering and Management

Air Force Institute of Technology

Air University

Air Education and Training Command

In Partial Fulfillment of the Requirements for the

Degree of Master of Science in Aeronautical Engineering

Christopher A. Hill, BAEM

Ensign, USN

June 2006

APPROVED FOR PUBLIC RELEASE; DISTRIBUTION UNLIMITED.

AFIT/GAE/ENY/06-J06

THEORETICAL MODELING OF THE TRANSIENT EFFECTS OF A TOWLINE USING THE METHOD OF CHARACTERISTICS

Christopher A. Hill, BAEM
Ensign, USN

Approved:

_____	_____
Dr. Ralph Anthenien (Chairman)	date
_____	_____
Lt Col Raymond Maple (Member)	date
_____	_____
Dr. Mark Reeder (Member)	date

Abstract

The use of decoys in combat has become more advanced in recent years. Some of the newest military aircraft, such as the US Navy's F/A-18E/F Superhornet, have the capability to deploy a towline with an attached decoy when entering hostile territory as a defense mechanism against enemy threats. In steady state, the towline extends behind and below the aircraft. A major concern is the position of the towline, as aircraft maneuvers can cause the line to enter the engine plume. The high exhaust heat can cause problems, such as damaging electrical equipment and severing the line. In order to better understand the behavior of the towline, as well as setting up a method to analyze the heat transfer to the towline, computer modeling has been utilized using numerical integration with the method of characteristics.

The method of characteristics has been applied to 4 hyperbolic equations of motion, leaving 2 parabolic equations of motion to be calculated at each timestep. The energy equation for heat transfer to the towline was also derived, which provides a means to find local air density and towline temperature. From these a model was created to observe towline behavior and temperature, which is shown to be consistent with past research. This model is applicable to any towed body in any medium with zero slack conditions.

The effects of transient aircraft maneuvers on towline behavior in a predetermined temperature field were analyzed under different conditions using a code developed in MATLAB®. This code is included such that aircraft maneuvers in unique temperature fields can be analyzed for future research.

To Mom and Dad, for your generosity over the years, to my fiancée, for your unending encouragement, patience, admiration, prayers, and support, and to God, the Maker of this world, for His continual blessings in Christ Jesus (Eph 1:3)

Acknowledgements

I would like to express my deepest appreciation to my thesis advisor, Dr. Ralph Anthenien. Without his help, this work would not have been possible. I would also like to thank my committee members, Lt Col Raymond Maple and Dr. Mark Reeder. Their advice was invaluable.

Christopher A. Hill

Table of Contents

List of Figures

Page

Page

List of Symbols Used

*All values for this analysis will be in SI units and radians.

ϕ, θ	= directional angles of towline defined as: ϕ is 1st rotation from space to towline (about spatial *z*-axis) θ is 2nd rotation from space to towline (about towline *X*-axis)
μ	= mass of towline per meter
x, y, z	= spatial coordinates of towline
u, v, w	= velocity components in space
F_x, F_y, F_z	= aerodynamic forces in space (per meter along towline)
TF_x, TF_y, TF_z	= total forces in space (minus tension)
D_x, D_y, D_z	= drag forces in space (per meter along towline)
X, Y, Z	= coordinates aligned with towline
U, V, W	= velocity components aligned with towline
F_X, F_Y, F_Z	= aerodynamic forces aligned with towline (per meter of towline)
D_X, D_Y, D_Z	= drag forces aligned with towline (per meter along towline)
$\vec{V}$	= total velocity
s	= arc length along the towline
t	= time
W_t	= weight of towline per meter
e	= extension of towline
T	= tension of towline
$\mathbf{T}$	= temperature
d_{TL}	= diameter of towline

D_{TL}	= total length across towline in direction of airflow
$C_{D,TL}$	= coefficient of pressure drag for towline
$C_{D,TL,sf}$	= coefficient of skin friction drag for towline
$C_{D,B}$	= coefficient of drag on body
d_B	= diameter of cylindrical towed body
Wb	= weight of towed body
Mb	= mass of towed body
Nu	= Nusselt number
Re_D	= Reynolds number
h	= convection coefficient of air
k	= thermal conductivity of air
$\dot{E}$	= rate of internal energy
Vol	= volume
A_s	= total surface area
F_α and F_β	= characteristic lines
G_α, G_β, H_α, H_β, J_α, J_β, K_α, K_β, L_α, and L_β	= characteristic equation coefficients

THEORETICAL MODELING OF THE TRANSIENT EFFECTS OF A TOWLINE USING THE METHOD OF CHARACTERISTICS

I: Introduction

1.1. Background and Problem Setup

As military aircraft design has advanced over the years, so has the ability to detect and destroy them. The beginning of military aviation saw aircraft used primarily for scouting. At the outbreak of World War I, pilots were flying around each other shooting with handguns or the occasional mounted gun. There were antiaircraft defenses, but they often missed their targets. The aircraft themselves were only mildly effective warfighting tools, and were thus not the focus of much of military strategy.

Over the years, however, military aviation has become a vital part of combat strategy. The turning point of the Pacific Theater of World War II was the Battle of Midway. A naval conflict, this battle was fought purely with aircraft, proving the effectiveness and necessity for air superiority. Indeed, at the end of the same war, Japan found itself minus two cities due to attacks from the air. One might wonder what would have happened had Japan's air defense been stronger such that it could have shot down the bombers.

The intense threat of air attacks has propelled an equally intense development of antiaircraft defenses. From the introduction of surface to air missiles in Vietnam to the

development of long range air to air missiles such as the Phoenix, military aircraft must increasingly be wary of threats from both the ground and air. Modern design of aircraft must keep these issues central to their design.

This advancement of aircraft design has meant that as technology progresses, much more care and work needs to be put into protecting aircraft due to the immense cost of each vehicle. Ball quotes an anonymous source in his book as saying, "the cost of modern aircraft weapon systems, coupled with the requirement that the system be *effective*, makes imperative the consideration of the aircraft's survivability throughout the life cycle of the system" (Ball, 2003: xxvii).

The development of aircraft for modern conflict must take careful consideration to the threats that are posed. This is the back and forth process that the history of technology in warfare has followed. Antiaircraft artillery was able to be more effective at the altitude the aircraft were flying, so aircraft were designed to fly higher. Heat seeking missiles were put into battle, so chaff and flare became standard defenses. Radar could detect threats and track aircraft, so stealth aircraft and radar jammers were designed.

A lot of the more modern advances have been in electro-magnetic warfare. Anything that uses the EM spectrum falls under the scope of EM warfare. This includes detection devices such as radar, as well as any type of communication device. Control of the electro-magnetic spectrum in modern conflicts has become one the most vital guarantors of effectiveness.

One way to protect against aircraft in the realm of EM warfare is the use of towed decoys. A towed decoy is nothing more than a relatively small body towed behind an aircraft going into combat that can emit EM signals. It is connected to the aircraft by a

towline that can send signals back and forth, thus eliminating any need for communication through the air. The towline also eliminates the need for a propulsion and guidance system on the towed body. The body contains equipment that can be used to confuse enemy radar into seeing multiple or different types of aircraft. This could deter an attacker from attempting an attack, or force a threat to reveal their location (by firing a SAM, for instance). If a weapon is fired, the weapon will track the towed body rather than the aircraft. Either way, the aircraft and her crew are protected and are allowed to complete their mission.

One of the more common towed decoy systems, Raytheon's AN/ALE-50 Towed Decoy System is currently used on many US military aircraft, including the F/A-18E/F Superhornet, the F-16 Falcon, and the B-1B Lancer. This system has been used for the last decade or so. More developments on towed decoys are underway. A drawing of this system is shown in Figure 1.1-1.

(used without permission) (The Raytheon Company, 2006)

Figure 1.1-1 Raytheon's AN/ALE-50 Towed Decoy System

The towed body has the potential to undergo movement in combat. It is often unwise and tactically foolish to fly straight and level when under fire. Thus, the towline and towed body may need to undergo significant maneuvers. This can put a lot of tension on the towline, and often causes it to drift into the engine plume. At such a close distance, the towline has the potential to be damaged or severed, thus making the towed body worthless.

This paper seeks to provide a way to model the behavior of the towed body and towline under transient conditions so that future work can use these results to better design the system. This paper also analyzes the convective transfer of heat to the towline, and develops a manner in which to transfer data through time and down the line

by using the method of characteristics. Computer coding done in MATLAB® is included that can be easily modified to account for temperature effects and transient maneuvers.

1.2. Assumptions

The assumptions in this report were such that the analysis of the system of towline and towed body can be applied to almost any towed body in any medium. Much of the work in this paper was based on the development of equations to model towed bodies underwater. The first set of assumptions involved the towline behavior. The second set involved the attachment of the towline to the body and the aircraft. The third set of assumptions involved the aerodynamic effects. The fourth set of assumptions involved heat transfer effects.

Regarding the towline behavior, the first assumption was that compression in the line is impossible (see discussion on Crist's work, Section 2.3). Thus, the minimum tension in the line is zero. The second assumption was that the towline was inextensible. This is reasonable, since the towed body is also assumed to be relatively small and the towline is assumed to be made of inelastic material. The third assumption is that the towline is assumed to be straight along each increment (ds), which allows for numerical integration at each point along the line.

Regarding the attachment of the towline to the body and the aircraft, the first assumption is that the towline at its attachment to the body and the aircraft has the same behavior as the body and the aircraft respectively. This allows for the computation of the upper and lower boundaries of the towline. The second assumption is that the towed body has no rotational forces on it. In other words, any moments acting upon it become negligible. If the towed body is loosely attached (i.e., allowed to move freely) at its

lower end, it should generally be parallel to the freestream velocity. Since many of these bodies are also designed to have a streamline shape with fins (to keep them in the freestream), this assumption is reasonable. The body is thus modeled as always being parallel to the freestream.

Regarding the aerodynamic effects, the first assumption is that the aircraft is flying at subsonic speeds. This prevents the need for any type of shock wave analysis. The second assumption is that turbulent effects are negligible, or rather that the length scale of turbulence is larger than the control volume. Thus, the wake of the aircraft and any disturbance from engine plume do not come into play, and all calculations are based on the assumption of local laminar flow. The third assumption is that skin friction parallel to the towline is negligible. Due to the problem of an increasing boundary layer along the towline, the solution for analyzing the boundary layer becomes tricky. However, this assumption is the same used in Richardson (Richardson, 2005:20), and should not significantly affect the results.

Regarding the heat transfer effects, the first assumption was that the temperature of the medium is known at every point in space and time. This can be provided by analyzing the behavior of the engine plume, the primary source of heat disturbances. The second assumption is that the towed body is sufficiently far behind the aircraft such that its temperature remains constant over time. This prevents the need for extra processes that would slow down the calculations. Since the primary concern regarding temperature analysis is the possibility of damaging or severing the towline, there is no need to find the heat transfer to the body. The entire towline is analyzed, however, all the way to the point of attachment to the towed body. The third assumption is that the temperature

change along the towline is gradual. Thus, all heat transfer comes from the convection due to airflow over the towline, and any conduction within the towline is negligible. The main concern is the maximum temperature in the line, so this is also a reasonable assumption. The fourth assumption is that air pressure is constant. Thus, values of air density, viscosity, and thermal conductivity are purely functions of air temperature.

1.3. Preview of Paper

There are 5 chapters in this thesis, the first one (here) giving an introduction to the project's topic. The rest of the paper is as follows:

Chapter 2 contains a summary of background reading that was utilized in researching this topic. Since this paper is not experimental, the previous work became vital in understanding the development of techniques to model towline behavior. The chapter concludes with a description of the method of characteristics, a vital aspect of the methodology.

The methodology is contained in chapter 3. The development of the governing equations, as well as converting the equations of motion using the method of characteristics is explained in great detail. A set of equations is determined that can model the behavior of the towline under different perturbations with given initial data. In addition, a methodology to analyze heat transfer is explored, and equations are developed to model heat transfer in a predetermined temperature field. These equations can be used with the aid of computer software, such as MATLAB® (used for this paper), to solve for the behavior of a towline under transient effects.

Results of the computer simulation are contained in chapter 4. Some example scenarios are offered and analyzed, including steady state behavior, single axis

perturbations, a multiaxial perturbation, and heat transfer to a moving towline under constant ambient temperature. These results were compared to previous work.

Chapter 5 offers general conclusions to the research. It also lays out some suggestions for future work, including the motivation for such work.

II: Literature Review

A lot of past research has been done on towed lines and is included here as a source for background information. Of particular note are the works of Richardson, as well as Schram and Reyle. Most of the research in this paper is based on their methodologies. The last section of the literature review will include a description of the method of characteristics.

2.1. Richardson

"Parametric Study of the Towline Shape of an Aircraft Decoy," completed 2005, develops a method to compute the steady state form of a towline behind and aircraft in flight. This thesis, completed by ENS Tyler Richardson (USNR), is the foundational work that this paper is continuing.

Richardson derived equations of motion by taking into account airflow across a towline with a towed body (causing drag), and the weight of both the towline and the body. These equations were manipulated such that seven governing differential equations could be used to describe the behavior of the towline from the body up to the aircraft. All equations were with respect to the arc length of the towline, were nondimensionalized, and could thus be integrated along the towline (see discussion on the method of characteristics, Section 2.8). These equations involved four second order ODE's, three of which described position (three axes) and one of which described tension, and three first order ODE's that described position (three axes). Essentially, only four equations were uniquely derived by Richardson, noting that the first order position

terms become the integrals of the second order terms (i.e., $\frac{dx}{dl} = \int \frac{d^2x}{dl^2} dl$, where *dl* is the change in length along the towline). These seven governing equations were placed into the *ode45* solver in MATLAB® and integrated along the towline from the body up to the aircraft. This procedure was repeated for different parameters (velocity, weight, etc.) in order to determine the steady state behavior of the line under various conditions.

The most important results from this work include MATLAB® code that takes initial data and outputs the position, velocity, and tension of a towline in steady state flight. Richardson's work was compared to real data and determined to be accurate. Thus his code will serve as a comparison here. Richardson's code was also used in this paper to set up the initial conditions for transient behavior. In addition, his work serves as a reference for developing the method by which to solve the problem at hand.

Although similar techniques were used for this paper, one primary difference that Richardson's thesis utilized was the *ode45* solver in MATLAB®. The method for the research of this paper does not allow for continuous integration, however, since a fixed grid system is to be set up in advance for numerical integration. Richardson analyzes a steady state position of the towline before he analyzes its behavior. This paper is, however, concerned with the transient behavior, and as a result deals with changing variables over time. Thus, Richardson converts all of his equations to functions of one independent variable, whereas this work requires the use of two (see discussion on the method of characteristics in Section 2.8). This addition of the time element precludes the use of the *ode45* solver. Richardson notes himself in his conclusions and remarks that "a numerical integration routine for the system of differential equations needs to be written for the transient case" (Richardson, 2005:51).

2.2. Schram and Reyle

"A Three-Dimensional Dynamic Analysis of a Towed System," published in 1968, explores the behavior of an underwater towed body behind a ship. Using a purely theoretical model, the paper starts off by deriving the equations of motion from Newton's second law in three dimensions. These take into account not only tension from the ship, but include hydrodynamic towline forces. A coordinate transformation was applied so that all values were respective of the towline itself. For boundary conditions, they assumed that "the towline at its point of attachment to the towing ship must have the same motion as the ship … [and] the towline must have the same motion as the body at its point of attachment" (Schram and Reyle, 1968:216). They also set the tow point to "coincide with the center of mass of the body" in order to eliminate pitch, roll, and yaw effects (Schram and Reyle, 1968:216). In order to understand the dynamic effects of towline motion, the method of characteristics was applied such that all values vary solely with length and time. They finished by developing a numerical procedure to solve the dynamic solution.

Schram and Reyle made a few conclusions that are important for this paper. First, they found that "the speed at which transverse disturbances are propagated in the *x*-*y* and the *z*-*y* planes are the same" (Schram and Reyle, 1968:217). Second, they found that "if a towline is not straight, each type of disturbance, transverse or longitudinal, influences the other" (Schram and Reyle, 1968:219). In other words, a solely longitudinal disturbance could cause transverse motion farther down the towline as well and vice versa. Lastly, they found that the transfer function, which is "the ratio of the resultant amplitude of the

body motion to the amplitude of the motion of the ship" (Schram and Reyle, 1968:220) decreases if either the towline length or towing speed increases. With a longer length, disturbances have a longer distance to travel, thus being subject to a greater amount of damping. With a faster speed, the towline's pitch angle is reduced, causing a greater percentage of disturbances to be transversal. Transverse disturbances were found to be damped significantly more than longitudinal disturbances.

The research was summarized in a paper published in the Journal of Hydronautics in 1968, which was used as a primary point of reference here. This paper was essentially a summarization of a PhD. thesis completed earlier the same year (Reyle was the PhD. advisor) at Rutgers University. Both the journal's paper and the PhD. thesis were used in conjunction to understand their methodology.

Schram and Reyle's research provides the basis of much of the methodology in this paper. Their method will not be explained in more detail here due to the complexity of it. However, the methodology section of this paper explains much of what they did. Their application of the method of characteristics in modeling the behavior of the towed body has been relied upon heavily. In addition, their conclusions for towline behavior will serve as a comparison. The results of this research will differ in the sense that Schram and Reyle studied underwater behavior behind a towing body at constant altitude and ignored heat transfer and temperature effects. This paper will explore the behavior of the towed body in air at differing altitudes and set up a method to analyze heat transfer and temperature effects.

2.3. Crist

"Analysis of the Motion of a Long Wire Towed from an Orbiting Aircraft," published in 1970, studies the behavior of a long cable towed behind an aircraft undergoing oscillations, to include wind shear effects on cable motion. The paper relies upon previous steady state research on the TACAMO (**TA**ke **C**harge **A**nd **M**ove **O**ut) cable. It assumes a lumped mass model of the cable and derives Lagrange's equations of motion. The equations were solved numerically for vertical oscillations of a towing aircraft in constant radius and altitude, as well as transition from orbit to straight and level flight. Crist gives the method for wind shear analysis, but does not provide results.

Crist's concludes that "the effects of slack cable must be included in most analyses," that "the tension at the drogue can be considerably higher than the equilibrium tension when the aircraft oscillates vertically," and that the "tension in the cable during transition from orbit can be considerable, even for a smooth transition from orbit" (Crist, 1970:73). Perhaps more importantly, he notes that "compressive force in the cable segment… is, of course, impossible since everyone knows 'you can't push on a rope'" (Crist, 1970:65). He also developed an analysis to calculate the motion of a towed cable behind an orbiting aircraft following a prescribed flight path. Due to the high speed of aircraft, however, slack conditions will not be analyzed in this paper, since they create negative tension errors. More on this will be discussed in the conclusions.

Crist's analysis of a towing cable undergoing aircraft motion will be used as a source for comparison for this paper. Due to computing power at the time his paper was written, a discrete mass approach was used in the analysis. Crist notes, however, that a good approximation can be made to a continuous mass approach with only a few mass

points (Crist, 1970:61). Since this paper is using numerical integration along a towline, it will also use the discrete mass approach, although more accurate results will be available due to much faster computing time. In addition, this paper will develop methods to analyze a whole range of motion, not just vertical oscillations or transition to straight and level flight. As in the Schram and Reyle paper, Crist does not consider heat transfer or temperature effects either.

2.4. Chapman

"Towed Cable Behaviour During Ship Turning Manoeuvres," published in 1984 explores the behavior of an underwater towed body in large and small radius turns. In large radius turns, the system behaves similarly to a steady state straight-tow behavior. However, in small radius turns, the system collapses, causing the towed body to drop in depth (no cable tension), followed by a quick tug (high cable tension). This paper's purpose was to determine a non-dimensionalized minimum radius at which collapse can be avoided.

Chapman concluded that "in a gradual turn (with a relatively slow rate of turn) the cable moves towards, and usually attains, an equilibrium configuration that is a slightly perturbed form of the profile adopted during straight towing. The [towed body] moves towards a circular course which is concentric with the ship's course but of slightly smaller radius. As a consequence the speed of the [towed body] is reduced resulting in a slight increase of depth" (Chapman, 1984: 353). Also, he concludes that in a sharp turn, the straight-tow profile collapses, causing the towed body to drop sharply. This results in increased tension at the top of the cable, and could cause slackness near the towed body.

Thus, the system will most likely never reach equilibrium in the turn. He found that the transition from equilibrium turns to a collapsed system happens over a very small range of radii, thus giving a fairly defined minimum turning radius.

Chapman's analysis and methods will be used in this paper to help understand small radius turns. His analyses involved an underwater body, which will exhibit significantly more drag than a body in air. Also, ship speeds will be significantly slower than those of aircraft. Thus, while the concern of a collapsed system in sharp turns will be considered, it will most likely not be an issue except in extreme cases. Due to the restriction in this paper of no slack, Chapman's research is referenced here since it can be used to prevent slack conditions for future work.

2.5. Dowling

"The Dynamics of Towed Flexible Cylinders Part I: Neutrally Buoyant Elements," published in 1987, investigates the transverse vibrations of a thin, flexible neutrally buoyant cylinder under nominally constant towing conditions. The cylinder is assumed to have a very small bending stiffness, and stretches out due to viscous forces along its length.

Dowling focuses primarily on a flexible towed body, whereas this paper's research is concerned with inflexible towed bodies. Also, he investigates underwater behavior with a towing body of constant altitude. This paper will be used primarily to develop methods for forces on the towed body.

2.6. Ames

Nonlinear Partial Differential Equations in Engineering, published in 1965, gives a detailed understanding of the method of characteristics, and provides a foundation for the mathematical understanding behind the derivations used in this paper. Specifically, this book helps set up the mesh scheme and the equations to carry data from one timestep to the next for the method of characteristics, which Ames notes is based on a previous scheme set up by Courant, Isaacson, and Rees. Ames notes that this mesh is based on a first-order scheme (Ames, 1965:446), which becomes significant in the error analysis of this work. This method is used in order to avoid the "messy two-dimensional interpolation in the characteristic grid" (Ames, 1965:444) by setting up the mesh points in advance and interpolating as the computation proceeds, making the interpolation one-dimensional.

Ames also proposes a "hybrid" method by Hartree, which provides a second-order truncation error. This method could be useful for future analysis, but is not used here due to the iteration requirement to solve the system of equations at each timestep. The method based on Courant, Isaacson, and Rees requires no iteration, and is the same method used in Schram and Reyle. Thus, this method will be used for the analysis of this paper.

Schram and Reyle relied heavily on the work of Ames, and this paper will follow in their footsteps. It will be used as a point of reference for much of the math, and will help with the derivation of any new equations.

2.7. Tannehill, Anderson, and Pletcher

Computational Fluid Mechanics and Heat Transfer, published in 1997, serves as a foundational basis for a lot of CFD work today. Since this paper's work depends on the stepping method of solving a system of equations, the CFD book is a vital resource in determining numerical differencing schemes, as well as understanding the method of characteristics. This book, like Ames, will be used primarily as a reference tool to develop the governing equations.

2.8. Method of Characteristics

As alluded to earlier, both Ames as well as Tannehill, Anderson, and Pletcher give detailed descriptions of the method of characteristics. These, in conjunction with Schram and Reyle, were used to understand the method of characteristics. This method will be explained in its general principles here.

The method of characteristics is a technique that is used to solve nonlinear hyperbolic partial differential equations. What this method does, in essence, is convert the equations of a system into new equations that are constant along characteristic lines. In the application here, the system of equations is rewritten to be a function of two independent variables, which can be held constant along the characteristic lines.

An analogy that can be used to describe this is a wave on the ocean traveling in space and time. From shore, looking straight along a line in the water, an observer sees the water move up and down in a different manner at every point along that line (Figure 2.8-1). Thus, the behavior is a function of time and location (i.e., position on the line the observer is concerned about). If the reference frame is changed, however, such that the

observer is on the top of one wave, with his line of sight along the top of that wave, the behavior will look the same at all time and position along his line of sight (Figure 2.8-2). The method of characteristics uses this type of technique in order to “march” data from one timestep to the next by finding characteristic lines on which the solution is constant. Applying the wave analogy to the towline problem, the towline at a certain time becomes a waveline in its direction of motion (left to right in figure), and the change in time is represented by each successive waveline (top to bottom in figure, and not to be confused with the time described in the analogy).

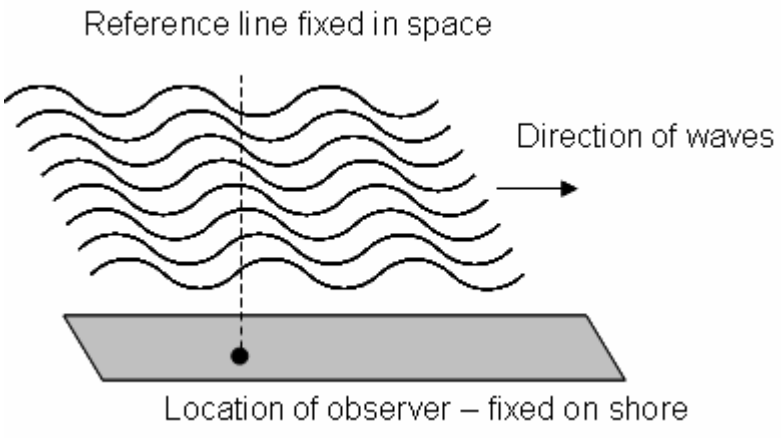

Figure 2.8-1 Initial Reference Frame

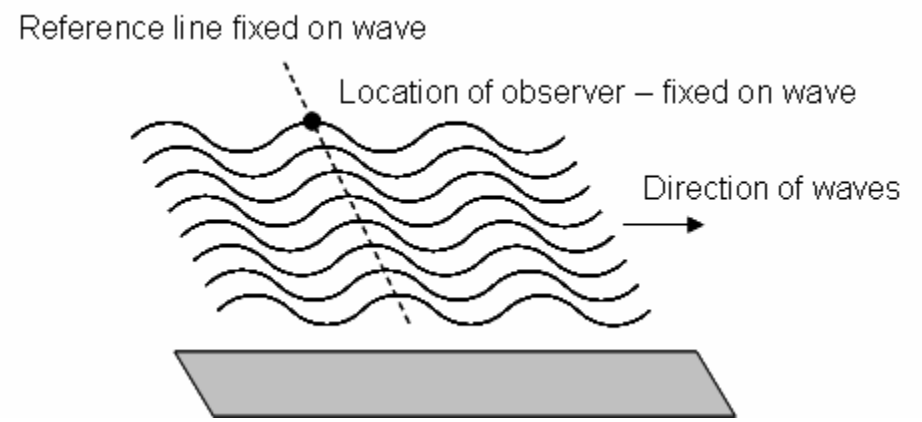

Figure 2.8-2 New Reference Frame - fixed to wave

This method is vital for finding a solution to the problems of this paper. What will be shown later is the development of six PDE equations of motion with respect to time and length along the towline. In order to get a total solution to the system, these equations will be converted into characteristic equations, solved for all positions along the towline for one timestep, then "marched" to the next timestep using the characteristic lines. To follow the wave analogy represented in Figure 2.8-2, the information at one point on the towline is carried to the next timestep at a different position on the towline. This new position is determined by the characteristic line and the change in time. Another way to show this is in Figure 2.8-3, which shows a solution in time and space that will be used for this paper, where *s* is the length along a towline and *t* is time. This figure is based on one devised by Tannehill, Anderson, and Pletcher (Tannehill, Anderson, and Pletcher, 1997:361), but could be found in most detailed descriptions of the method of characteristics.

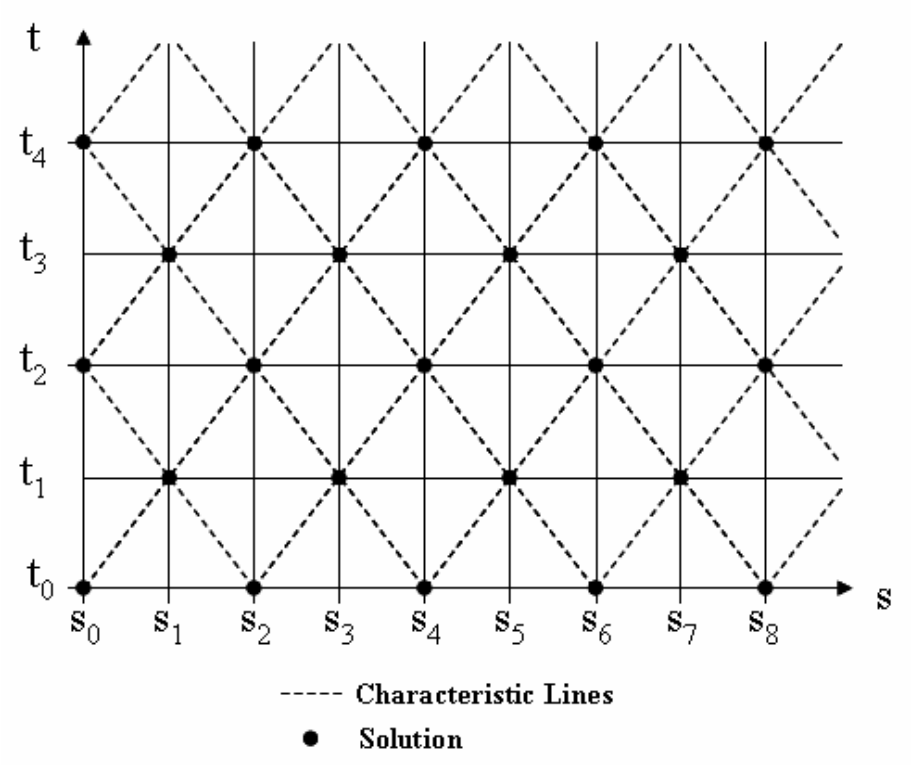

Figure 2.8-3 Characteristic Net

Note that the solution can be found at every intersection of the characteristic lines. Thus, new data is available at every interval. Since the characteristic lines carry constant data along their entire path, middle steps can be skipped if desired. If new lines were started from every *s* and *t* position, the density of the mesh would double. In fact, the mesh size can be reduced to be as small as desired by noting that any new used data point can transfer information along newly created characteristic lines from that point.

The characteristic net is defined by the characteristic lines. The positive sloped characteristic lines all have the same slope, but start at equally spaced positions along the *s*-axis. Similarly, the negative sloped lines all have the same slope, starting at the same positions as their counterparts. Due to the hyperbolic nature of the equations used in the method of characteristics, these two slopes are different only in sign, and are found by

finding the roots of the system of equations. These roots are called the "characteristic lines," and make up the "characteristic net" shown in Figure 2.8-3.

Thus, the application of the method of characteristics necessitates first that characteristic equations are derived such that they remain constant along the characteristic lines. This is done by converting a set of hyperbolic PDE's into a set of ordinary differential equations where each ODE comes from two separate PDE's. Each new ODE is then integrated along the characteristic lines. Ames (Ames, 1965: 422) notes that these calculations must, in most cases, be carried out numerically. Exact integration by this method is very rare. This paper will use the method of characteristics with numerical integration.

III: Methodology

The subsequent derivations for towline motion come from an adaptation of those in Schram and Reyle. While their work is heavily relied upon here, they were not always followed directly. Effort has been made to note when their work was followed. The heat transfer derivations were completely independent of any past work.

3.1. Derivation of Governing Equations

The governing equations and their derivations rely very heavily upon work done by Schram and Reyle (1968). Similar notation and procedure will be used, and a great deal of effort has been used to reduce any ambiguity in their work, and to make the procedure used in this paper as clear as possible.

Axis Transformation.

In order to derive a system of equations for use with the method of characteristics, all variables will need a manner to convert between coordinate axes aligned with space (aircraft at steady state), and those aligned with the towline. Thus, a matrix [A] must be found, which will allow for the transformation of components (position, velocity, etc.) between space and towline axes. This transformation is shown in Figure 3.1-1, Figure 3.1-2, and Figure 3.1-3

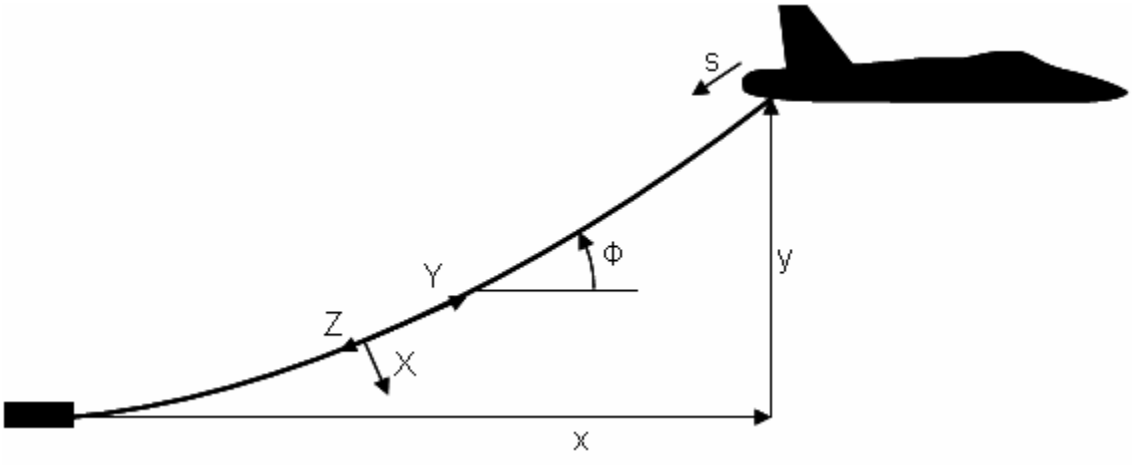

Figure 3.1-1 Spatial orientation of x-y plane

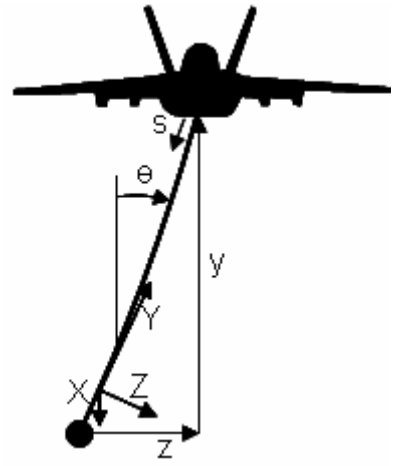

Figure 3.1-2 Spatial orientation of z-y plane

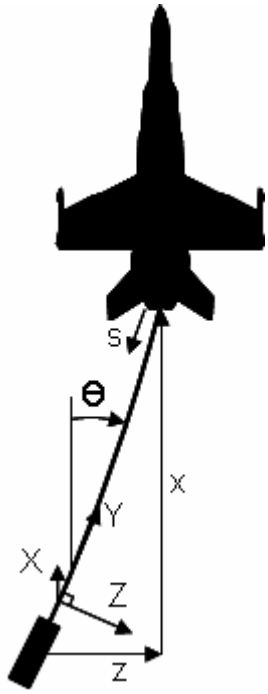

Figure 3.1-3 Spatial orientation of z-x plane

where ϕ is the azimuth angle and θ is the polar angle. A note should be made about θ in regards to its appearance in the diagrams. This angle refers to a second transform about the towline *X*-axis, and the two-dimensional silhouette of Figure 3.1-2 and Figure 3.1-3 do not show the fact that θ can go in or out of the page as well. A better visual representation is in Figure 3.1-6, while making sure to note the transitional *y'*-axis.

The spatial axes are oriented with the *y*-axis aligned directly vertical, the *x*-axis aligned with the direction of the aircraft, and the *z*-axis aligned perpendicular to the aircraft's line of flight. The towline axes are oriented with the *Y*-axis aligned directly along the towline, the *X*-axis aligned downward from the towline and in the *x*-*y* plane, and the *Z*-axis aligned perpendicular to the towline and the *X*-axis. Figure 3.1-4 sets up a three dimensional plot for transformation.

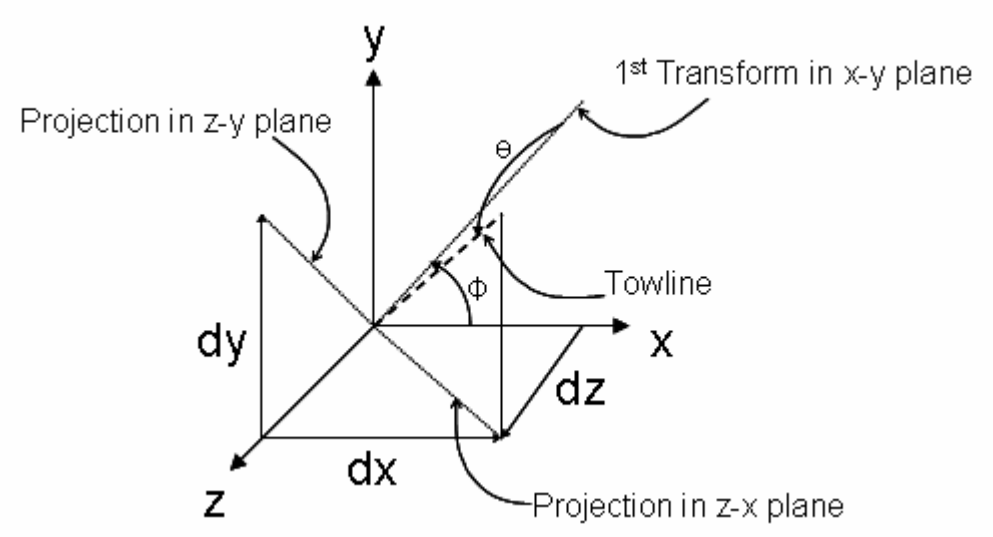

Figure 3.1-4 Towline in spatial axes

The first transformation changes the spatial coordinates into the towline *X*-axis and a mid-step *y'*-axis by rotating about the *z*-axis. This is shown in Figure 3.1-5. The angle ϕ is used here and exists only in the spatial *x-y* plane. Thus, ϕ is not hard to represent in the other diagrams of this paper.

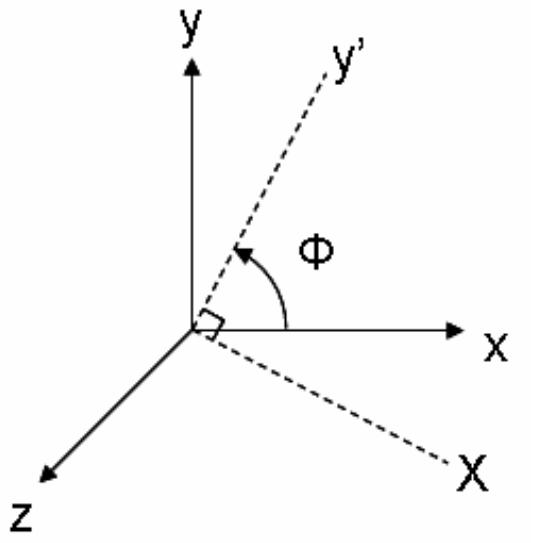

Figure 3.1-5 First Transformation

Note that ϕ is defined as positive up from the *x*-axis such that a zero value lines up the *y'* and *x* axes.

From here, the following are derived:

$$f(X) = f(x)\sin\phi - f(y)\cos\phi \qquad 1.1$$

$$f(y') = f(x)\cos\phi + f(y)\sin\phi \qquad 1.2$$

where *f*( ) refers to any variable in each respective axis. Note that the *y'*-axis has no real value except for its use in the process of coordinate transformation. As will be seen in the next transformation, however, a θ angle of zero makes the *y'* and *y* axes line up, and Figure 3.1-5 is sufficient to model the axis transformation.

At this point, the transformation from space to the *X* towline component is complete. The second transformation will provide a solution for the *Y* and *Z* components in the towline by rotating about the new *X*-axis. This transformation is shown in Figure 3.1-6. As an aside, the angle θ, used for the second transformation, exists in the *z*-*y'* plane, where *y'* is the transitory axis. Thus, it is hard to represent accurately in many of the diagrams.

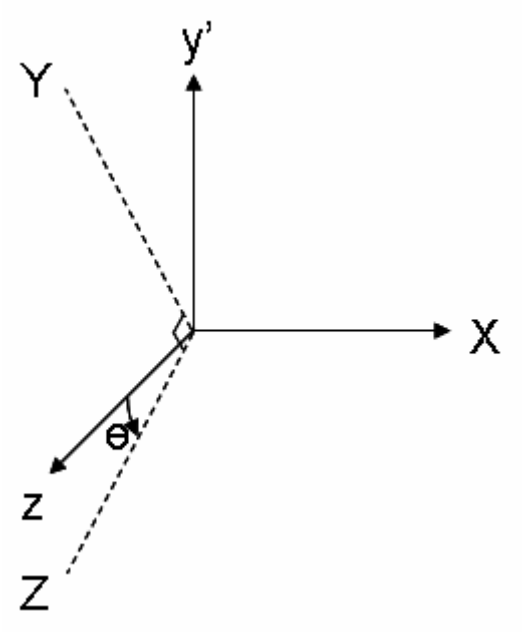

Figure 3.1-6 Second Transformation

Thus, the following are derived:

$$\begin{aligned} f(Y) &= f(y')\cos\theta + f(z)\sin\theta \\ &= f(x)\cos\phi\cos\theta + f(y)\sin\phi\cos\theta + f(z)\sin\theta \end{aligned} \tag{1.3}$$

$$\begin{aligned} f(Z) &= -f(y')\sin\theta + f(z)\cos\theta \\ &= -f(x)\cos\phi\sin\theta - f(y)\sin\phi\sin\theta + f(z)\cos\theta \end{aligned} \tag{1.4}$$

From these equations, a matrix [A] is generated such that all axis transformations can be computed in a simple manner. By taking the components of *x*, *y*, and *z*, one generates the matrix as follows:

$$[A] = \begin{bmatrix} \sin\phi & -\cos\theta & 0 \\ \cos\phi\cos\theta & \sin\phi\cos\theta & \sin\theta \\ -\cos\phi\sin\theta & -\sin\phi\sin\theta & \cos\theta \end{bmatrix} \tag{1.5}$$

This matrix can be used to transform from space to towline, and vice versa. This is accomplished quite easily, and is printed here for reference (to prevent confusion, *TL* and *S* will denote towline and space respectively):

$$\begin{bmatrix} f(X) \\ f(Y) \\ f(Z) \end{bmatrix}_{TL} = [A] \begin{bmatrix} f(x) \\ f(y) \\ f(z) \end{bmatrix}_{S} \tag{1.6}$$

$$\begin{bmatrix} f(x) & f(y) & f(z) \end{bmatrix}_{S} = \begin{bmatrix} f(X) & f(Y) & f(Z) \end{bmatrix}_{TL} [A] \tag{1.7}$$

Now that a manner in which to transform between the spatial and towline axes has been determined, the governing equations may be developed.

Equations of Motion.

Since this system contains six unknowns (U,V,W,ϕ,θ,T) in the towline reference frame at any point in time and space, six equations of motion will be needed to describe the entire behavior of the towline.

Using Newton's Second Law of Motion (flipped from standard notional for convenience)

$$ma = F \tag{1.8}$$

and applying it to the free body diagram of the towline in its spatial coordinates (Figure 3.1-4), Schram cites Cristescu (Schram, 1968:6) with determining that the equations of motion for an elastic line become:

$$\mu \frac{\partial^2 x}{\partial t^2} = \frac{\partial}{\partial s}\left(\frac{T}{(1+e)} \frac{\partial x}{\partial s} \right) + \mathrm{F}_x \tag{1.9}$$

$$\mu \frac{\partial^2 y}{\partial t^2} = \frac{\partial}{\partial s}\left(\frac{T}{(1+e)} \frac{\partial y}{\partial s} \right) + \mathrm{F}_y - W_t \tag{1.10}$$

$$\mu \frac{\partial^2 z}{\partial t^2} = \frac{\partial}{\partial s}\left(\frac{T}{(1+e)} \frac{\partial z}{\partial s} \right) + \mathrm{F}_z \tag{1.11}$$

It should be noted that these terms are all per meter of towline length.

In these equations, tension is divided by a percent change in extension of the towline. Assuming an inextensible towline, which this paper will assume just as Schram and Reyle did, the extension terms drop out. The $\partial x/\partial s$, $\partial y/\partial s$, and $\partial z/\partial s$ terms are used to project tension into the respective axes, since tension is purely directed along the towline (the *s*-direction is used here, which is interchangeable with the *Y*-axis). Through a simple application of the matrix transformation represented in Equation 1.7, these terms become:

$$\frac{\partial x}{\partial s} = -\cos\theta\cos\phi \tag{1.12}$$

$$\frac{\partial y}{\partial s} = -\cos\theta\sin\phi \tag{1.13}$$

$$\frac{\partial z}{\partial s} = -\sin\theta \tag{1.14}$$

where the negative term is due to the orientation of *s* being positive down the towline towards the body.

Substituting Equations 1.12 through 1.14 into Equations 1.9 through 1.11, replacing the second derivative (acceleration) terms with equivalent velocity terms, and rearranging slightly, these equations reduce to:

$$\frac{\partial u}{\partial t} = \frac{1}{\mu}\left[\frac{\partial}{\partial s}\left(-T\cos\theta\cos\phi\right) + \mathrm{F}_x\right] \tag{1.15}$$

$$\frac{\partial v}{\partial t} = \frac{1}{\mu}\left[\frac{\partial}{\partial s}\left(-T\cos\theta\sin\phi\right) + \mathrm{F}_y - W_t\right] \tag{1.16}$$

$$\frac{\partial w}{\partial t} = \frac{1}{\mu}\left[\frac{\partial}{\partial s}\left(-T\sin\theta\right) + \mathrm{F}_z\right] \tag{1.17}$$

Taking the three towline acceleration terms and applying them to the axis transformation in Equation 1.6 yields the equations of motion in towline form, noting first the velocity transformations:

$$U = u\sin\phi - v\cos\phi \tag{1.18}$$

$$V = u\cos\phi\cos\theta + v\sin\phi\cos\theta + w\sin\theta \tag{1.19}$$

$$W = -u\sin\theta\cos\phi - v\sin\theta\sin\phi + w\cos\theta \tag{1.20}$$

Thus, the equations of motion become:

$$\frac{\partial U}{\partial t} = \left[\frac{\partial u}{\partial t}\sin\phi - \frac{\partial v}{\partial t}\cos\phi\right] + \left(u\cos\phi + v\sin\phi\right)\frac{\partial\phi}{\partial t} \tag{1.21}$$

$$\begin{aligned}\frac{\partial V}{\partial t} = &\left[\left(\frac{\partial u}{\partial t}\cos\phi + \frac{\partial v}{\partial t}\sin\phi\right)\cos\theta + \frac{\partial w}{\partial t}\sin\theta\right] \\ &+ \left(v\cos\phi - u\sin\phi\right)\cos\theta\frac{\partial\phi}{\partial t} - \left((u\cos\phi + v\sin\phi)\sin\theta + w\cos\theta\right)\frac{\partial\theta}{\partial t}\end{aligned} \tag{1.22}$$

$$\begin{aligned}\frac{\partial W}{\partial t} = &\left[-\left(\frac{\partial u}{\partial t}\cos\phi + \frac{\partial v}{\partial t}\sin\phi\right)\sin\theta + \frac{\partial w}{\partial t}\cos\theta\right] \\ &- \left(-u\sin\phi + v\cos\phi\right)\sin\theta\frac{\partial\phi}{\partial t} - \left(\left(u\cos\phi + v\sin\phi\right)\cos\theta + w\sin\theta\right)\frac{\partial\theta}{\partial t}\end{aligned} \tag{1.23}$$

The bracketed terms come from the direct transformation of the *U*, *V*, and *W* towline variables (Equations 1.18, 1.19, and 1.20), while the extra terms come from the derivative due to the product rule. By utilizing Equation 1.7, the spatial velocity terms can also be transformed into their towline forms:

$$u = U\sin\phi + V\cos\phi\cos\theta - W\cos\phi\sin\theta \tag{1.24}$$

$$v = -U\cos\phi + V\cos\theta\sin\phi - W\sin\theta\sin\phi \tag{1.25}$$

$$w = V\sin\theta + W\cos\theta \tag{1.26}$$

The spatial forces, F_x, F_y, and F_z, are also transformed in the same manner to the towline forces F_X, F_Y, and F_Z. Combining the above equations by replacing all of the spatial terms with towline terms, everything can now be transformed into towline parameters. Thus, the equations of motion in towline axes become:

First Three Equations of Motion:

$$\mu\left[-\frac{\partial U}{\partial t}+\left(V\cos\theta-W\sin\theta\right)\frac{\partial\phi}{\partial t}\right]=-T\cos\theta\frac{\partial\phi}{\partial s}-F_X-W_t\cos\phi \qquad \textbf{1.27}$$

$$\mu\left[\frac{\partial V}{\partial t}-W\frac{\partial\theta}{\partial t}+U\cos\theta\frac{\partial\phi}{\partial t}\right]=-\frac{\partial T}{\partial s}+F_Y-W_t\sin\phi\cos\theta \qquad \textbf{1.28}$$

$$\mu\left[U\sin\theta\frac{\partial\phi}{\partial t}-V\frac{\partial\theta}{\partial t}-\frac{\partial W}{\partial t}\right]=T\frac{\partial\theta}{\partial s}-F_Z-W_t\sin\phi\sin\theta \qquad \textbf{1.29}$$

These equations will be useful later in the method of characteristics, and provide the first 3 equations of motion. All partial derivatives are with respect to either time or arc length (s), which is valuable since the two independent variables used in the method of characteristics will be time and arc length.

The next three equations can be found by simply taking the partial derivative of the towline accelerations with respect to the arc length of the towline. These equations become exactly the same as Equations 1.21, 1.22, and 1.23, except that the partial derivatives are now in terms of s instead of t:

$$\frac{\partial U}{\partial s}=\left[\frac{\partial u}{\partial s}\sin\phi-\frac{\partial v}{\partial s}\cos\phi\right]+u\cos\phi\frac{\partial\phi}{\partial s}+v\sin\phi\frac{\partial\phi}{\partial s} \qquad 1.30$$

$$\begin{aligned}\frac{\partial V}{\partial s}=&\left[\left(\frac{\partial u}{\partial s}\cos\phi+\frac{\partial v}{\partial s}\sin\phi\right)\cos\theta+\frac{\partial w}{\partial s}\sin\theta\right]\\&+\left(v\cos\phi-u\sin\phi\right)\cos\theta\frac{\partial\phi}{\partial s}-\left((u\cos\phi+v\sin\phi)\sin\theta+w\cos\theta\right)\frac{\partial\theta}{\partial s}\end{aligned} \qquad 1.31$$

$$\frac{\partial W}{\partial s} = \left[-\left(\frac{\partial u}{\partial s}\cos\phi + \frac{\partial v}{\partial s}\sin\phi \right)\sin\theta + \frac{\partial w}{\partial s}\cos\theta \right] \\ -\left(-u\sin\phi + v\cos\phi\right)\sin\theta\frac{\partial\phi}{\partial s} - \left(\left(u\cos\phi + v\sin\phi\right)\cos\theta + w\sin\theta\right)\frac{\partial\theta}{\partial s} \tag{1.32}$$

The partial derivatives of the spatial velocities with respect to arc length can be easily related in the following manner with the use of Equations 1.12, 1.13, and 1.14:

$$\frac{\partial u}{\partial s} = \frac{\partial}{\partial s}\left(\frac{\partial x}{\partial t}\right) = \frac{\partial}{\partial t}\left(\frac{\partial x}{\partial s}\right) = \frac{\partial}{\partial t}(-\cos\theta\cos\phi) \tag{1.33}$$

$$\frac{\partial v}{\partial s} = \frac{\partial}{\partial s}\left(\frac{\partial y}{\partial t}\right) = \frac{\partial}{\partial t}\left(\frac{\partial y}{\partial s}\right) = \frac{\partial}{\partial t}(-\cos\theta\sin\phi) \tag{1.34}$$

$$\frac{\partial w}{\partial s} = \frac{\partial}{\partial s}\left(\frac{\partial z}{\partial t}\right) = \frac{\partial}{\partial t}\left(\frac{\partial z}{\partial s}\right) = \frac{\partial}{\partial t}(-\sin\theta) \tag{1.35}$$

By combining these with the velocity relationships from Equations 1.24, 1.25, and 1.26, one derives the final three equations of motion in towline form:

Last Three Equations of Motion:

$$\frac{\partial U}{\partial s} = \frac{\partial\phi}{\partial t}\cos\theta + (V\cos\theta - W\sin\theta)\frac{\partial\phi}{\partial s} \tag{**1.36**}$$

$$\frac{\partial V}{\partial s} = W\frac{\partial\theta}{\partial s} - U\cos\theta\frac{\partial\phi}{\partial s} \tag{**1.37**}$$

$$\frac{\partial W}{\partial s} = -\frac{\partial\theta}{\partial t} - V\frac{\partial\theta}{\partial s} + U\sin\theta\frac{\partial\phi}{\partial s} \tag{**1.38**}$$

Just as in the first three equations of motion, these equations will be useful later in the method of characteristics. All partial derivatives here are also with respect to either time or arc length (*s*), where *s* is positive down the towline towards the body.

3.2. Applying the Method of Characteristics

Mathematical Character of Equations.

A few comments should be made here regarding the behavior of parabolic versus hyperbolic equations using a stepping method such as the method of characteristics. Of most importance, perhaps, is the fact that only hyperbolic PDE's can be used with the method of characteristics. Tannehill, Anderson, and Pletcher (Tannehill, Anderson, and Pletcher, 1997:26-32) discuss the behaviors of hyperbolic versus parabolic PDE's, noting the dependence that each equation has with respect to a length-time mesh. They note that hyperbolic equations are dependent only upon the solution contained within the bounds set by the characteristics at the previous timestep. This solution is represented in Figure 3.2-1 (similar figure in Tannehill, Anderson, and Pletcher, 1997:27), where it can be seen that a single solution exists at the intersection of the characteristic lines.

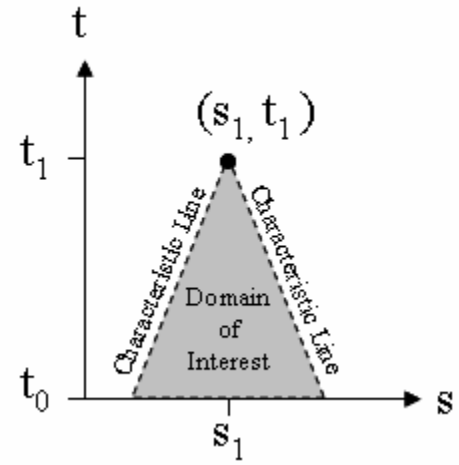

Figure 3.2-1 Hyperbolic Characteristic Lines & Domain of Interest

Tannehill, Anderson, and Pletcher note, however, that parabolic equations, unlike hyperbolic equations, are dependent upon the entire physical domain, and thus have no characteristic lines; or rather, the slopes of the characteristic lines are zero. This is why

the method of characteristics cannot be applied to parabolic PDE's. The dependence of a parabolic solution is shown in Figure 3.2-2 (similar figure in Tannehill, Anderson, and Pletcher, 1997:31), where it can be seen that an infinite number of solutions exist at t_1; or rather, the solution is dependent on everything at its current timestep.

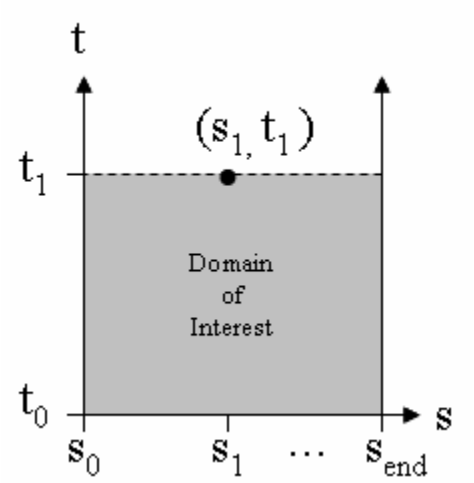

Figure 3.2-2 Parabolic Domain of Interest

In order to determine whether an equation is hyperbolic or parabolic, an attempt must be made to find the characteristic roots (these are the slopes of the characteristic lines). If the roots exist and are distinct and real, the equation is hyperbolic. If there is only one distinct real root, the equation is parabolic. Another case exists where the roots are complex or no real root exists, causing the equation to by elliptical. This last case turns out to not be relevant here, however.

Equations 1.28 and 1.37 are both parabolic (Schram and Reyle, 1968: 216), whereas the rest of the equations of motion are hyperbolic. The zero characteristic roots that appear in the parabolic equations are due to the towline's inextensible assumption. Equations 1.28 and 1.37 can be shown to be parabolic, with the rest being hyperbolic, by a little work and inspection.

Tannehill, Anderson, and Pletcher note the forms of hyperbolic, parabolic, and elliptical PDE's (Tannehill, Anderson, and Pletcher, 1997:25) in the following manner. Hyperbolic PDE's exist in the two forms of Equations 2.1 and 2.2:

$$\frac{\partial^2 f}{\partial t^2} - \frac{\partial^2 f}{\partial s^2} = g_1\left(\frac{\partial f}{\partial t}, \frac{\partial f}{\partial s}, f, t, s\right) \tag{2.1}$$

$$\frac{\partial^2 f}{\partial t \partial s} = g_2\left(\frac{\partial f}{\partial t}, \frac{\partial f}{\partial s}, f, t, s\right) \tag{2.2}$$

where both equations are necessary. Parabolic PDE's exist in the form of either Equation 2.3 or 2.4:

$$\frac{\partial^2 f}{\partial t^2} = g\left(\frac{\partial f}{\partial t}, \frac{\partial f}{\partial s}, f, t, s\right) \tag{2.3}$$

$$\frac{\partial^2 f}{\partial s^2} = g\left(\frac{\partial f}{\partial t}, \frac{\partial f}{\partial s}, f, t, s\right) \tag{2.4}$$

Elliptical PDE's exist in the form of Equation 2.5:

$$\frac{\partial^2 f}{\partial t^2} + \frac{\partial^2 f}{\partial s^2} = g\left(\frac{\partial f}{\partial t}, \frac{\partial f}{\partial s}, f, t, s\right) \tag{2.5}$$

where $g(\ )$ denotes some function of the included variables.

To determine if Equations 1.27 through 1.29, and Equations 1.36 through 1.38 are hyperbolic, parabolic, or elliptical, they need to be converted into a second order form. This is done by noting that the velocity terms of the equations in question can be replaced with their respective position derivative (i.e., $U = \partial X/\partial t$, thus $\partial U/\partial t = \partial^2 X/\partial t^2$). The angles can also be converted into position terms by manipulating Equations 1.12 through 1.14 into the following:

$$\phi = \tan^{-1}\left(\frac{\partial y}{\partial x}\right) \tag{2.6}$$

$$\theta = -\sin^{-1}\left(\frac{\partial z}{\partial s}\right) \tag{2.7}$$

From here, one can convert all six equations of motion to forms that have derivatives of solely position variables. Another transformation between space and towline forms would be required for consistency, although to simply determine the character of the equations by inspection this would not be necessary since it would not add more derivative terms. In other words, *x* and *X* are interchangeable for the inspection technique.

The details of this procedure are not vital to understanding the methodology of this paper, and will thus not be included here. Suffice it to say that Equations 1.28 and 1.37 are both parabolic, whereas the rest of the equations of motion are hyperbolic. Since only hyperbolic equations can be applied to the method of characteristics, the parabolic equations cannot be transformed in the subsequent sections.

Finding Roots of Equations.

The roots of the hyperbolic equations can be found by setting up a generalized Eigenvalue problem. Generalized Eigenvalues are defined as

$$[\upsilon][M] = \lambda[\upsilon][N] \tag{2.8}$$

where

$$\det(M - \lambda N) = 0 \tag{2.9}$$

[*M*] and [*N*] are coefficient matrices of a system and [υ] is chosen such that equation 2.8 holds true (in reality, [υ] is said to be non-zero for the system to have Eigenvalues, thus its values do not matter for finding roots, since it follows that the determinant must be zero for the system to hold). Solving for λ finds the roots of the system. Schram and

Reyle model the system of hyperbolic equations based on a technique they developed from Ames (Schram and Reyle, 1968:216-217). In this they converted the four hyperbolic equations (1.27, 1.29, 1.36, 1.38) into one single system of matrices.

$$[M][\gamma]_s + [N][\gamma]_t + [P] = [0] \tag{2.10}$$

where

$$[M] = \begin{bmatrix} 0 & 0 & \dfrac{T\cos\theta}{\mu} & 0 \\ 0 & 0 & 0 & -\dfrac{T}{\mu} \\ 1 & 0 & -(V\cos\theta - W\sin\theta) & 0 \\ 0 & 1 & -U\sin\theta & V \end{bmatrix} \tag{2.11}$$

$$[N] = \begin{bmatrix} -1 & 0 & (V\cos\theta - W\sin\theta) & 0 \\ 0 & -1 & U\sin\theta & -V \\ 0 & 0 & -\cos\theta & 0 \\ 0 & 0 & 0 & 1 \end{bmatrix} \tag{2.12}$$

$$[\gamma] = \begin{bmatrix} U \\ W \\ \phi \\ \theta \end{bmatrix} \tag{2.13}$$

$$[P] = \frac{1}{\mu}\begin{bmatrix} F_X + W_t\cos\phi \\ W_t\sin\phi\sin\theta + F_Z \\ 0 \\ 0 \end{bmatrix} \tag{2.14}$$

and the *s* and *t* subscripts refer to the partial derivatives of the matrix variables.

From this, one can find the general Eigenvalues of the system, which represent the characteristic roots. This is done by solving for λ in equation 2.9. The roots of the system are thus represented by

$$F_{\alpha} = \sqrt{\frac{T}{\mu}} \tag{2.15}$$

$$F_{\beta} = -\sqrt{\frac{T}{\mu}} \tag{2.16}$$

which are each repeated twice (four equations gives four roots). The subscripts α and β refer to the characteristic directions. These values turn out to be the speed at which disturbances are propagated along the towline. In other words,

$$\frac{ds}{dt} = \pm\sqrt{\frac{T}{\mu}} \tag{2.17}$$

This is consistent with the value that can be found in any textbook for propagation of disturbances along an inextensible line in tension.

Finding Characteristic Equations.

Schram and Reyle (Schram and Reyle, 1968:217) note that the characteristic equations can be determined by some manipulation of the hyperbolic equations. This can be done by multiplying Equations 1.27 and 1.29 by *dt* and adding them to their counterpart Equations 1.36 and 1.38 multiplied by *ds*. This provides two equations that have partial derivative terms with respect to both *s* and *t*. By noting that the total derivative is defined as

$$df(s,t) = \frac{\partial f}{\partial s} ds + \frac{\partial f}{\partial t} dt \tag{2.18}$$

the partial derivative terms of these two equations can be combined (this process involves some simple but lengthy equations and will thus not be included here). Replacing the *ds*/*dt* term with the characteristic root of Equation 2.17, this provides two equations with no partial derivatives:

$$dU + d\phi\left[\pm\sqrt{\frac{T}{\mu}}\cos\theta - V\cos\theta - W\sin\theta\right] - \frac{dt}{\mu}(F_X + W_t\cos\phi) = 0 \qquad 2.19$$

$$dW + d\theta\left[V \mp \sqrt{\frac{T}{\mu}}\right] - U\sin\theta d\phi - \frac{dt}{\mu}(W_t\sin\phi\sin\theta + F_Z) = 0 \qquad 2.20$$

These equations are the total derivatives in the characteristic directions. It should be noted that the parabolic equations, had they been attempted to be converted in this manner, would have remaining partial derivative terms and would thus have no benefit in converting their form.

By taking the derivative of these equations with respect to the characteristic directions, one finds the characteristic equations that can be used for integration:

$$\frac{dU}{d\alpha} + \frac{d\phi}{d\alpha}\left[F_\alpha\cos\theta - V\cos\theta - W\sin\theta\right] - \frac{dt}{d\alpha}\frac{1}{\mu}(F_X + W_t\cos\phi) = 0 \qquad \mathbf{2.21}$$

$$\frac{dU}{d\beta} + \frac{d\phi}{d\beta}\left[F_\beta\cos\theta - V\cos\theta - W\sin\theta\right] - \frac{dt}{d\beta}\frac{1}{\mu}(F_X + W_t\cos\phi) = 0 \qquad \mathbf{2.22}$$

$$\frac{dW}{d\alpha} + \frac{d\theta}{d\alpha}\left[V - F_\alpha\right] - U\sin\theta\frac{d\phi}{d\alpha} - \frac{dt}{d\alpha}\frac{1}{\mu}(W_t\sin\phi\sin\theta + F_Z) = 0 \qquad \mathbf{2.23}$$

$$\frac{dW}{d\beta} + \frac{d\theta}{d\beta}\left[V - F_\beta\right] - U\sin\theta\frac{d\phi}{d\beta} - \frac{dt}{d\beta}\frac{1}{\mu}(W_t\sin\phi\sin\theta + F_Z) = 0 \qquad \mathbf{2.24}$$

It should be noted that α and β are the characteristic directions in the *z-y* plane, but since the characteristic roots are repeated, these changes are the same in both the *z-y* and the *x-y* planes (Schram and Reyle, 1968:218).

3.3. Numerical Methods

Setting up the Mesh and the Characteristic Equations.

As mentioned in Section 2.6, the numerical method used in this paper is one developed by Courant, Isaacson, and Rees, presented in Ames (Ames, 1965: 446), and applied to this type of problem by Schram and Reyle (Schram and Reyle, 1968:218). This technique uses a preset space-time mesh in order to reduce the amount of calculations required. As a result, the mesh size must be sufficiently small enough to ensure straight characteristic lines between timesteps.

Using this understanding as background, one may rewrite Equations 2.21 through 2.24 into a set of simplified characteristic ODE's

$$dU + G_\alpha d\phi + H_\alpha dt = 0 \tag{3.1}$$

$$dU + G_\beta d\phi + H_\beta dt = 0 \tag{3.2}$$

$$dW + J_\alpha d\theta + K_\alpha d\phi + L_\alpha dt = 0 \tag{3.3}$$

$$dW + J_\beta d\theta + K_\beta d\phi + L_\beta dt = 0 \tag{3.4}$$

where the coefficients are defined as

$$G_\alpha = W \sin\theta - V \cos\theta + F_\alpha \cos\theta \tag{3.5}$$

$$G_\beta = W \sin\theta - V \cos\theta + F_\beta \cos\theta \tag{3.6}$$

$$J_\alpha = V - F_\alpha \tag{3.7}$$

$$J_\beta = V - F_\beta \tag{3.8}$$

$$K_\alpha = -U \sin\theta \tag{3.9}$$

$$K_\beta = -U \sin\theta \tag{3.10}$$

$$H_\alpha = \frac{1}{\mu}(-F_X - W_t \cos\phi) \tag{3.11}$$

$$L_\alpha = \frac{1}{\mu}\left(-F_Z - W_t \sin\phi \sin\theta\right) \tag{3.12}$$

For the towline, the following coefficients are defined as

$$H_\beta = \frac{1}{\mu}(-F_X - W_t \cos\phi) \tag{3.13}$$

$$L_\beta = \frac{1}{\mu}\left(-F_Z - W_t \sin\phi \sin\theta\right) \tag{3.14}$$

At the body, however, these are defined as

$$H_\beta = \frac{1}{Mb}(-F_X - Wb \cos\phi) \tag{3.15}$$

$$L_\beta = \frac{1}{Mb}\left(-F_Z - Wb \sin\phi \sin\theta\right) \tag{3.16}$$

where the forces are calculated on the body, noting that only the β characteristic lines affect the lower boundary, and of these β characteristic parameters, only the force terms become different (thus only two terms need to be changed). It should also be noted that the characteristic root changes at the lower boundary, thus,

$$F_\beta = -\sqrt{\frac{T}{Mb}} \tag{3.17}$$

at the towed body.

These equations are applied to every point down the towline, in order to "march" the data to the next timestep. This is represented in Figure 3.3-1. Points *a*, *b*, and *c* are points along the towline where data is known. Points *p* and *q* are set by the F_α and F_β characteristic lines by noting that these lines are defined as *ds*/*dt*. Thus, *ds*, which is the

distance along the *s*-axis between both *q* and *b* as well as *b* and *p*, can be defined as either $|F_\alpha|\mathrm{d}t$ or $|F_\beta|\mathrm{d}t$.

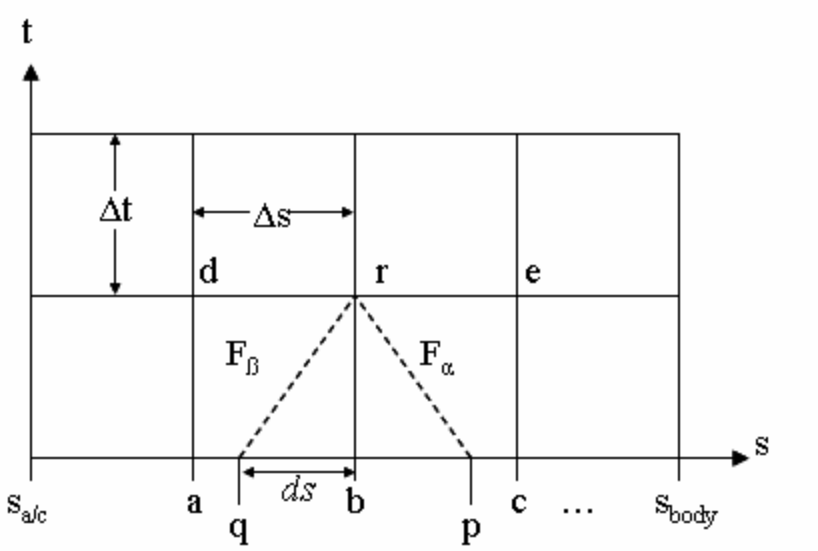

Figure 3.3-1 Character Mesh with Characteristic Lines

The data associated with the points *p* and *q* can be found by interpolating between the known data points (*a*, *b*, and *c*) in the following manner:

$$f(q) = \frac{1}{\Delta s}\left[f(a)ds + f(b)(\Delta s - ds)\right] \qquad 3.18$$

$$f(p) = \frac{1}{\Delta s}\left[f(c)ds + f(b)(\Delta s - ds)\right] \qquad 3.19$$

where *f*( ) refers to any type of data stored at the respective points (i.e., velocity).

As can be seen in Figure 3.3-1, the stability of the preset mesh is restricted by the points *p* and *q* being between *a* and *c*. The maximum values of the characteristic lines are thus limited in this mesh to $\Delta t/\Delta s$. These values force *q* to line up with *a*, and *p* to line up with *c*. In other words, the stability of this system is restricted by

$$\left|F_\alpha\right|\frac{\Delta t}{\Delta s} \le 1 \qquad 3.20$$

$$\left|F_\beta\right|\frac{\Delta t}{\Delta s} \le 1 \qquad 3.21$$

which forces *ds* to not go beyond Δs. Thus the mesh remains stable.

This setup produces two sets of equations (one from each characteristic line) for every point in time and space for all data (i.e., velocity) except at the boundary conditions, which only have one characteristic line at each end (the upper boundary condition only uses F_α and the lower boundary condition only uses F_β). By going back and writing the characteristic equations (Equations 3.1 through 3.4) in difference notation form, the equations for numerical integration along the line are completed. It should be noted that all the coefficient variables (Equations 3.5 through 3.16) are evaluated at point *b* on the mesh, which Ames notes as well (Ames, 1965:447).

Characteristic Equations:

$$U_r - U_p + G_\alpha(\phi_r - \phi_p) + H_\alpha dt = 0 \qquad \textbf{3.22}$$

$$U_r - U_q + G_\beta(\phi_r - \phi_q) + H_\beta dt = 0 \qquad \textbf{3.23}$$

$$W_r - W_p + J_\alpha(\theta_r - \theta_p) + K_\alpha(\phi_r - \phi_p) + L_\alpha dt = 0 \qquad \textbf{3.24}$$

$$W_r - W_q + J_\beta(\theta_r - \theta_q) + K_\beta(\phi_r - \phi_q) + L_\beta dt = 0 \qquad \textbf{3.25}$$

These equations can be combined in order to solve for the four unknowns: U_r, W_r, ϕ_r, and θ_r.

Since the two parabolic equations (Equations 1.28 and 1.37) were not transformed by the method of characteristics, these must be directly translated here into difference notation so that they can be used. Schram and Reyle use a central differencing technique in order to ensure a more accurate result (Schram and Reyle, 1968:219), nothing that Equation 3.26 is a central differencing about an averaged value (halfway between *e* and *r*).

Parabolic Equations:

$$V_e - V_r = \left(\frac{W_e + W_r}{2}\right)(\theta_e - \theta_r) - \left(\frac{U_e + U_r}{2}\right)\cos\left(\frac{\theta_e + \theta_r}{2}\right)(\phi_e - \phi_r) \qquad \textbf{3.26}$$

$$T_d - T_e = \delta s\left[\frac{\mu}{\delta t}\left[(V_r - V_b) - W_r(\theta_r - \theta_b) + U_r\cos\theta_r(\phi_r - \phi_b)\right] - F_{Y,r} + W_t\sin\phi_r\cos\theta_r\right] \qquad \textbf{3.27}$$

where δs is the distance between the two points, which becomes $2\Delta s$ here, and δt is the distance between time steps, which becomes Δt.

These equations must be applied after the characteristic equations have been used to find the values down the entire line. The boundary conditions (discussed later) must be defined at the upper boundary in advance for Equation 3.26. This equation can then be used for all values including the lower boundary (a different equation will be used later, however). The boundary conditions must also be defined at the lower end in advance for *T* since it is to be found starting at the towed body and calculated back up the towline to the aircraft (see Figure 3.5-1 at the end of this chapter). Since the central differencing technique of Equation 3.28 cannot be applied at the first point up the towline from the lower boundary, a forward differencing scheme is used instead (Schram and Reyle, 1968:219).

$$T_d - T_L = \delta s\left[\frac{\mu}{\delta t}\left[(V_d - V_a) - W_d(\theta_d - \theta_a) + U_d\cos\theta_d(\phi_d - \phi_a)\right] - F_{Y,d} + W_t\sin\phi_d\cos\theta_d\right] \qquad \textbf{3.28}$$

where δs is Δs and δt is Δt.

This produces a set of six equations (plus a seventh, but only due to the issue of central differencing) that can describe the behavior down the entire line except for at the boundaries. The boundary conditions for the mesh used here exist at $s = s_{a/c}$ and $s = s_{body}$.

In addition, the initial conditions at $t = 0$ must be known before any kind of stepping technique is used.

Initial Conditions.

The initial conditions are determined by prior research using MATLAB® code to develop a steady state solution (Richardson, 2005:Appendix A). The method by which this code was developed is discussed in Section 2.1. Another way to set the initial conditions is by setting the angles of the towline and its velocities in all three axes manually. The tension can be found up the entire line by calculating the body and towline forces (shown later) from the known angles and velocities.

Boundary Conditions.

In order to find the values at the upper and lower boundaries, new equations must be developed to work with the characteristic lines. This is due to the fact that there must be two equations for every point in order to determine the values at that point. The characteristic lines carry data to the boundary conditions as can be seen for the upper boundary conditions in Figure 3.3-2.

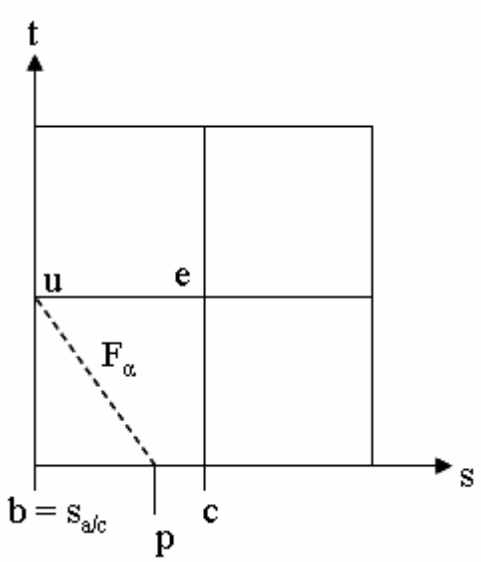

Figure 3.3-2 Characteristic Line to find upper BC data

Since it is assumed that the towline at the point where it connects to the aircraft has the same motion as the aircraft, the new equations for the upper boundary conditions in towline form become the transformation of coordinates from Equation 1.6. Thus, the upper boundary conditions can be described by:

$$\left[\vec{V}\right]_u = [A][\vec{v}]_u \qquad 3.29$$

where $\left[\vec{V}\right]_u$ refers to the velocity matrix in towline coordinates at the upper limit (i.e., the aircraft), and $[\vec{v}]_u$ refers to the velocity matrix in spatial coordinates at the upper limit. By multiplying through, the upper boundary equations are found:

Upper Boundary Conditions:

$$U_u = u_u \sin\phi_u - v_u \cos\phi_u \qquad \mathbf{3.30}$$

$$V_u = u_u \cos\theta_u \cos\phi_u + v_u \cos\theta_u \sin\phi_u + w_u \sin\theta_u \qquad \mathbf{3.31}$$

$$W_u = -u_u \sin\theta_u \cos\phi_u - v_u \sin\theta_u \sin\phi_u + w_u \cos\theta_u \qquad \mathbf{3.32}$$

Equation 3.22

Equation 3.24

The equations are all combined to find the values at the upper boundary: U_u, V_u, W_u, ϕ_u, and θ_u (T_u will be found later by 3.27). Schram and Reyle (Schram and Reyle, 1968:219) note that an iterative procedure must be used to find ϕ_u and θ_u such that these equations are satisfied.

The lower boundary conditions become a little trickier. However, a few assumptions can be made that simplify the process. The characteristic line used at the lower boundary can be seen in Figure 3.3-3.

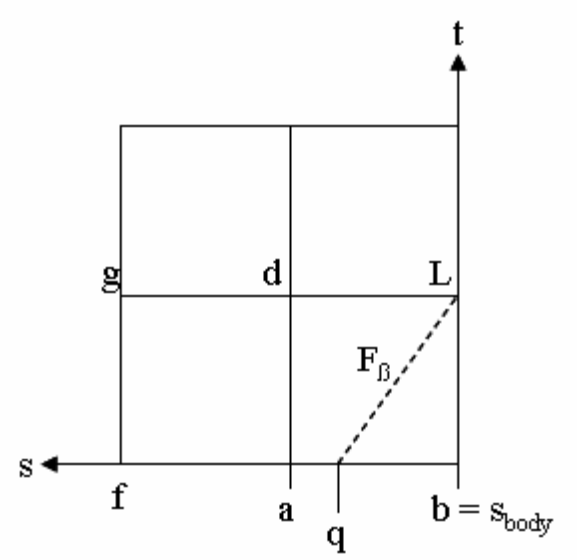

Figure 3.3-3 Characteristic Line to find lower BC data

With the assumption that the towline at the towed body has the same motion as the body, one can develop the lower boundary conditions. This requires a little understanding of the geometry. For the sake of simplicity, the body will be assumed to be rigid, small, and always parallel to the freestream direction, thus producing negligible moment effects. In other words, the body will be assumed to be reducible to a point mass in how its behavior transfers to the towline.

By taking Equations 1.36, 1.37, and 1.38 and writing them in finite difference form using a central differencing technique about point *d* in Figure 3.3-3, one finds three equations of motion at the lower boundary:

$$U_L = U_g + \frac{\delta s}{\delta t}(\phi_L - \phi_b)\cos\theta_d + (V_d \cos\theta_d - W_d \sin\theta_d)(\phi_L - \phi_g) \quad \textbf{3.33}$$

$$V_L = V_g - U_d \cos\theta_d(\phi_L - \phi_g) + W_d(\theta_L - \theta_g) \quad \textbf{3.34}$$

$$W_L = W_g - \frac{\delta s}{\delta t}(\theta_L - \theta_b) - V_d(\theta_L - \theta_g) + U_d \sin\theta_d(\phi_L - \phi_g) \quad \textbf{3.35}$$

Central differencing is used due to the fact that forward differencing creates a set of five nonlinear equations that have no exact symbolic solution. Central differencing prevents the need for using iteration to solve the system for a best value. It should be noted that due to this setup, δs is set to twice the Δs value. Thus, $\frac{\delta s}{\delta t} = 2\frac{\Delta s}{\Delta t}$.

Combining these three equations with Equations 3.23 and 3.25, five equations have now been determined for the lower boundary, which contain five unknown variables. ϕ_L can be determined explicitly and θ_L becomes a function of only ϕ_L from these equations by first creating two new equations. This is found by rewriting Equations 3.23 and 3.25 in difference notation at the lower boundary:

$$U_L = U_q - G_\alpha(\phi_L - \phi_p) - H_\alpha dt \quad 3.36$$

$$W_L = W_q - J_\beta(\theta_L - \theta_p) - K_\beta(\phi_L - \phi_q) - L_\beta dt \quad 3.37$$

These two equations are then combined with Equations 3.33 and 3.35 respectively to form two new equations, the first dependent solely on ϕ_L and the second on both θ_L and ϕ_L:

$$U_g + \frac{\delta s}{\delta t}(\phi_L - \phi_b)\cos\theta_d + (V_d \cos\theta_d - W_d \sin\theta_d)(\phi_L - \phi_g) - U_q + G_\beta(\phi_L - \phi_q) + H_\beta dt = 0 \quad 3.38$$

$$W_g - \frac{\delta s}{\delta t}(\theta_L - \theta_b) - V_d(\theta_L - \theta_g) + U_d \sin\theta_d(\phi_L - \phi_g) - W_q + J_\beta(\theta_L - \theta_q) + K_\beta(\phi_L - \phi_q) + L_\beta dt = 0 \quad 3.39$$

As can be seen, the only unknown in Equation 3.38 is ϕ_L. Thus, the equation can be rearranged to reveal

$$\phi_L = \frac{\frac{\delta s}{\delta t}\phi_b \cos\theta_d + (V_d \cos\theta_d - W_d \sin\theta_d)\phi_g - U_g - H_\beta dt + U_q + G_\beta \phi_q}{G_\beta + V_d \cos\theta_d - W_d \sin\theta_d + \frac{\delta s}{\delta t}\cos\theta_d} \quad \mathbf{3.40}$$

Similarly, Equation 3.39 can be rearranged to reveal

$$\theta_L = \frac{W_g + \frac{\delta s}{\delta t}\theta_b + V_d\theta_g + U_d \sin\theta_d(\phi_L - \phi_g) - W_q - J_\beta\theta_q + K_\beta(\phi_L - \phi_q) + L_\beta dt}{\frac{\delta s}{\delta t} + V_d - J_\beta} \quad \mathbf{3.41}$$

By solving for these two values, the values for U_L, V_L, and W_L can now be solved.

Thus, the lower boundary conditions are defined by the following equations, noting that values for U_L and W_L can be solved by two different equations and that

Equations 3.40 and 3.41 must be solved first:

Lower Boundary Conditions:

Equation 3.40

Equation 3.41

Equation 3.36 or 3.33

Equation 3.37 or 3.35

Equation 3.34

The values for U_L, V_L, W_L, ϕ_L, and θ_L have been determined. These new values are, then, used to solve for tension.

Body Forces.

The forces on the body must be found in order to model the towline's movement and tension. This is best done by finding a coordinate system aligned with the body. Since the body is assumed to be attached to the towline such that it has no rotation, the body axes become the towline axes at attachment. Schram developed a manner in which to analyze rotation in the body (Schram, 1968:119-120) using Euler angles, which will not be used or discussed here. His method becomes quite rigorous, and the assumptions here involve negligible moment effects (thus no angular acceleration is included). A manner in which to account for angular acceleration is included in Appendix A. The body orientation is represented in Figure 3.3-4 and Figure 3.3-5. Again, it should be noted that θ is in a unique plane set by ϕ, and could be coming in or out of the page.

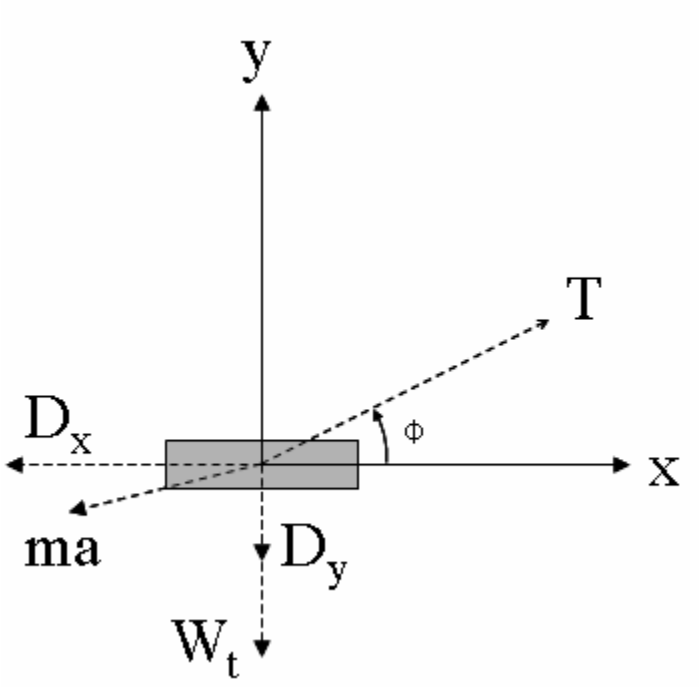

Figure 3.3-4 Towed Body Force Components (x-y axis)

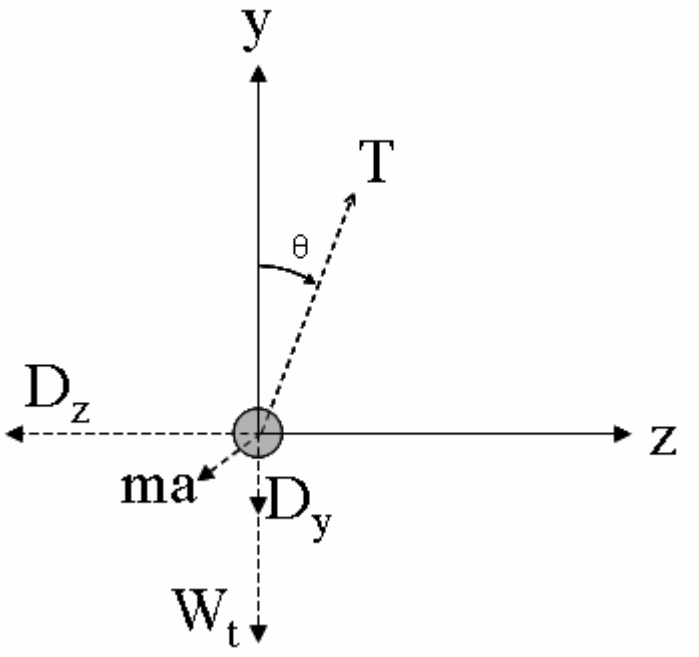

Figure 3.3-5 Towed Body Force Components (z-y axis)

To calculate the forces in each axis, the drag components must first be found. Since it is assumed that the body is always aligned with the freestream flow, drag is always acting along the body, which allows for the use of a single drag coefficient. The values will be calculated in the spatial coordinate system, since weight will have to be added later. The spatial velocities can be found from the towline velocities at the lower boundary by the transformation of Equation 1.7. Noting that the total drag force as a function of components is defined as $D_{TOT}^2 = D_X^2 + D_Y^2 + D_Z^2$, and velocity must be decomposed based on these forces,

$$D_x = \frac{1}{2}\rho \vec{V}_L u_L C_{D,B} \frac{d_B{}^2 \pi}{4} = -F_x \tag{3.42}$$

$$D_y = \frac{1}{2}\rho \vec{V}_L v_L C_{D,B} \frac{d_B{}^2 \pi}{4} = -F_y \tag{3.43}$$

$$D_z = \frac{1}{2}\rho \vec{V}_L w_L C_{D,B} \frac{d_B{}^2 \pi}{4} = -F_z \tag{3.44}$$

where

$$\vec{V}_L = \sqrt{u_L{}^2 + v_L{}^2 + w_L{}^2} \tag{3.45}$$

Note that the negative sign on the force terms is due to their orientation being in the positive direction in each axis. Since drag acts the same direction as airflow, these force terms must have a negative sign.

It is assumed that there is no lift on the body. A lift force can be easily added into the equations, although it will not be done here. The aerodynamic force terms are therefore the drag terms and were put into the above equations for consistency with prior equations (3.15, 3.16).

Additional forces based on the body's acceleration must by found by Newton's Second Law (Equation 1.8). The acceleration can be found through the use of a backward differencing method outlined in Tannehill, Anderson, and Pletcher (Tannehill, Anderson, and Pletcher, 1997:50)

$$\dot{u} = \frac{3u(t) - 4u(t-1) + u(t-2)}{2dt} + O(dt^2) \tag{3.46}$$

as well as a simple backward differencing method

$$\dot{u} = \frac{u(t) - u(t-1)}{dt} + O(dt) \tag{3.47}$$

for the first timestep. The more complex method is used in order to reduce truncation errors, which are one order higher than the simpler method.

Thus, the force terms due to inertia for all three axes become:

$$F_{accel,x} = \dot{u}_L Mb \tag{3.48}$$

$$F_{accel,y} = \dot{v}_L Mb \tag{3.49}$$

$$F_{accel,z} = \dot{w}_L Mb \tag{3.50}$$

It should be noted that, due to Newton's Third Law, these forces act away from the aircraft. In other words, a positive acceleration creates a negative force. Also of important mention is the fact there can be no compressive forces in the line. Thus, any acceleration that would theoretically compress the line cannot be factored into the forces for tension. Since compression is impossible, the acceleration has no effect on tension. This produces abnormal results in the code, thus the mass and drag coefficient must be monitored.

These forces can all be summed up to determine the total forces on the body (not including tension), noting that the drag acts in the same direction as airflow, the

acceleration is oriented away from the aircraft, and the force due to weight must be added to the *y*-axis term:

$$TF_x = -\dot{u}_L Mb - \frac{1}{2}\rho \vec{V}_L u_L C_{D,B} \frac{{d_B}^2 \pi}{4} \tag{3.51}$$

$$TF_y = -\dot{v}_L Mb - \frac{1}{2}\rho \vec{V}_L v_L C_{D,B} \frac{{d_B}^2 \pi}{4} - Wb \tag{3.52}$$

$$TF_z = -\dot{w}_L Mb - \frac{1}{2}\rho \vec{V}_L w_L C_{D,B} \frac{{d_B}^2 \pi}{4} \tag{3.53}$$

The tension acts purely in the towline *Y*-axis, and since the angles were found for the lower boundary, the transformation of Equation 1.6 can be applied. This yields:

$$T_L = -\left(TF_x \cos\phi \cos\theta + TF_y \sin\phi \cos\theta + TF_z \sin\theta\right) \tag{3.54}$$

where the negative sign is due to the tension being opposite the direction of total force such that the sum of all forces in the *Y*-axis is zero. Thus, T_L is found at the lower end, and can be calculated back up the towline by the use of Equations 3.27 and 3.28, noting the towline forces derived in the next section.

Towline Forces.

The towline forces (circular towline with no rotation) can be calculated in a similar manner. The drag forces on the towline are modeled in Figure 3.3-7 and Figure 3.5-1.

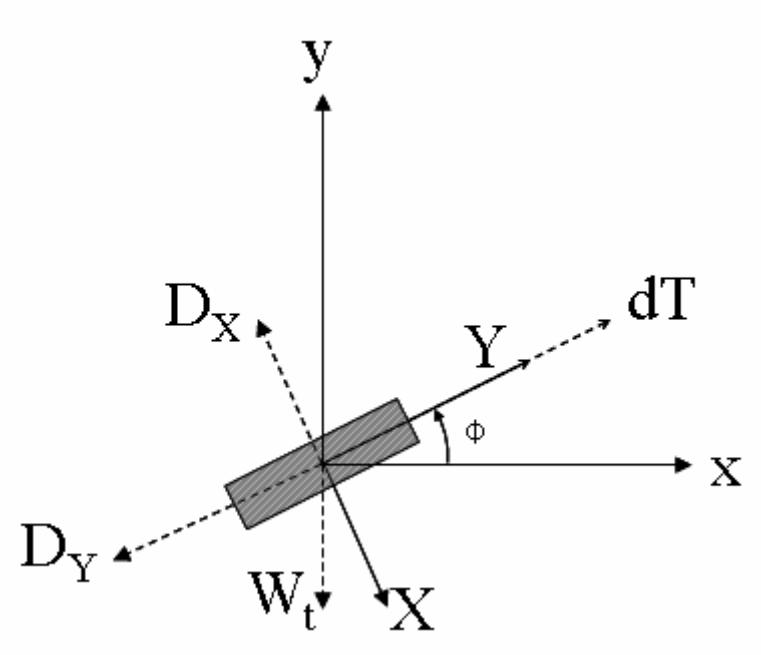

Figure 3.3-6 Towline Force Components (x-y plane)

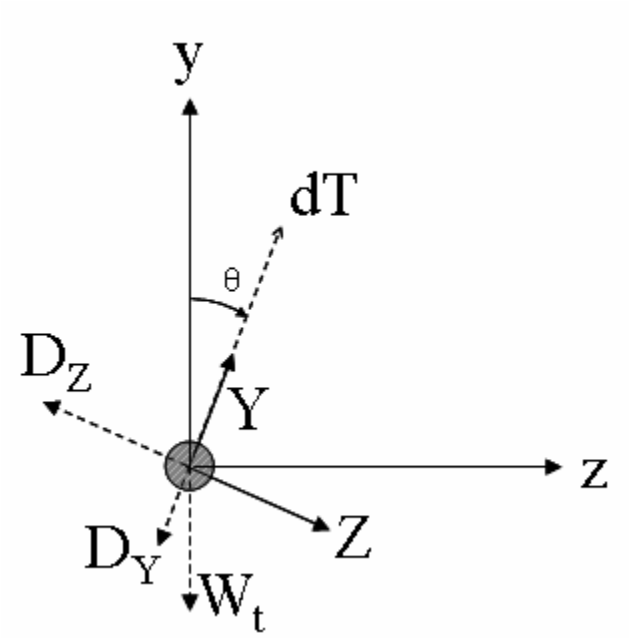

Figure 3.3-7 Towline Force Components (z-y plane)

One major difference, however, is that the towline is not considered to be facing the freestream velocity. Although drag is to be considered a total force (i.e., it must first be determined based on total velocity before decomposition into axial components),

Richardson notes that the drag on a cylinder (i.e., the towline) can be effectively decomposed into perpendicular and parallel components. By noting the assumption of zero drag parallel to the towline, the total drag can be represented as

$$D_{Towline} = \frac{1}{2}\rho d_B \vec{V}_{perp}{}^2 \left(C_{D,TL} + C_{D,TL,sf} \right) \tag{3.55}$$

where $C_{D,TL,sf}$ is the skin friction drag coefficient set at 0.04 (Richardson, 2005:20), $C_{D,TL}$ is the perpendicular drag coefficient (set at 1.1 for this paper) acting in both the *X* and *Z* axes, and drag force is per unit length (i.e., per meter). Also:

$$\vec{V}_{perp} = \sqrt{U^2 + W^2} \tag{3.56}$$

These forces can be decomposed into their respective axial forces by noting that the parallel force acts purely in the *Y*-axis, and the perpendicular force acts in the *X*-*Z* plane. Drag forces are decomposed for the *X*-*Z* plane by the relationship, $D_{TOT}{}^2 = D_X{}^2 + D_Z{}^2$. Thus,

$$D_X = \frac{1}{2}\rho d_B \vec{V}_{perp} U \left(C_{D,TL} + C_{D,TL,sf} \right) = -F_X \tag{3.57}$$

$$D_Y = 0 = -F_Y \tag{3.58}$$

$$D_Z = \frac{1}{2}\rho d_B \vec{V}_{perp} W \left(C_{D,TL} + C_{D,TL,sf} \right) = -F_Z \tag{3.59}$$

Note again, the force terms are to be in the positive direction, hence their negative sign. Since there are no lift forces, the aerodynamic forces become the drag forces, and can be applied to the previous equations (3.11 through 3.14, 3.27, and 3.28).

3.4. Heat Transfer

The entire system is assumed to be in a predetermined temperature field. Thus, the temperature of the air is known at every point in space and time. In order to determine the heat transfer in the system, an energy equation must be found that relates the rate of internal energy transfer between the air and the towline. The orientation of the control volume at each incremental length of towline is represented in Figure 3.4-1.

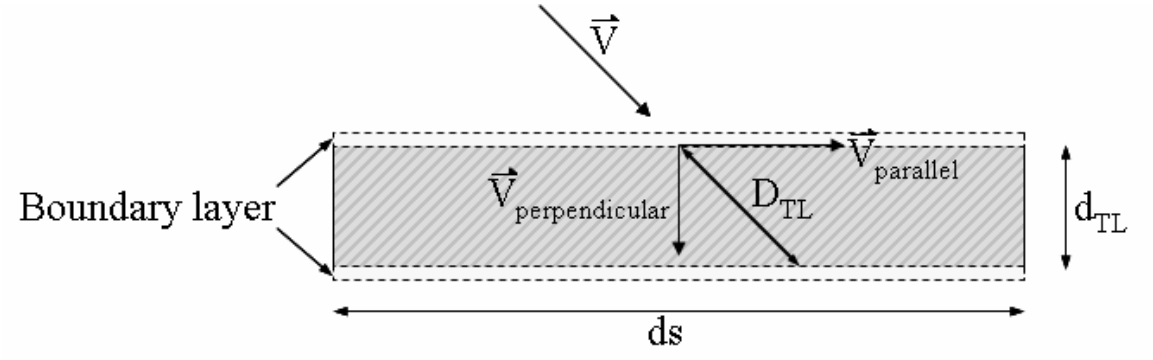

Figure 3.4-1 Airflow Over Towline

Due to conservation of energy, the energy balance equation may be written as

$$\dot{E}_{in} - \dot{E}_{out} + \dot{E}_{generated} - \dot{E}_{stored} = 0 \qquad 4.1$$

where all values are in terms of the rate of internal energy. Since the towline is not generating any energy, this equation becomes

$$\dot{E}_{in} = \dot{E}_{stored} \qquad 4.2$$

assuming there is one dimensional heat transfer from the air to the towline. If it were the other way around, the sign on $\dot{E}_{in}$ would be switched (essentially becoming -$\dot{E}_{out}$), so Equation 4.2 holds true for both heat being transferred to the line and away from it.

To solve for the energy rate into the towline, Newton's law of cooling can be used:

$$\dot{E}_{in} = hA_s(\mathbf{T}_\infty - \mathbf{T}_s) \tag{4.3}$$

where A_s is the total surface area over which the air flows, and h is the convection coefficient. $\mathbf{T}_\infty$ is used here since the heat transfer is between the far field flow and the towline surface ($\mathbf{T}_s$).

Since a thin boundary layer forms about the towline, film temperature will be used to find the properties of the air at the towline's surface. Film temperature is assumed to be the average temperature between the far field and the towline and is defined as

$$\mathbf{T}_f = \frac{\mathbf{T}_\infty - \mathbf{T}_s}{2} \tag{4.4}$$

The convection coefficient can be defined as

$$h = \frac{Nu}{D_{TL}}k \tag{4.5}$$

where Nu is the Nusselt number, k is the thermal conductivity of the air, and D_{TL} is the total distance across the towline (see Figure 3.4-1). The distance across the towline can be defined in the following manner, noting the perpendicular and parallel components of the velocity across the line, which create an angle at which the airflow acts:

$$\vec{V}_{perpendicular} = \sqrt{U^2 + W^2} \tag{4.6}$$

$$\vec{V}_{parallel} = V \tag{4.7}$$

$$FlowAngle = \tan^{-1}\left(\frac{\vec{V}_{perpendicular}}{\vec{V}_{parallel}}\right) \tag{4.8}$$

Thus,

$$D_{TL} = \frac{d_{TL}}{\sin(FlowAngle)} \tag{4.9}$$

for airflow that completely crosses the towline in the perpendicular direction (i.e., it does not completely cross the parallel direction). Otherwise,

$$D_{TL} = \frac{ds}{\cos(FlowAngle)} \tag{4.10}$$

for airflow that completely crosses the towline in the parallel direction. The towline's true diameter (d_{TL}) will be used for now, however, as will be shown later in the discussion of the Nusselt number.

The value for *k* can be calculated directly from the film temperature. This is shown by a power fit to experimental data (personal communication, Ralph Anthenien) as

$$k = (0.0002235)\mathbf{T}_f^{\,0.8302} \tag{4.11}$$

where $\mathbf{T}_f$ is in Kelvin.

The Nusselt number is calculated experimentally. Currently, an approximation for the Nusselt number could not be found for a cylinder with different angles to the freestream. Also, the boundary layer cannot be assumed to be very small down the towline (boundary layer thickness increases along the towline), which will affect heat transfer. Thus, only the perpendicular component of heat transfer will be calculated as if the only flow across the towline is perpendicular (i.e., thin boundary layer assumption), leaving a better Nusselt number approximation for future work. This is consistent with the rest of the paper, which assumes no drag parallel to the towline. Thus, the D_{TL} term in Equation 4.5 becomes d_{TL}. For perpendicular flow across a cylinder, *Nu* for Reynolds

numbers within the range $1 < Re_D < 10^4$ is shown by Kramer as reproduced in White (White, 1991:186) as

$$Nu = 0.42Pr^{0.2} + 0.57Pr^{1/3}\sqrt{Re_D} \tag{4.12}$$

This formula was determined from a curve fit of experimental data. *Pr* is the Prandtl number, assumed to be ~0.7 for air in the range of ~275–850 Kelvin. The Prandtl number changes very little as a function of temperature, and this approximation could be applied to even a greater range of temperatures. The Reynolds number is calculated by

$$Re_D = \frac{\vec{V}_{perpendicular} d_{TL}}{\nu} \tag{4.13}$$

where ν is the kinematic viscosity, which can calculated directly by a fit to experimental data (personal communication, Ralph Anthenien) based on the film temperature:

$$\nu = 8 \text{ x } 10^{-10} \mathbf{T}_f^{\,1.7235} \tag{4.14}$$

where $\mathbf{T}_f$ is again in Kelvin. Future development of a Nusselt number approximation that accounts for parallel flow will also have to develop a new Reynolds number approximation as well, assuming that *Nu=f*(*Re*).

In order to determine the stored energy in the towline, specific heat is used. Specific heat is defined as the amount of heat per unit mass required to raise the temperature one degree Kelvin. Since heat can be defined by the change in stored internal energy over the change in temperature, specific heat for the towline is represented as

$$c = \frac{\dot{E}_{stored}}{\rho V_{ol} \dfrac{d\mathbf{T}}{dt}} \tag{4.15}$$

Here, ρ and V_{ol} are the density and volume of the towline respectively, and $d\mathbf{T}/dt$ is the change in temperature over time. The *dt* term comes in because the stored internal energy is a rate as well.

Rearranging this gives the change in energy storage due to the temperature change

$$\dot{E}_{stored} = c\rho V_{ol}\frac{d\mathbf{T}}{dt} \tag{4.16}$$

where the specific heat value used in this analysis was an approximate value for steel of 450 J/kg-K. Combining Equations 4.2, 4.3, and 4.16 yields the energy equation at the surface of the towline

$$hA_s(\mathbf{T}_f - \mathbf{T}_s) = c\rho V_{ol}\frac{d\mathbf{T}}{dt} \tag{4.17}$$

Thus, temperature can be calculated at any point by knowing the position, velocity, and previous temperature of the towline:

$$\mathbf{T}_{s,t+1} = \mathbf{T}_s + \frac{hA_s(\mathbf{T}_f - \mathbf{T}_s)}{c\rho V_{ol}} \tag{4.18}$$

where $\mathbf{T}_s$ is the temperature at the surface at the current time and $\mathbf{T}_{s,t+1}$ is the new surface temperature at the new time.

A new film temperature can then be calculated based on the new surface temperature value through the use of Equation 4.4. This is used to calculate the air density in the boundary layer around the towline, which is used in turn to find the forces on the towline. Density can be calculated by fit to experimental data in SI units (personal communication, Ralph Anthenien) as

$$\rho = (357.88)\mathbf{T}_f^{-1.0041} \tag{4.19}$$

where it should again be noted that temperature is in Kelvin.

3.5. Integration Procedure

Enough equations have now been derived to model the behavior of the towline and body, as well as the heat transfer to the towline, at all points in time and space. These equations were written into MATLAB® code following the numerical integration procedure as can be seen in Figure 3.5-1. The code is attached in Appendices A through D.

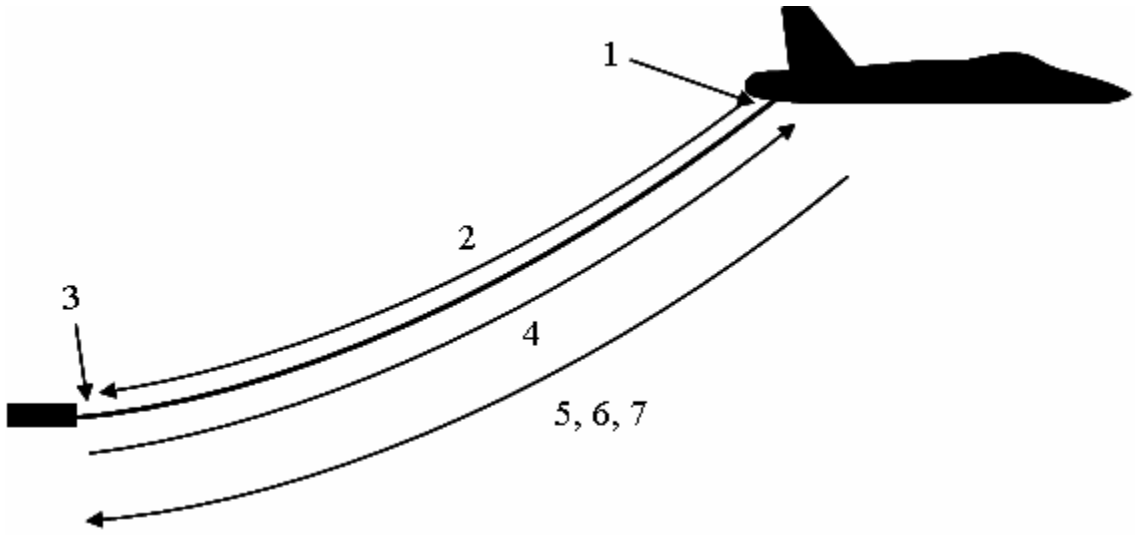

1. Find upper boundary conditions (U,V,W,Θ,Φ) from previous time and current a/c velocity (u,v,w).
2. Calculate Φ,U,Θ, and W down entire line from previous time, then find V from these values.
3. Find Θ explicitly at lower boundary from previous time and values one step up line, then find Φ,U,V, and W.
4. Calculate T at lower boundary from forces on the body, then find T up entire line and at upper boundary.
5. Find x,y,z spatial positions along line.
6. Find temperature and density at every point along line.
7. Go to next timestep.

Figure 3.5-1 Numerical Integration Procedure

IV: Results and Discussion

The MATLAB® code was written such that a change in initial conditions and system values could be easily altered. The behavior of the towline was initially modeled with the aircraft under a constant speed with the towline extended directly back behind the aircraft at a constant angle down the line of 0.01 (a zero angle gives a negative tension error almost immediately). These results were compared to the steady state values from Richardson. This same procedure was also applied using the initial conditions from Richardson to test for constant values under steady state. The system was then modeled under different perturbations, starting with the constant angle position of the towline from above. Lastly, the heat transfer to the towline was modeled under a steady state position over time. Due to the dynamic behavior of the code, and since no specific situations were under investigation, the general behavior of the towline is represented.

Although not shown in this paper (due to the difficulty of showing dynamic behavior in printed material), the towline can also be modeled as a pendulum at near zero velocity (zero velocity causes a slack condition). This representation reveals a damped oscillation about a hanging position, with curvature in the line as the body gets farther from its final steady state. This test, which was used to test the MATLAB® code for reasonable response, is an easy way to show that the methods used work.

4.1. Initial Conditions

The initial conditions for the towline parameters and step sizes for a towline length of 30 meters were set as follows:

$$ds = 5\ m$$
$$dt = .01\ s$$
$$d_{TL} = .00127\ m$$
$$\mu = .0096\ \frac{kg}{m}$$
$$C_{D,TL} = 1.1$$
$$C_{D,TL,sf} = .04$$
$$C_{D,B} = 1$$
$$d_B = .496\ \text{m}$$
$$Mb = 1\ \text{kg}$$

where most of these values were taken from previous work by Richardson. The value for towline mass per unit length (μ) is based on an approximated average density for most steels of ~7600 kg/m^3, and is a function of both density and diameter (d_{TL}). Schram and Reyle indicated (Schram and Reyle, 1968:218) that the value of *ds/dt* should be around 1000 to get good results and ensure stability for small perturbations. The values used here seemed to be stable for most cases, however. Greater changes in velocity may require different values, and the code prints an error statement if either stability cannot be maintained (Equations 3.20 and 3.21), or tension becomes negative.

The code is unable to accommodate negative tension (i.e., compression) in the towline, due to the creation of imaginary numbers in the characteristic directions (Equations 3.20 and 3.21). This is consistent, however, with the assumptions noted by Crist (see Section 2.3) in the fact that the minimum tension a line hanging freely can have is zero. Thus, slack conditions take place at zero tension (tension cannot equal zero in code due to division by zero errors, so slack is assumed to happen at near zero values).

Unfortunately, the code is also currently unable to account for slack conditions. This is because the characteristic lines become zero with zero tension. A line of slope

zero will never be able to transfer data between timesteps (see Figure 3.3-1). Thus, consideration must be made in the towed body's drag and mass, which can be altered to prevent slack. It was found that usually either reducing the mass, or increasing the towed body's drag coefficient or frontal area (i.e., increase the drag) prevented this condition. Although Crist notes that "the effects of slack cable must be included in most analyses" (Crist, 1970:73), the design of many towed bodies are made to prevent slack in the line, and it is assumed that an aircraft in combat will work at high enough speeds such that slack becomes nonexistent. Line slack will create adverse effects such as line jerk that are undesirable anyway. The values for mass and drag are changed in some of the following scenarios to prevent this effect, and any future work should note the restriction on this method.

4.2. Steady State Analysis

Using the steady state values from Richardson's code, the towline behavior should remain relatively stable. If the code was started from a towline hanging position (either back or down, noting an initial nonzero angle must be given for the backward position), the behavior should eventually reach, or maintain (if given initial steady state values), a steady state value close to that from Richardson's code.

Indeed, a steady state value is found that is consistent with that from Richardson. Using the initial values from Richardson, any towline movement is negligible, and a final shape can be seen to directly overlap the one from his code. This is shown in a 50 m/s horizontal velocity simulation plotted in Figure 4.2-1, where the towline was started at Richardson's steady state position.

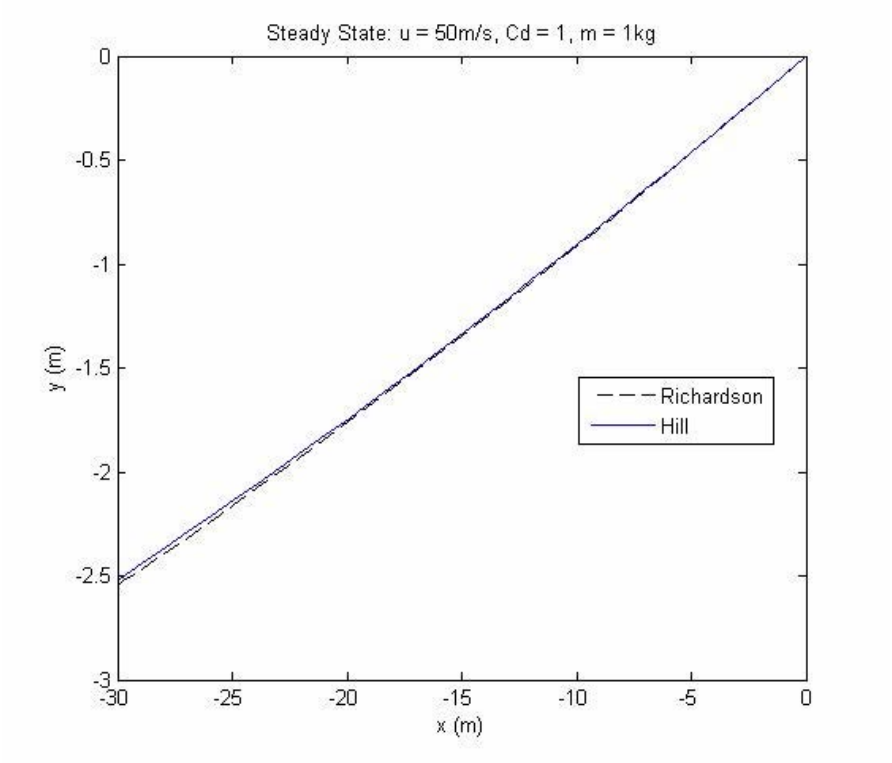

Figure 4.2-1 Steady State Comparison

It should be noted that the mesh spacing was reduced to a *ds* value of 1 meter and a *dt* value of .001 seconds to increase accuracy. Note the very slight difference between the two methods near the towed body. This difference is small enough to be negligible. Any difference is most likely due to the accuracy of the method of characteristics, which is not as accurate as the procedure Richardson used. His work utilized MATLAB®'s *ode45* solver, which is a 4^{th} order Runge-Kutta integration scheme. The method of characteristics for this work used a preset mesh with straight characteristic lines, which is only 1^{st} order accurate. Thus, some small discrepancies may be found between the two procedures. As mentioned, however, these are mostly negligible.

A final shape can be seen by also modeling the hanging position. As mentioned before, the towline was started at a constant angle of $\phi = 0.01$ radians and released. The aircraft was kept at a constant speed of 50 m/s, and the simulation took place over 50

seconds. The results can be shown in Figure 4.2-2 through Figure 4.2-6. The steady state values from Richardson are included on these plots in order to see the oscillations about steady state and model the damped response. The towline eventually reaches the same steady state position as shown previously in Figure 4.2-1. Tension is included in these results to show how it behaves over time. Note that the tension is always less at the body than at the aircraft.

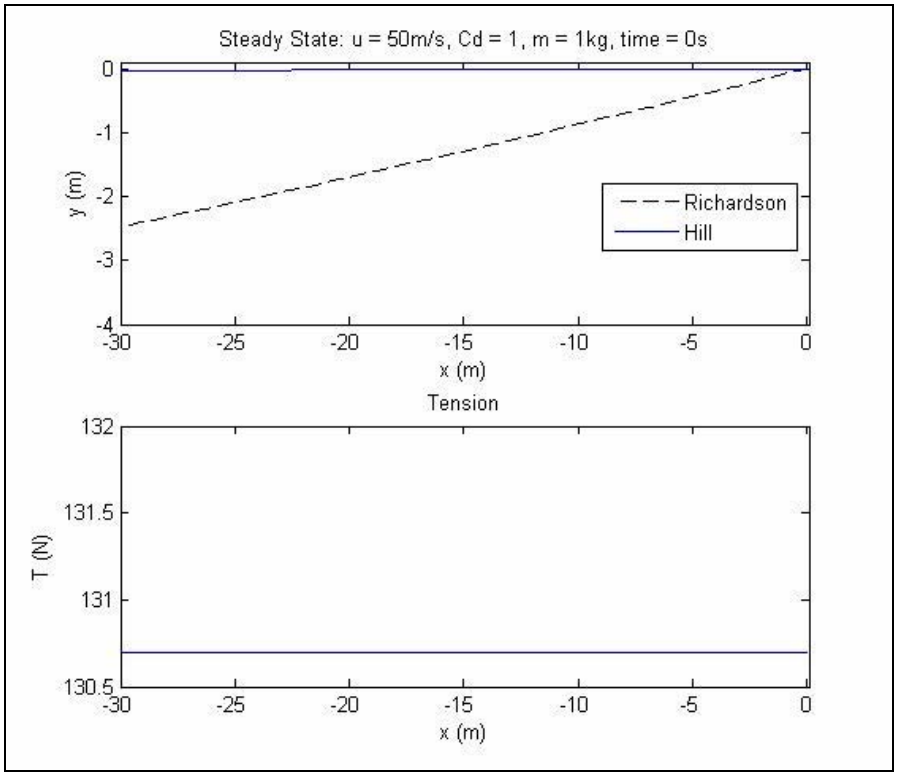

Figure 4.2-2 Steady State Drop t=0s

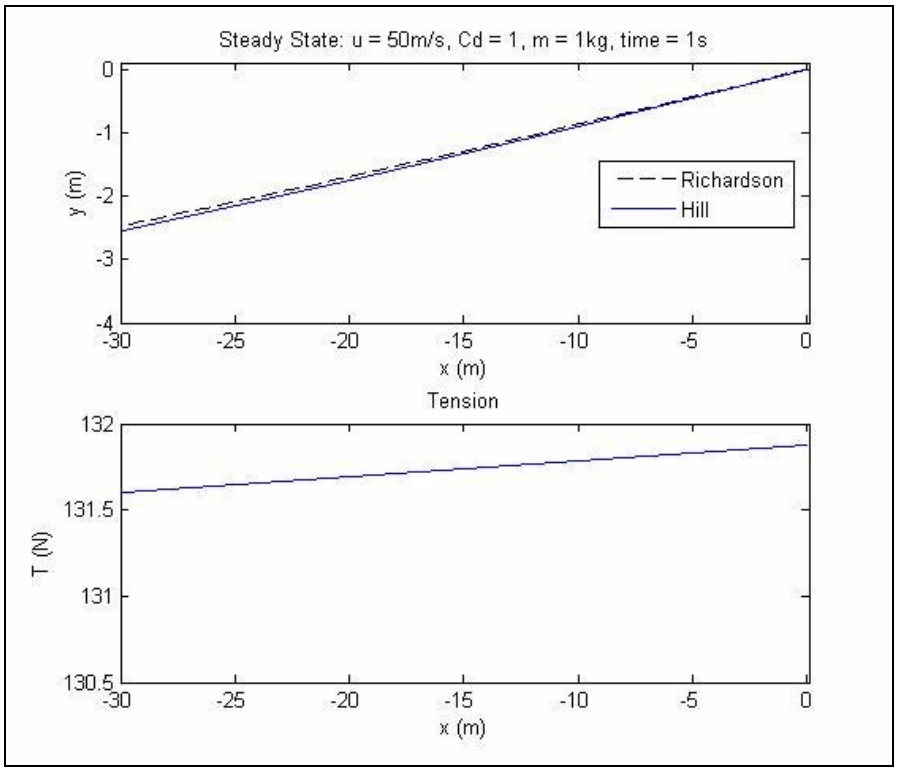

Figure 4.2-3 Steady State Drop t=1s

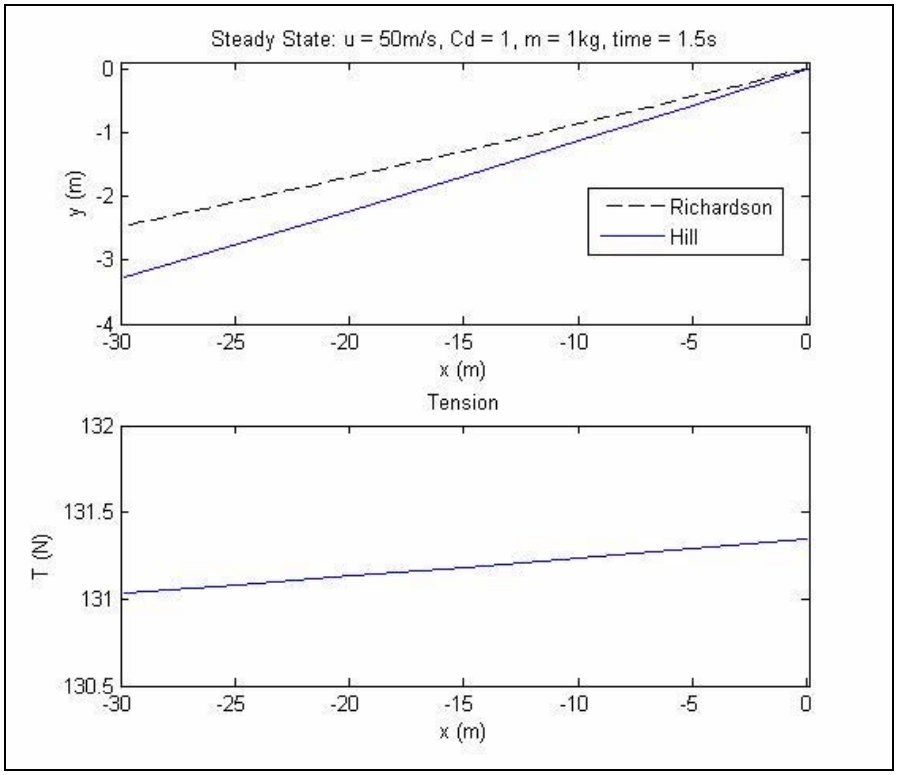

Figure 4.2-4 Steady State Drop t=1.5s

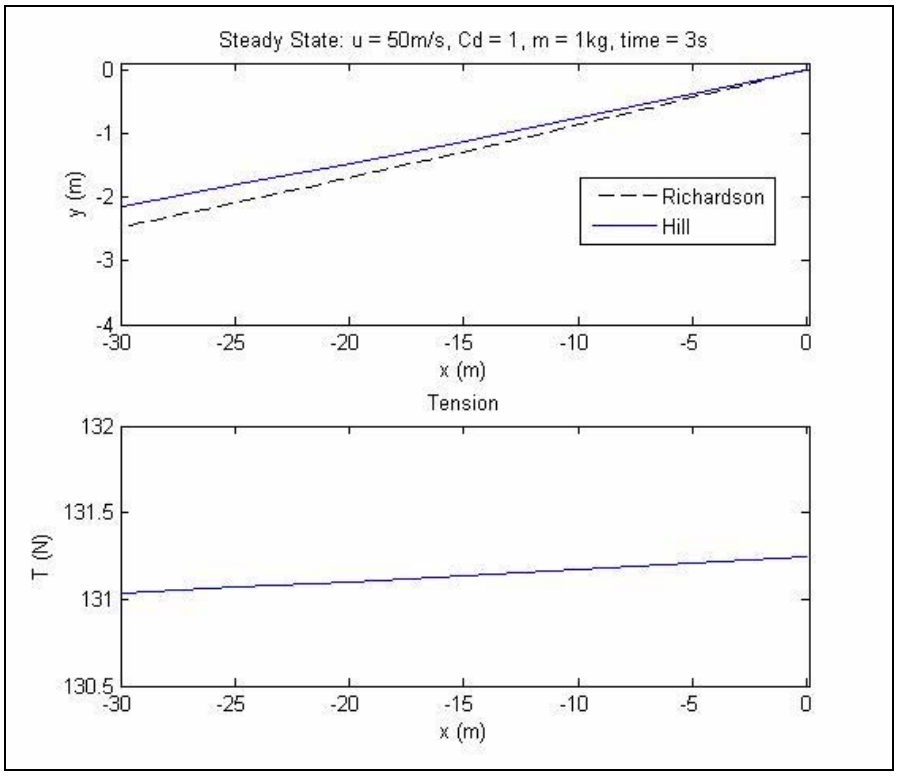

Figure 4.2-5 Steady State Drop t=3s

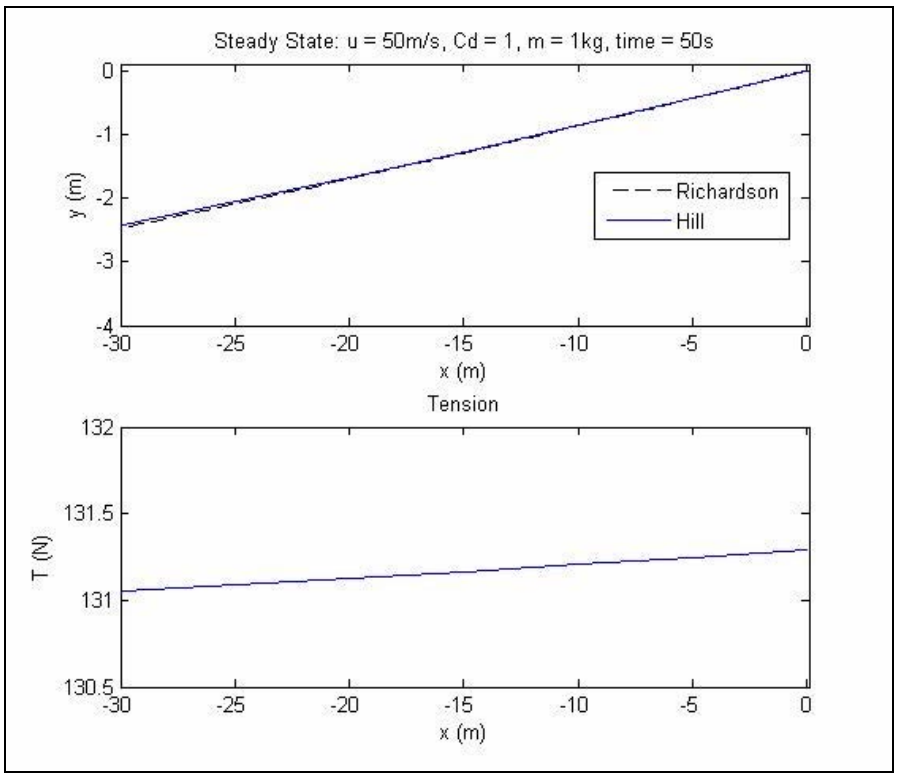

Figure 4.2-6 Steady State Drop t=50s

The towline initially goes down, crossing the steady state value. The tension increases until this value starts to be crossed. At this point, the tension decreases, and the towline starts to slow down. What happens physically during this time is that the drag forces on the line and body start to catch up to the gravitational forces, thus reducing the tension. The towline then goes back up past the steady state value, but not as far. This oscillation happens until a steady state value is reached. This value is very close to that of Richardson, such that the differences are negligible, and is the same shape as that shown in Figure 4.2-1.

4.3. Single Perturbation

The aircraft was set at an initial horizontal velocity of 100 m/s in a similar manner as in the steady state analysis. The reference frame for all of these plots is in the aircraft's initial velocity and direction (100 m/s horizontal velocity, which is to the right in the *x*-*y* plane). A way to visualize this is to think of being in a chase aircraft, traveling at a constant velocity with the initial velocity of the aircraft carrying the towline.

The code is set such that the acceleration is constant over a predetermined period of time. This creates a jerk effect in the tension (not shown here), which could be reduced by ramping the acceleration. Since the jerk is in acceleration, which is the second derivative of position, this has no noticeable effect on how the system behaves in space, and thus is mentioned only as an explanation of how the code works.

Horizontal Perturbation.

The decoy mass was set to 4 kg for this scenario. The first perturbation had the aircraft slow down to 70 m/s over a period of 1 second, then immediately sped back up to

100 m/s over a period of 1 second. The horizontal acceleration is shown in Figure 4.3-1 through Figure 4.3-7.

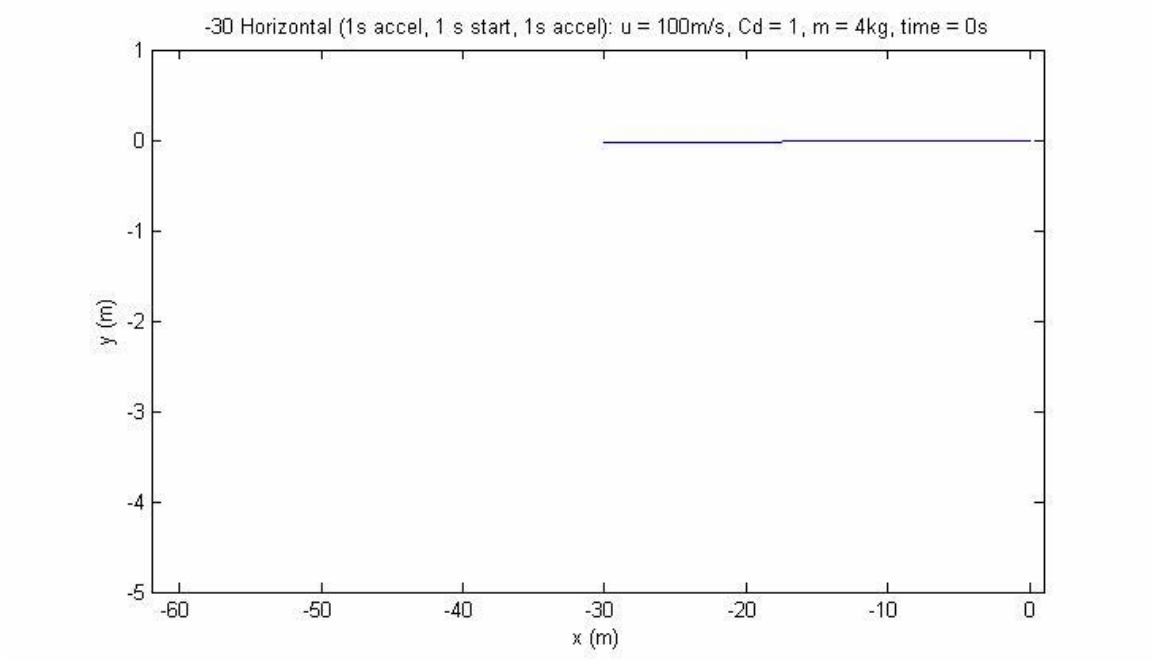

Figure 4.3-1 Horizontal Perturbation t=0s

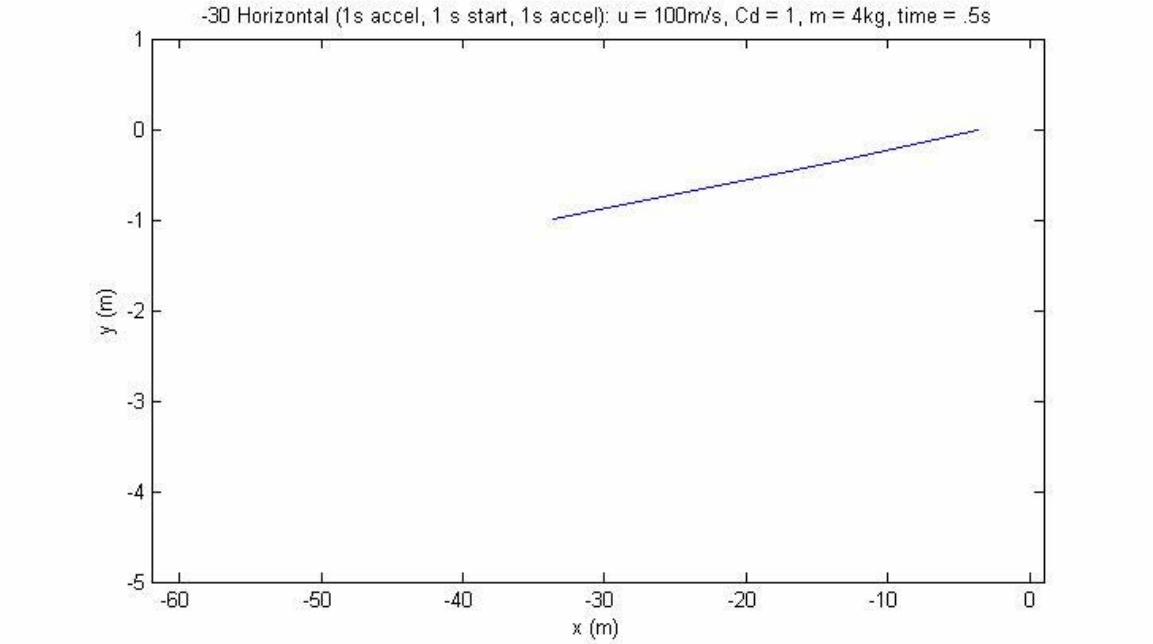

Figure 4.3-2 Horizontal Perturbation t=0.5s

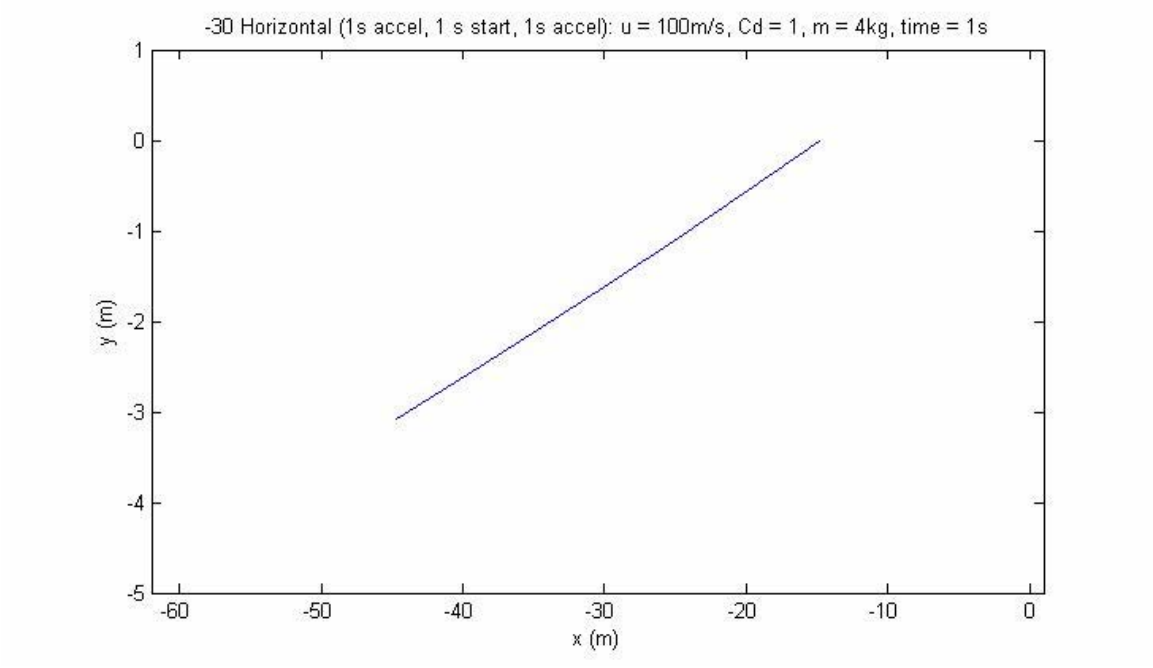

Figure 4.3-3 Horizontal Perturbation t=1s

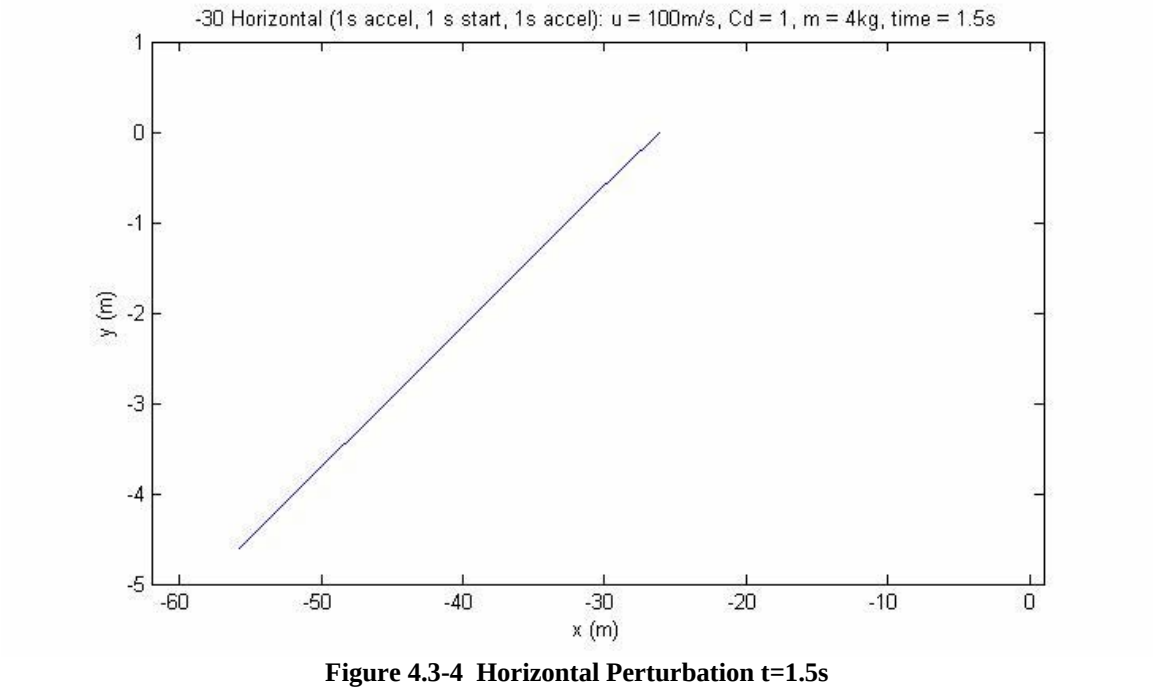

Figure 4.3-4 Horizontal Perturbation t=1.5s

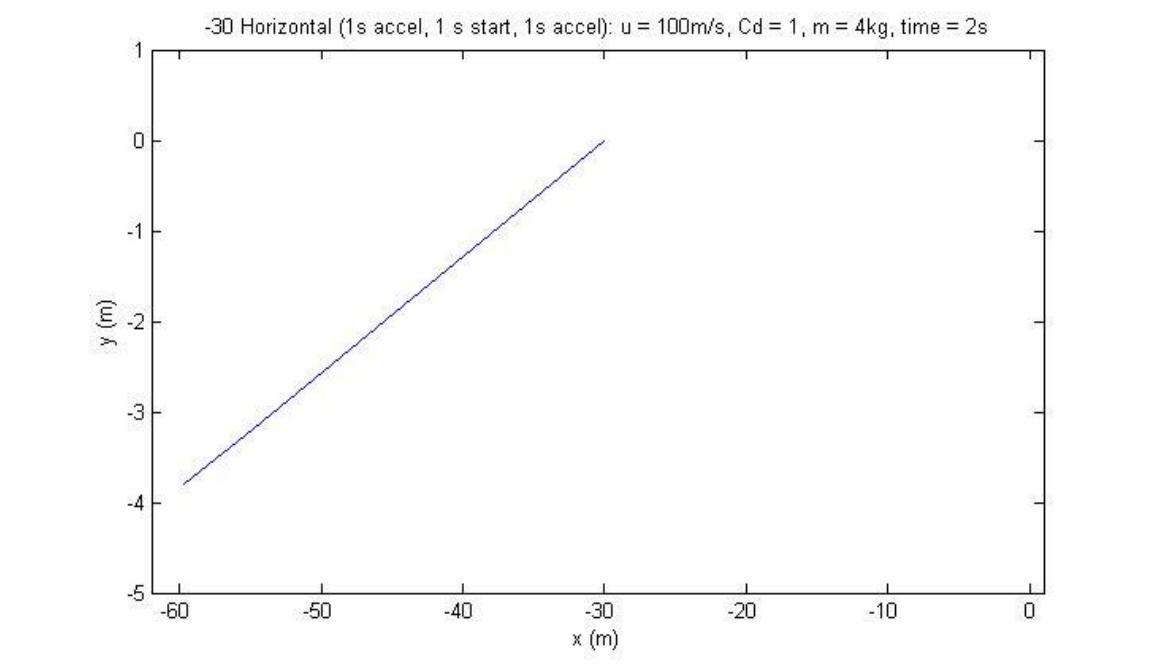

Figure 4.3-5 Horizontal Perturbation t=2s

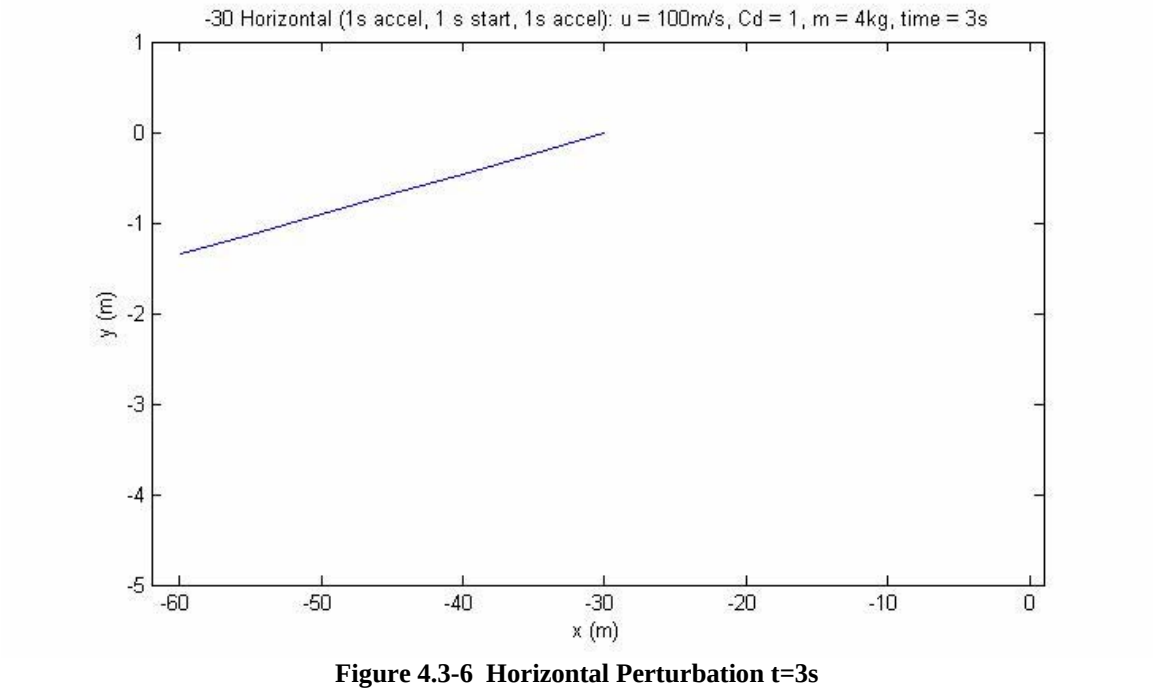

Figure 4.3-6 Horizontal Perturbation t=3s

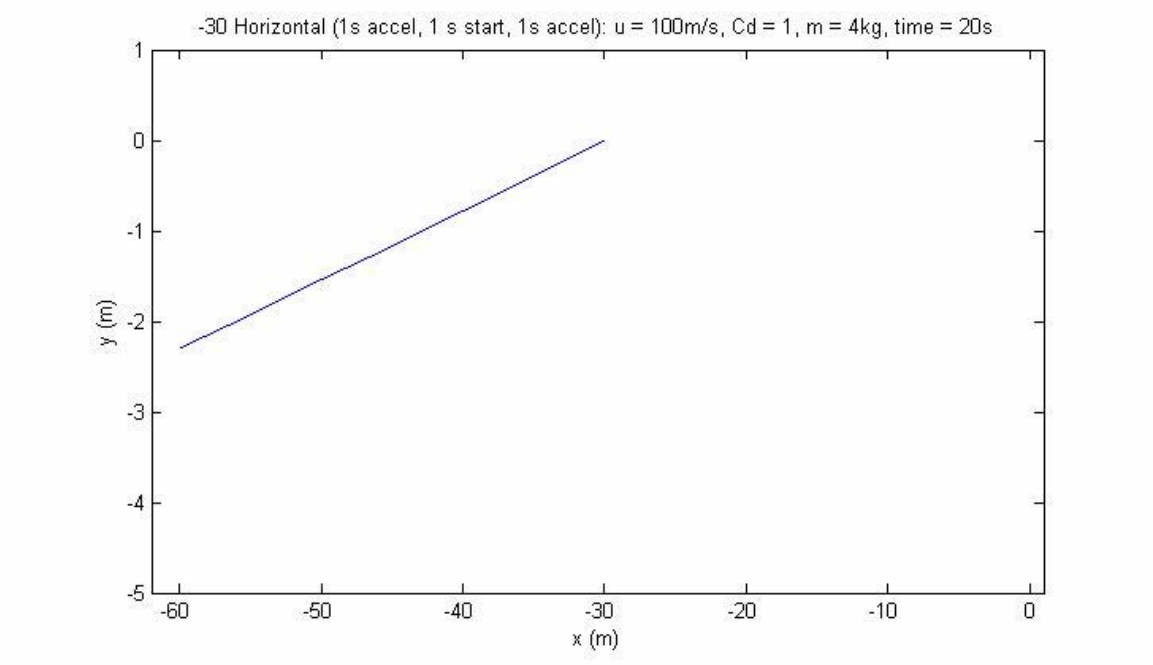

Figure 4.3-7 Horizontal Perturbation t=20s

As can be seen, the entire system slows down and the body drops below its initial and final steady state value. Upon acceleration back to 100 m/s, the body then comes up past its steady state value, and after oscillating about this value settles down in the original steady state position.

Vertical Perturbation.

This scenario also used a 4 kg mass. The aircraft was accelerated to a 30 m/s vertical velocity over 1 second of acceleration. This velocity was kept constant until 2 seconds, at which point it was accelerated back to its initial vertical velocity of 0 m/s over a period of 1 second. The results can be seen in Figure 4.3-8 through Figure 4.3-16.

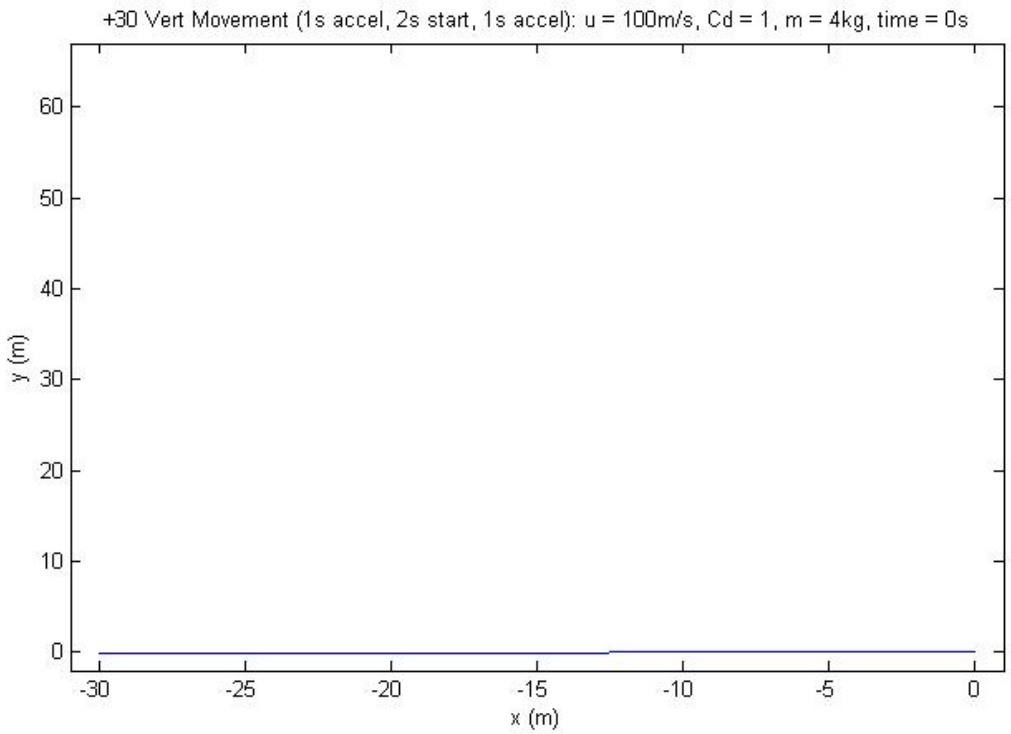

Figure 4.3-8 Vertical Perturbation t=0s

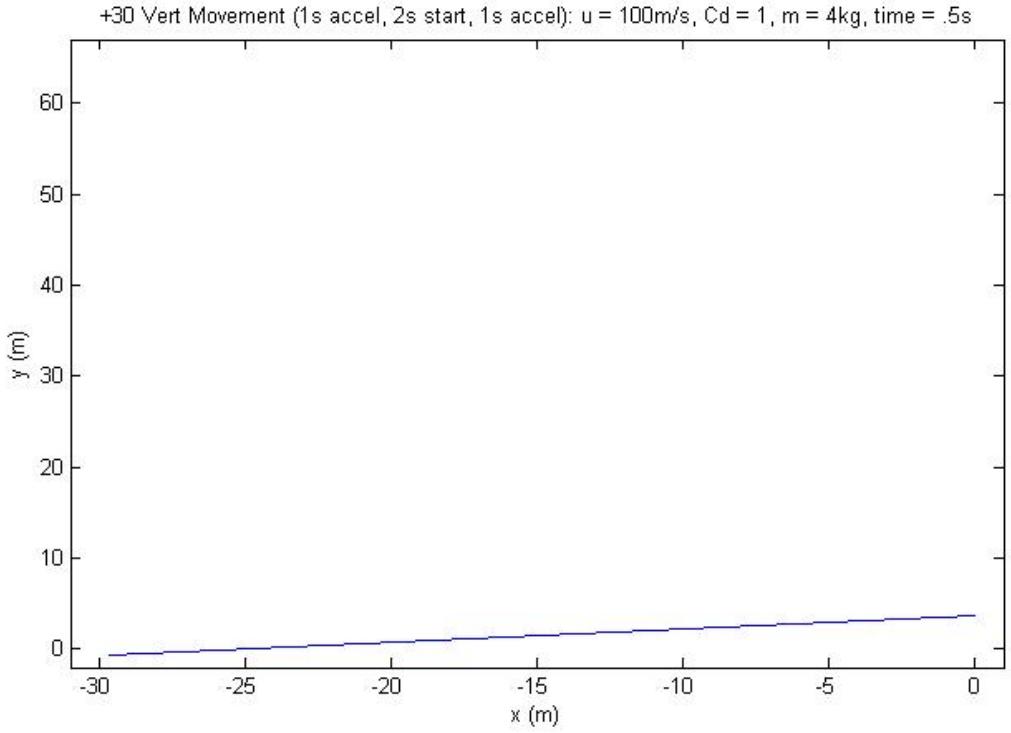

Figure 4.3-9 Vertical Perturbation t=0.5s

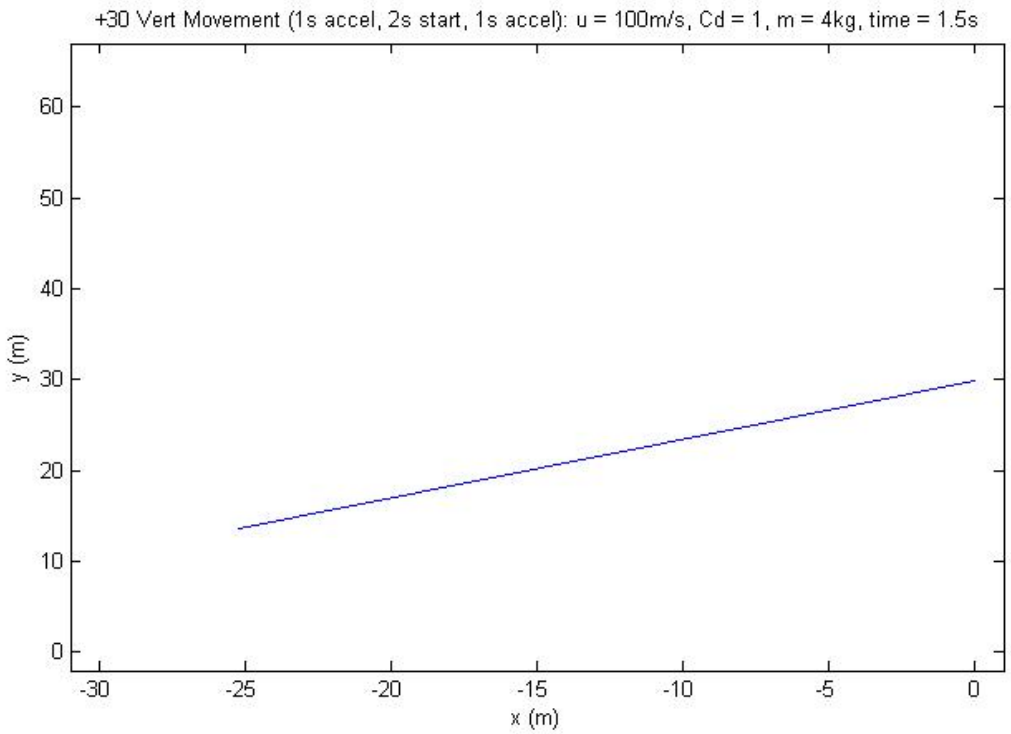

Figure 4.3-10 Vertical Perturbation t=1.5s

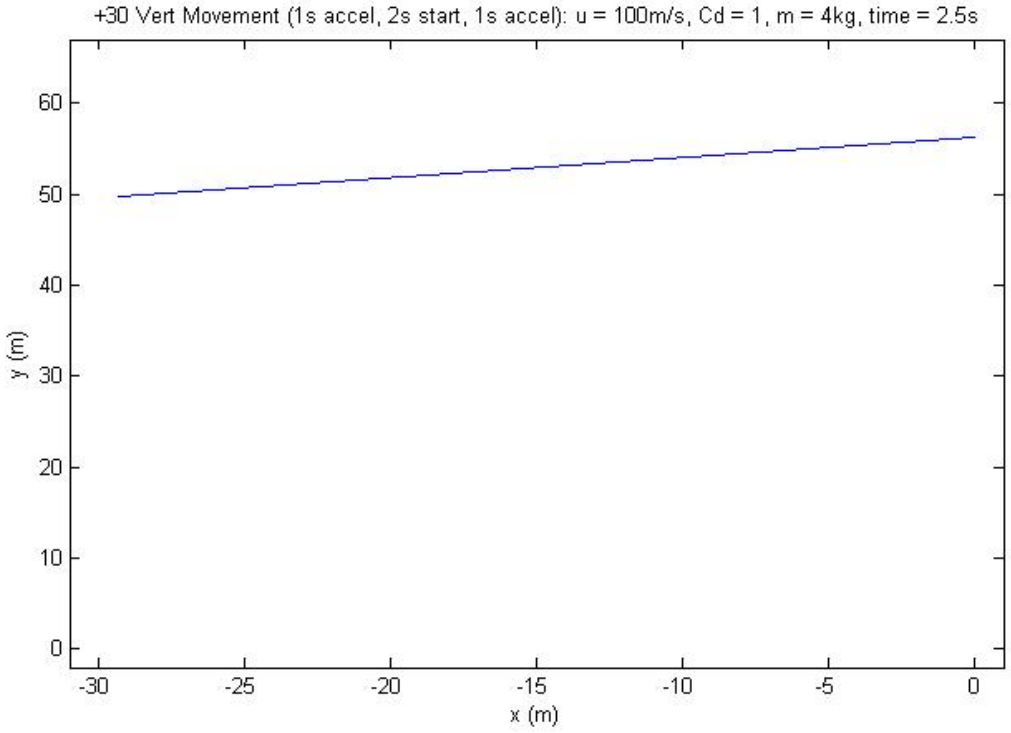

Figure 4.3-11 Vertical Perturbation t=2.5s

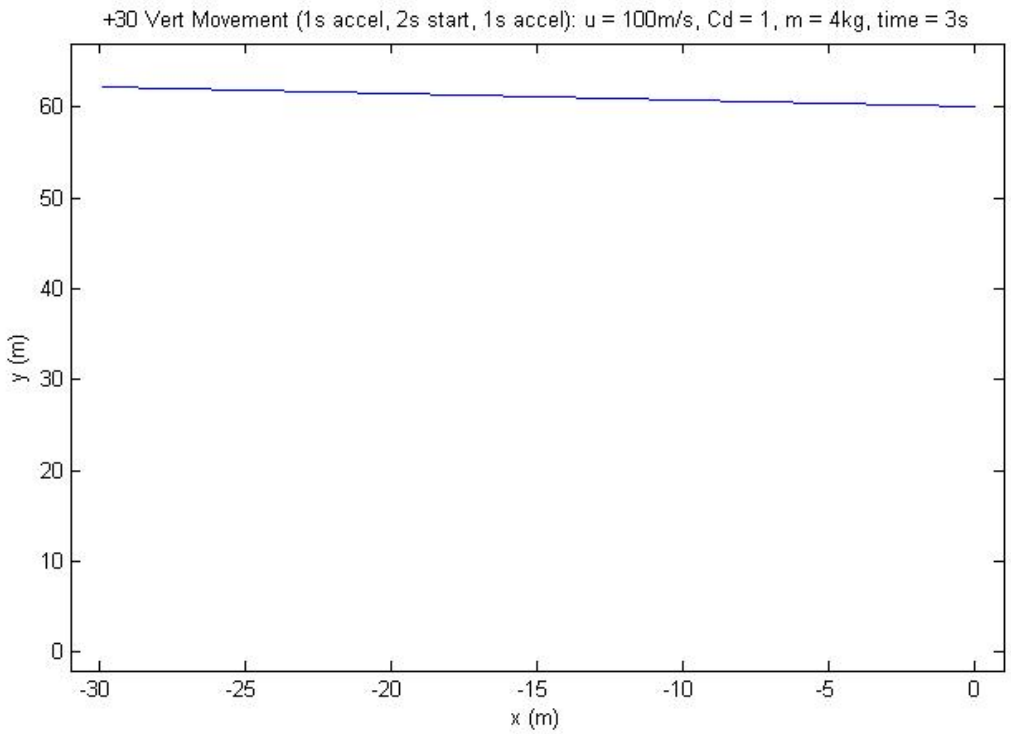

Figure 4.3-12 Vertical Perturbation t=3s

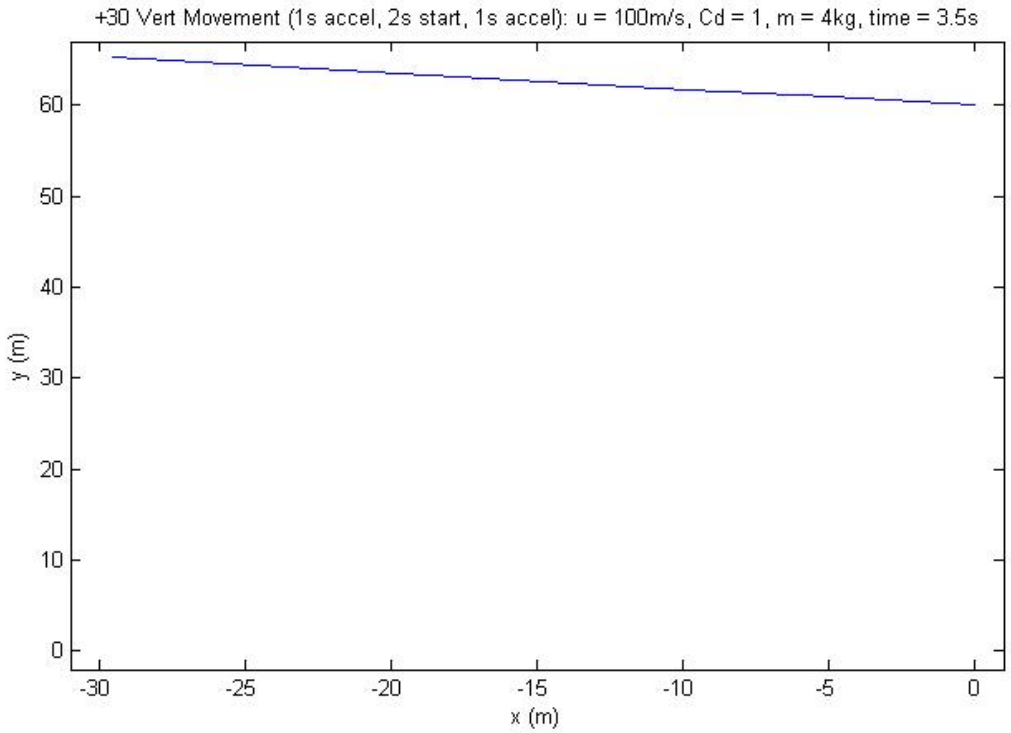

Figure 4.3-13 Vertical Perturbation t=3.5s

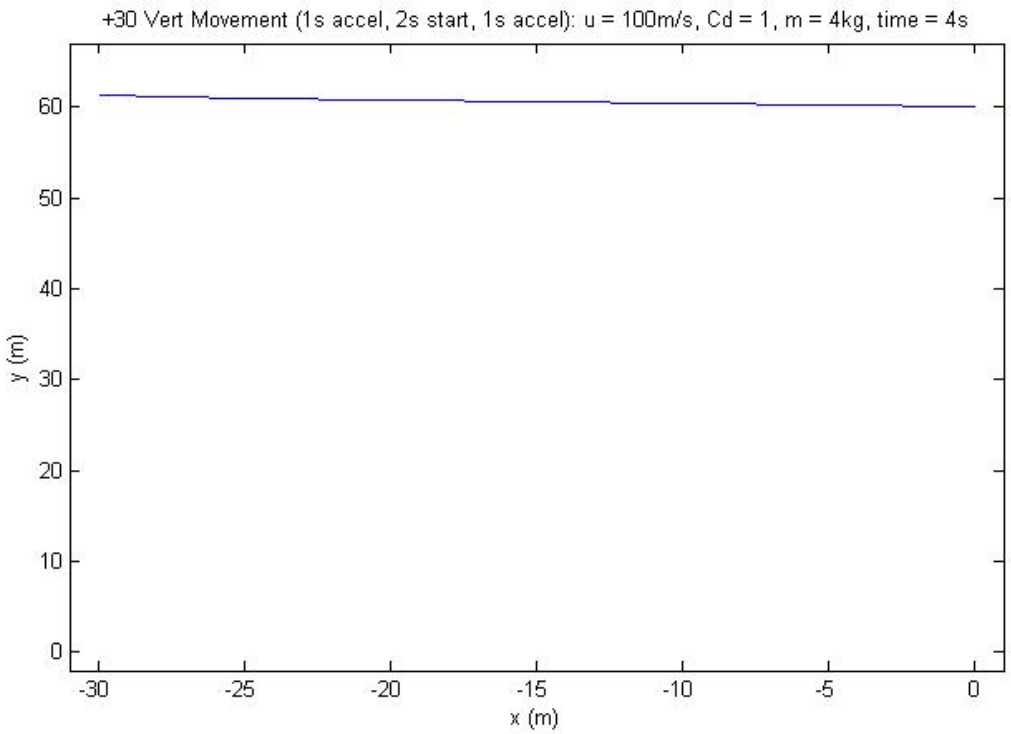

Figure 4.3-14 Vertical Perturbation t=4s

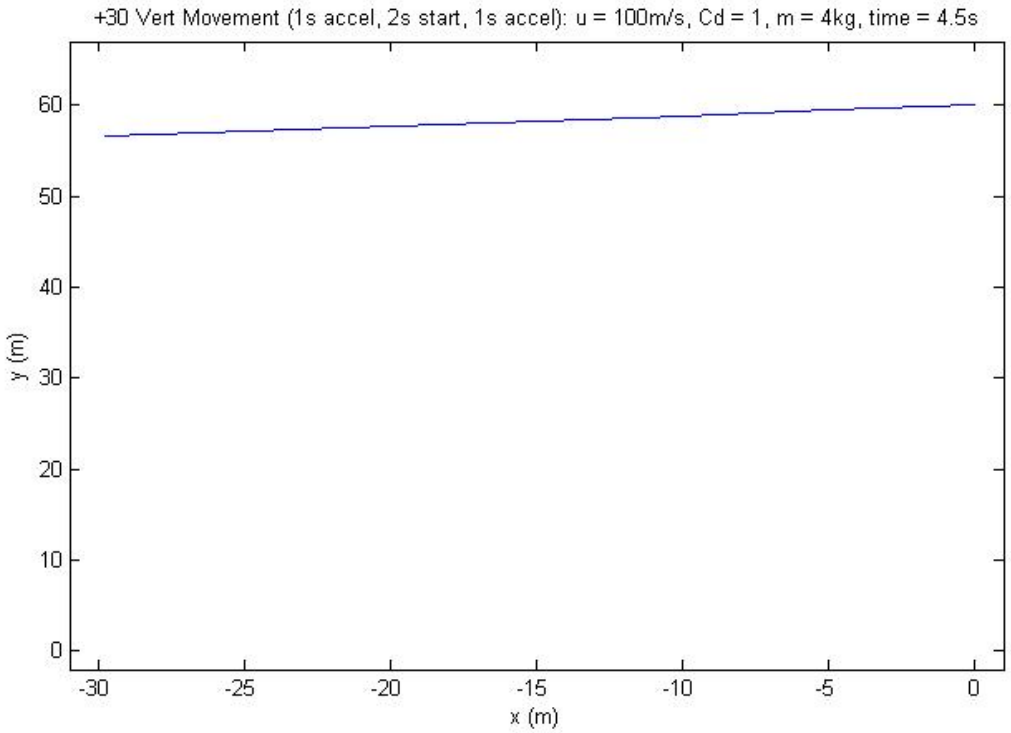

Figure 4.3-15 Vertical Perturbation t=4.5s

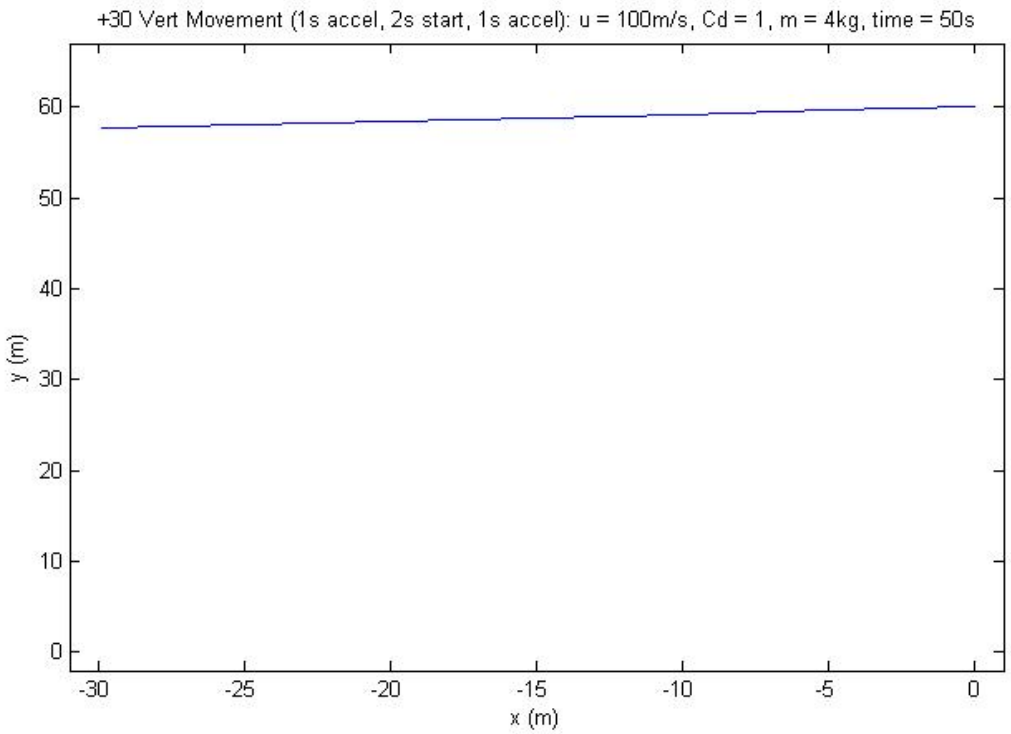

Figure 4.3-16 Vertical Perturbation t=50s

Note the overshoot as the system returns to its initial vertical velocity. When applying this to the concern of the towline crossing behind the engine, assuming that the engine plume is always in the horizontal direction, the towline can be seen to cross right down the middle of the plume. This effect is not desirable when concerned about heat transfer to the line. Since the towline is generally not deployed exactly behind the engine, and behavior represented here is only in the vertical direction, this is not necessarily the worst case. However, it is one that should be avoided.

Although it is not very noticeable in these plots, the towline exhibits a curvature in the overshoot, which is expected. The reason for the small amount of curvature is that the mass is contributing a large force in the *y*-axes due to weight. The inertia from the overshoot is what causes the curvature, but since gravity is always acting on the body, the

force in the *y*-axis does not change enough to create a significant curving effect. Essentially, the weight serves to damp the curvature from inertia.

Transverse Perturbation.

This scenario also used a 4 kg mass. The aircraft was accelerated to a 30 m/s velocity in the transverse direction (*z*-axis) over 1 second of acceleration. At 1 second, this velocity was accelerated back to its initial vertical velocity of 0 m/s over a period of 1 second. The results can be seen in Figure 4.3-17 through Figure 4.3-26.

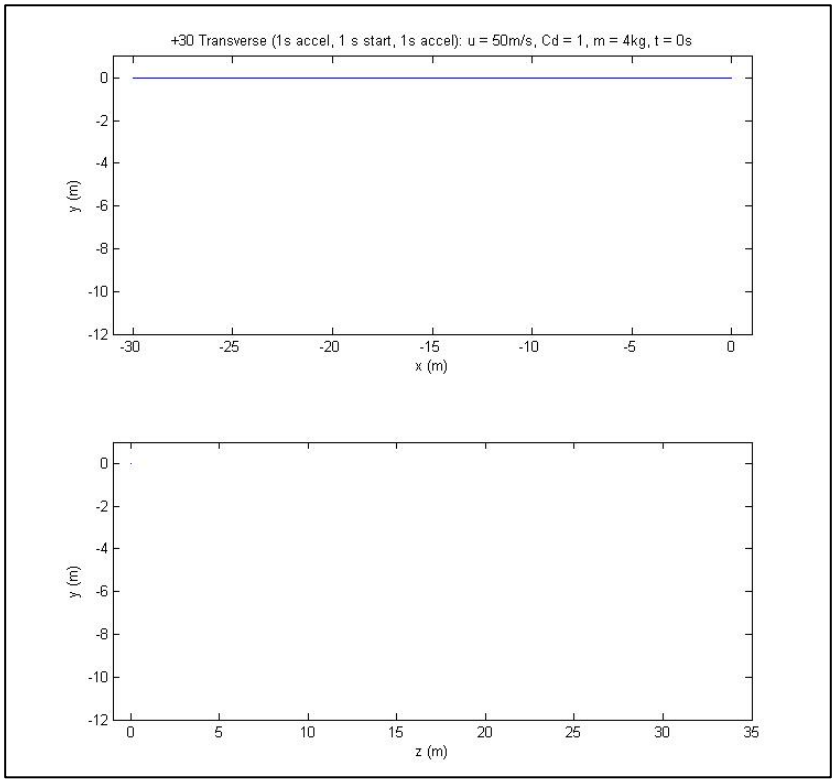

Figure 4.3-17 Transverse Perturbation t=0s

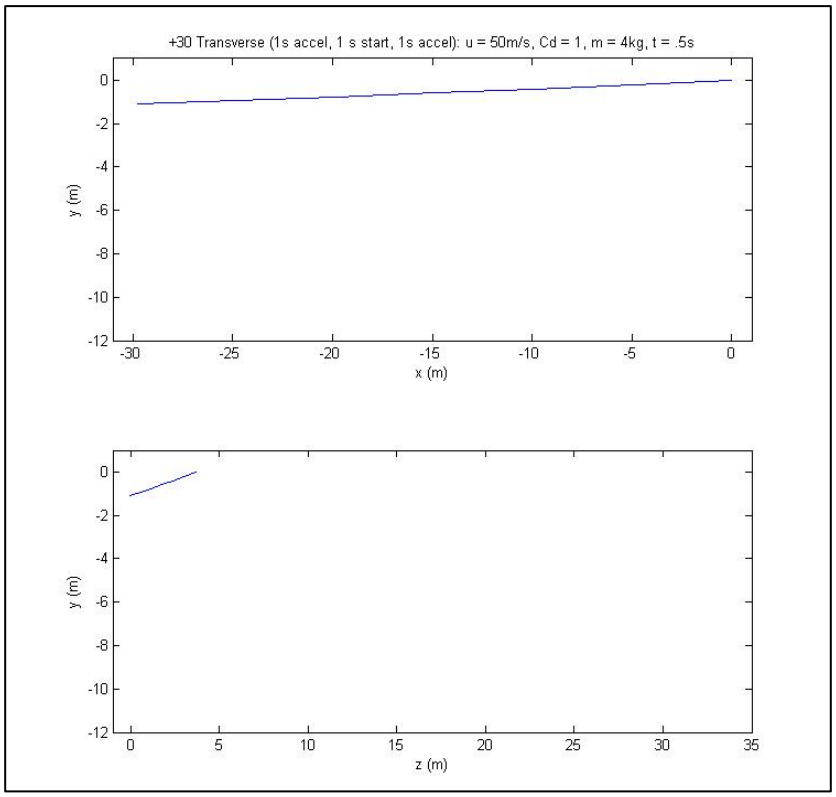

Figure 4.3-18 Transverse Perturbation t=0.5s

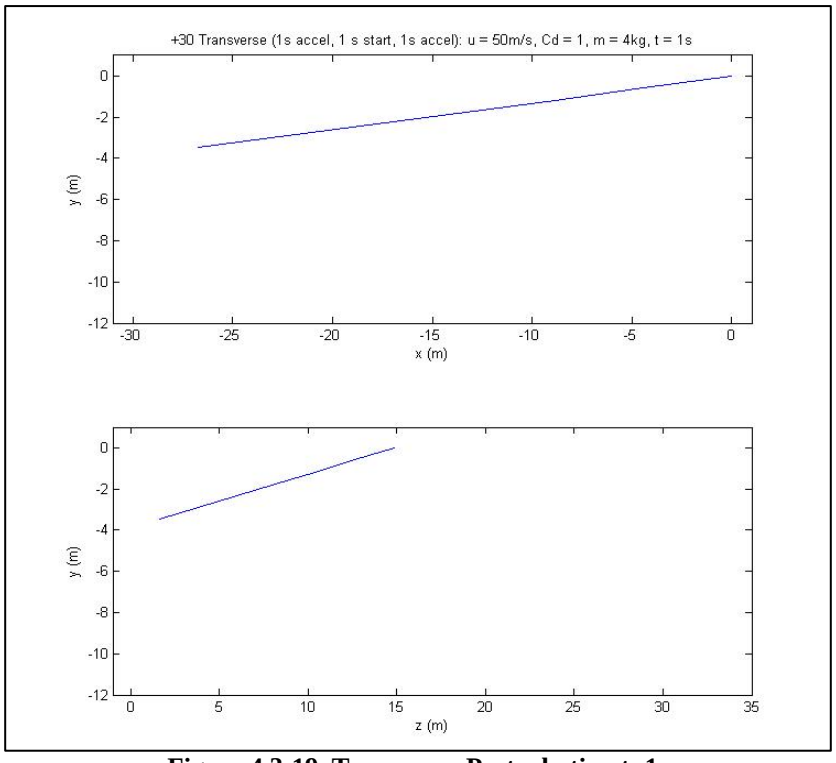

Figure 4.3-19 Transverse Perturbation t=1s

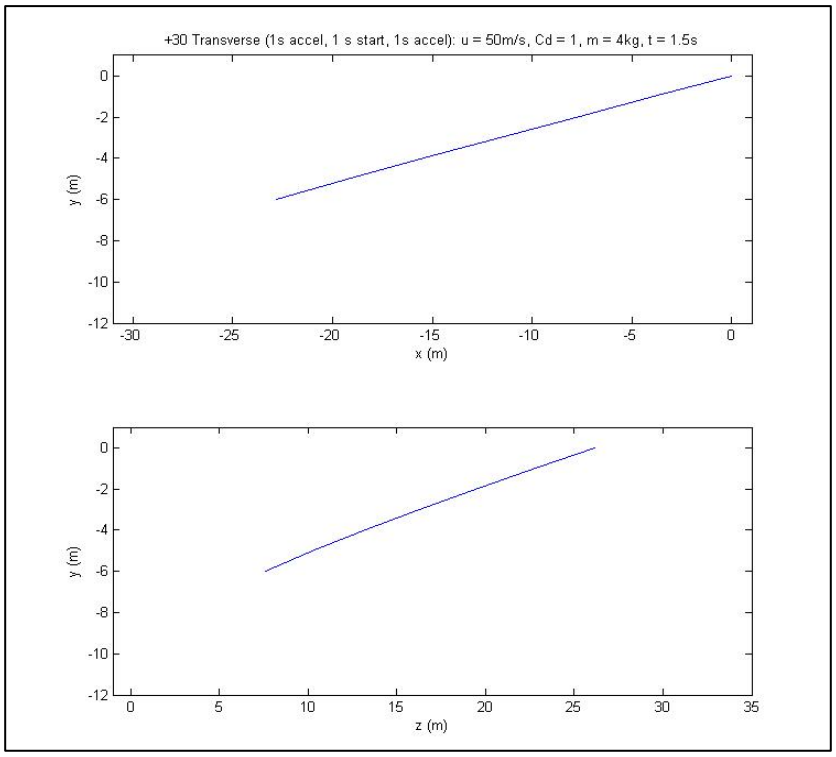

Figure 4.3-20 Transverse Perturbation t=1.5s

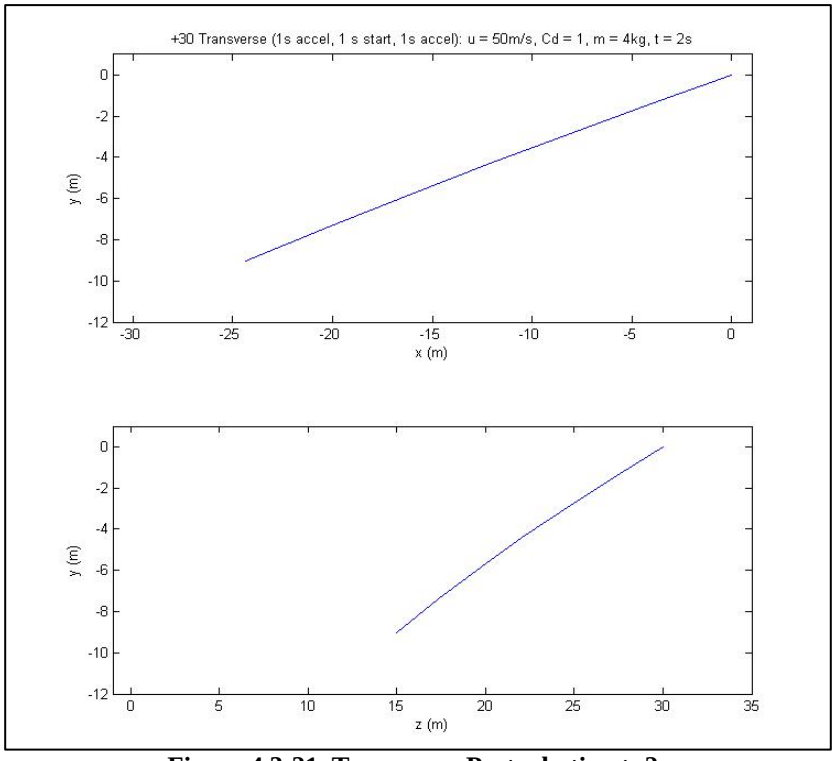

Figure 4.3-21 Transverse Perturbation t=2s

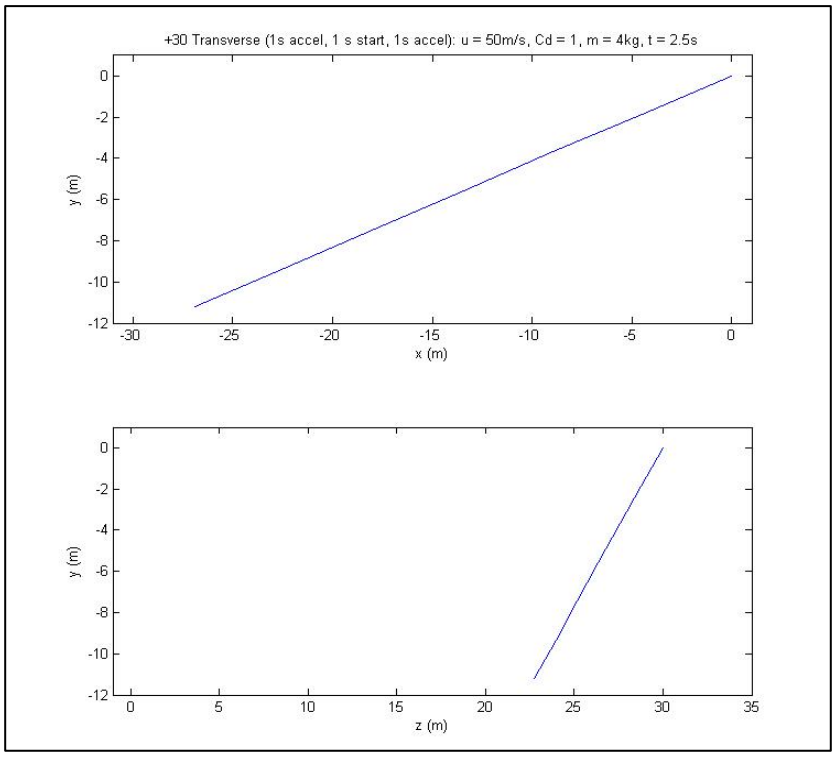

Figure 4.3-22 Transverse Perturbation t=2.5s

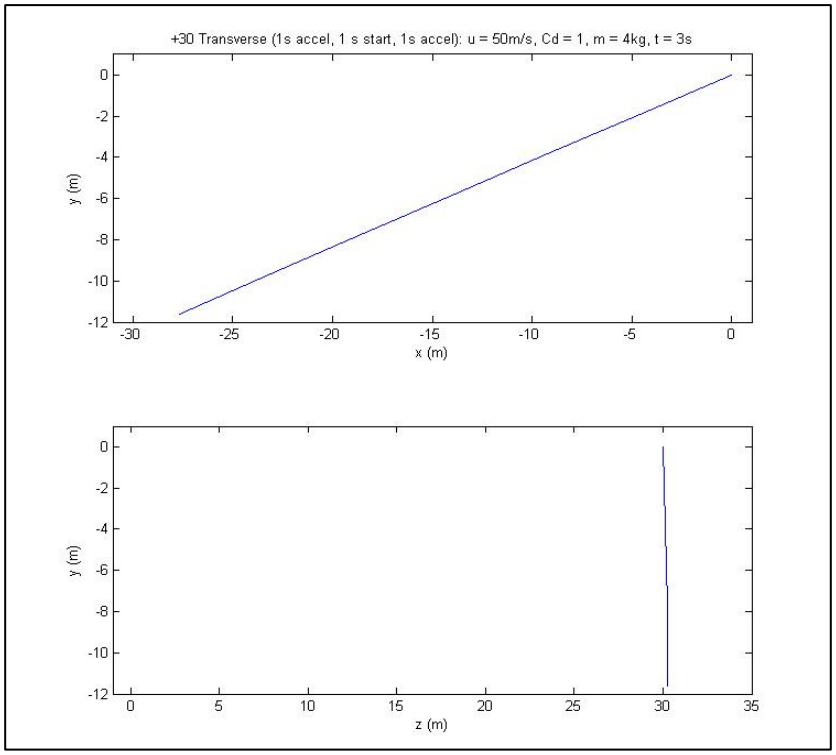

Figure 4.3-23 Transverse Perturbation t=3s

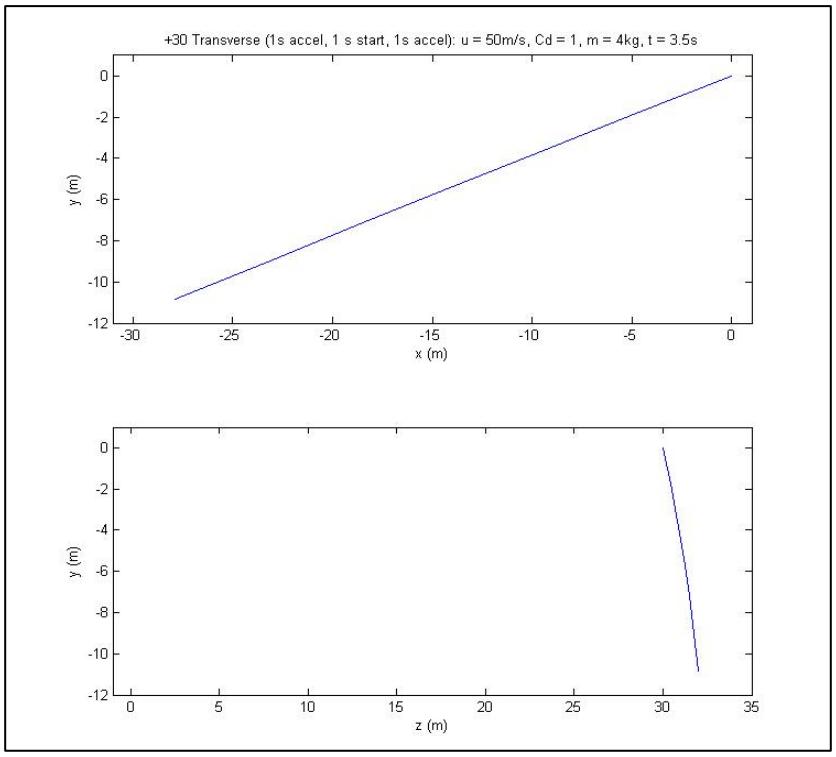

Figure 4.3-24 Transverse Perturbation t=3.5s

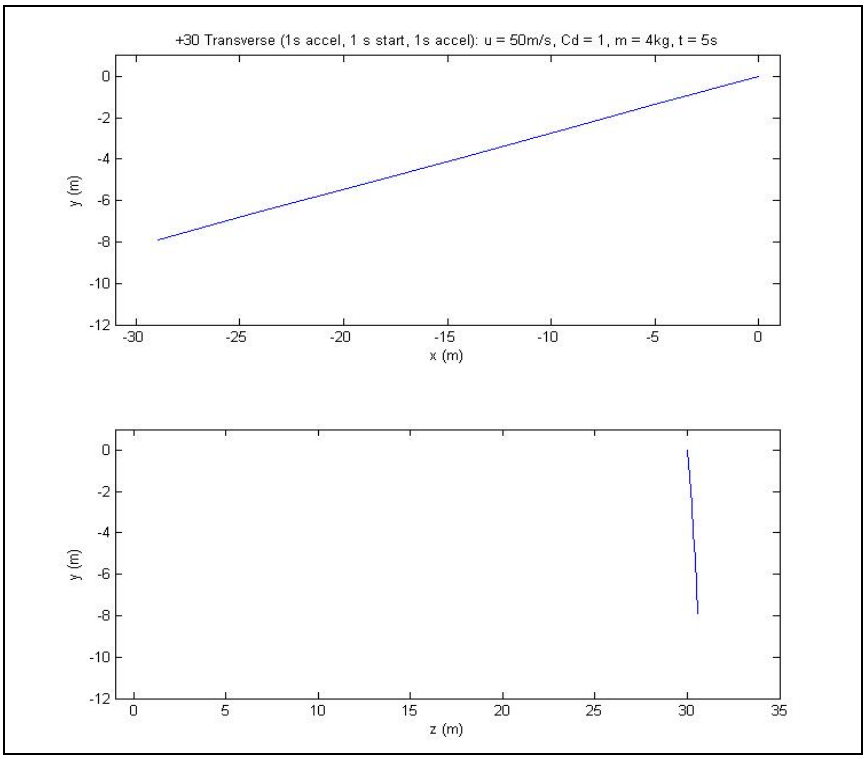

Figure 4.3-25 Transverse Perturbation t=5s

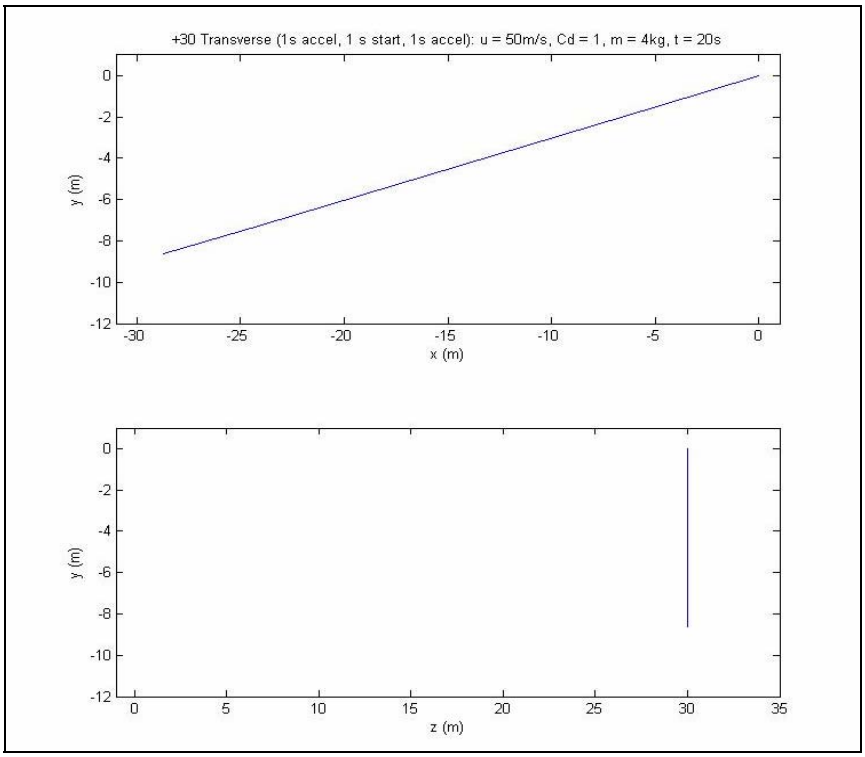

Figure 4.3-26 Transverse Perturbation t=20s

Since the towline was not initially in a steady state position, the change in both the *x*-*y* and the *z*-*y* planes can be seen. Although not explicitly clear here, the changes in the transverse direction affect the changes in the vertical direction and vice versa. The curvature of the line is more distinct in these perturbations, since the weight only works in the *y*-axis. Thus, the inertia in the *z*-axis becomes significant, causing curvature. Of interesting note is that although the line goes past its steady state value, it does not come back and cross this position, which is most likely due to the small amount of overshoot. Since the force from weight is what brings the line back to steady state, and this force is relatively small due to the small angle the towline goes past its steady state value, the towline approaches its final position at a slow rate, thus producing little to no overshoot when it comes back. A greater acceleration in the transverse direction would produce a noticeable overshoot on the return here.

4.4. Multiaxial Perturbation

Using the same values for the previous simulations with a 4 kg mass, the last two maneuvers from Section 4.3 were combined to produce an upward and rightward movement. Here, however, the transverse velocity did not begin to accelerate back to zero until the 2 second mark. The results can be seen in Figure 4.4-1 through Figure 4.4-10, noting the scaling in the *z-y* plane, which changes so that the results can be more easily seen.

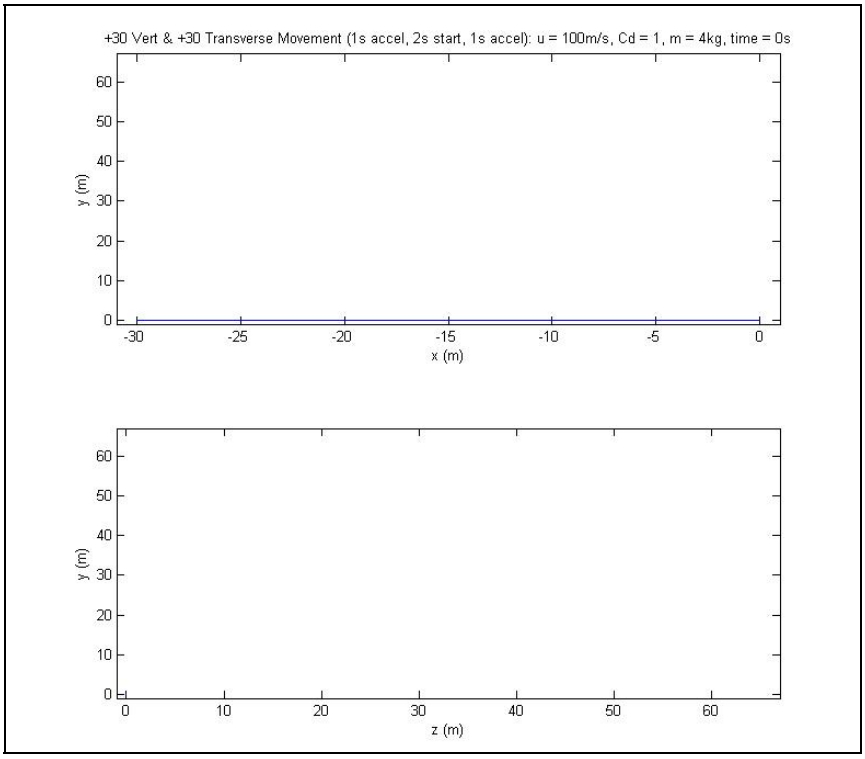

Figure 4.4-1 Multiaxial Perturbation t=0s

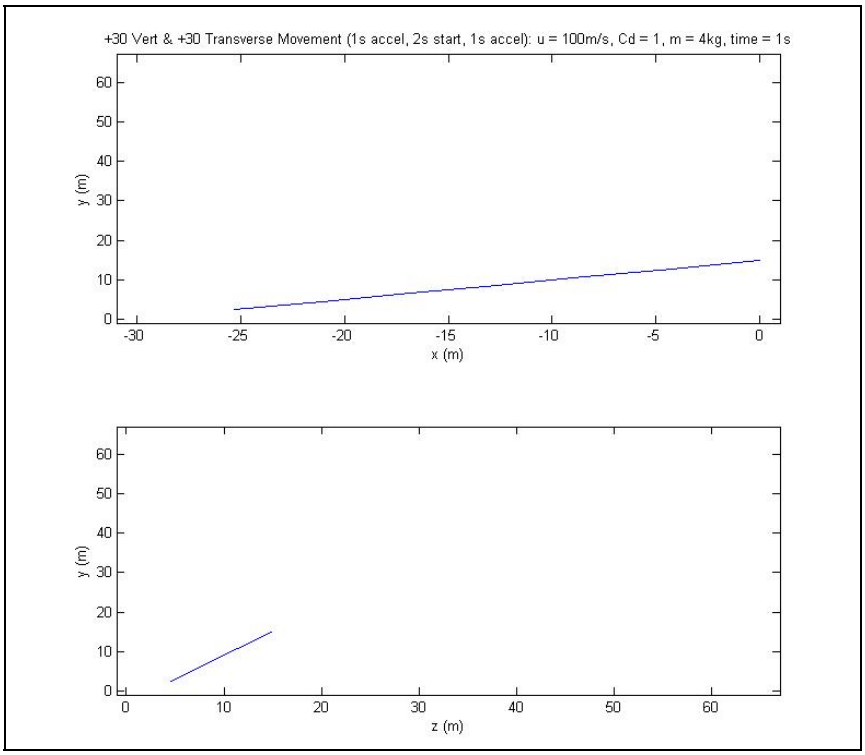

Figure 4.4-2 Multiaxial Perturbation t=1s

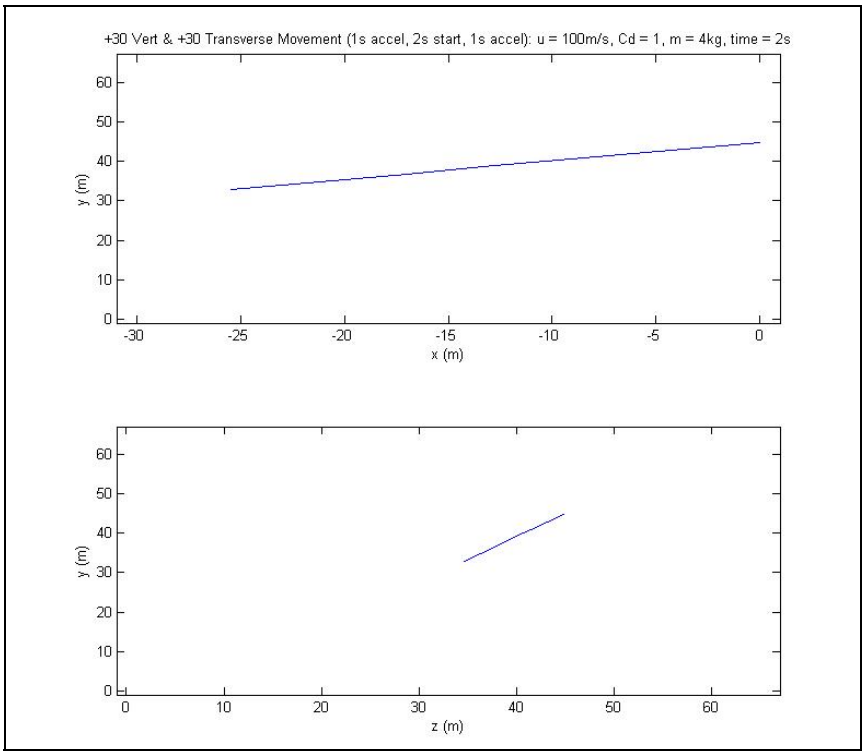

Figure 4.4-3 Multiaxial Perturbation t=2s

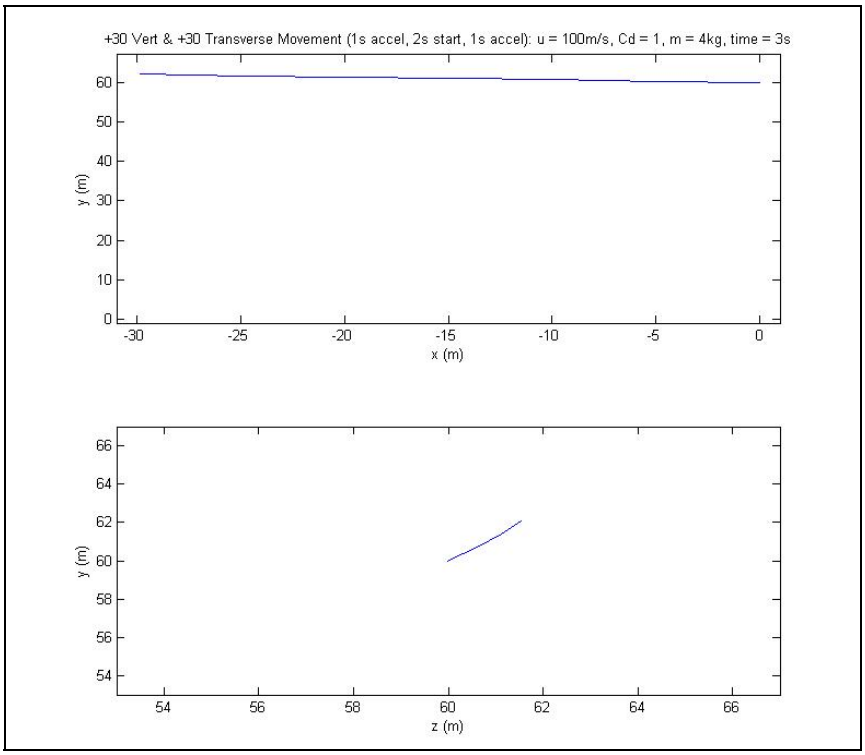

Figure 4.4-4 Multiaxial Perturbation t=3s

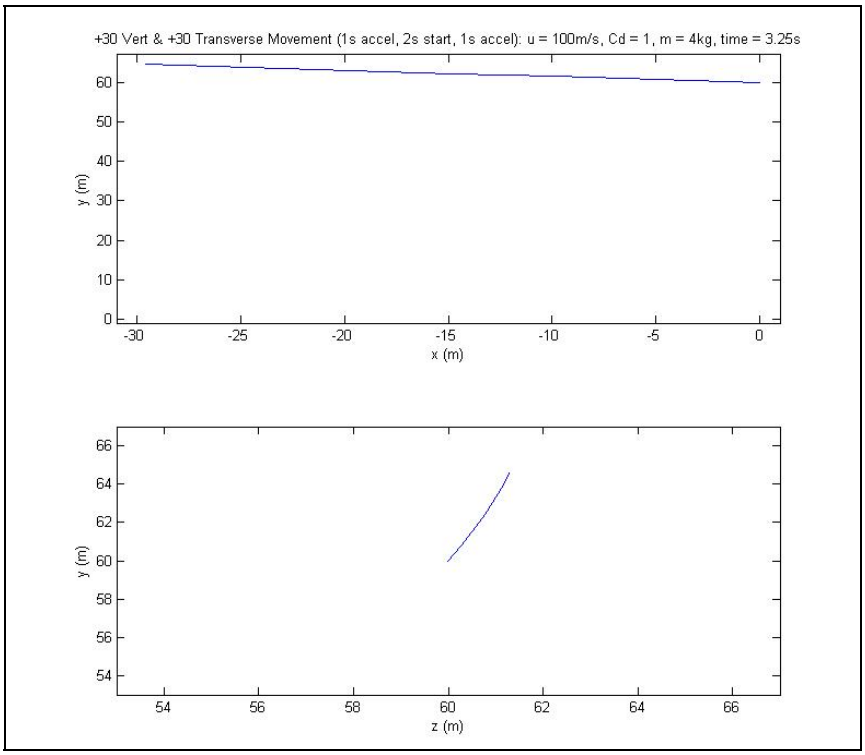

Figure 4.4-5 Multiaxial Perturbation t=3.25s

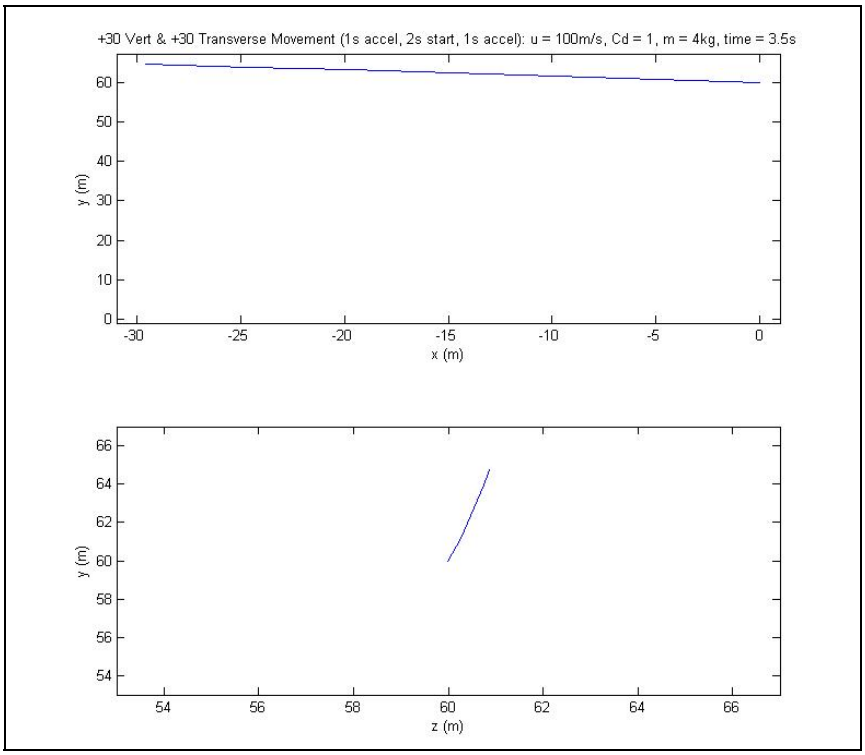

Figure 4.4-6 Multiaxial Perturbation t=3.5s

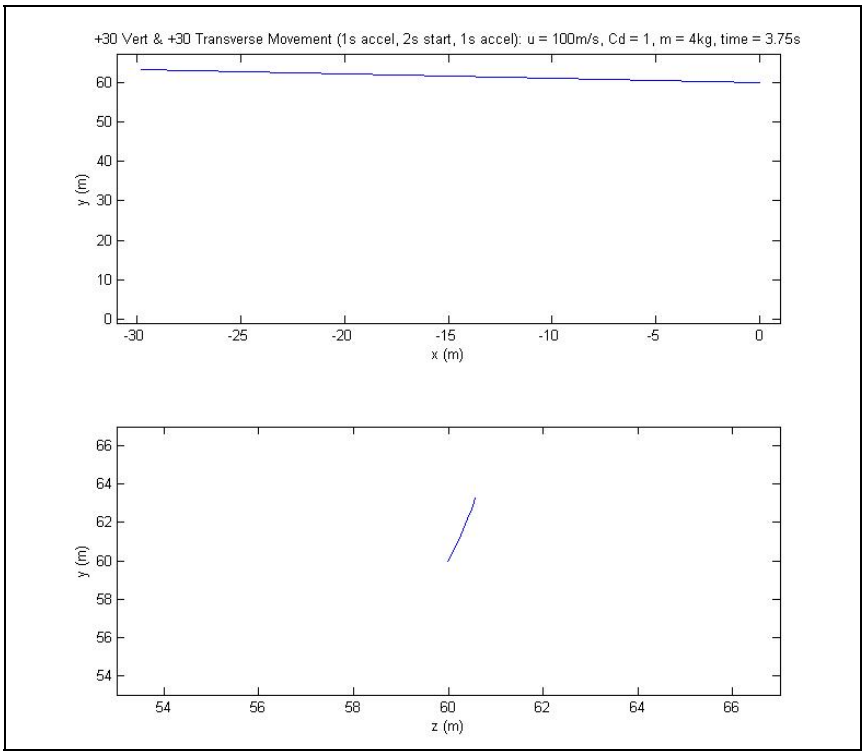

Figure 4.4-7 Multiaxial Perturbation t=3.75s

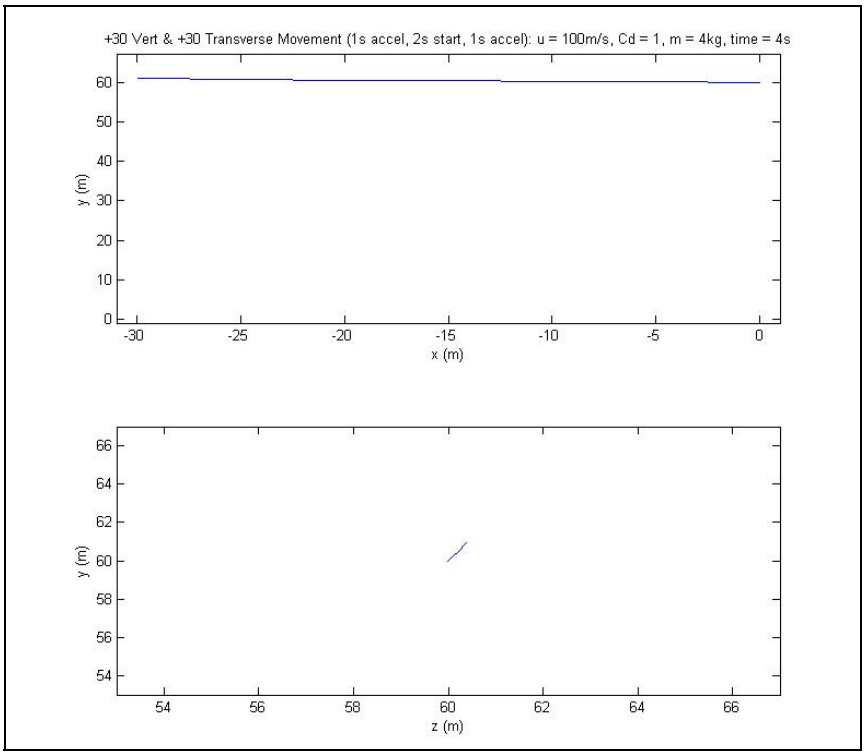

Figure 4.4-8 Multiaxial Perturbation t=4s

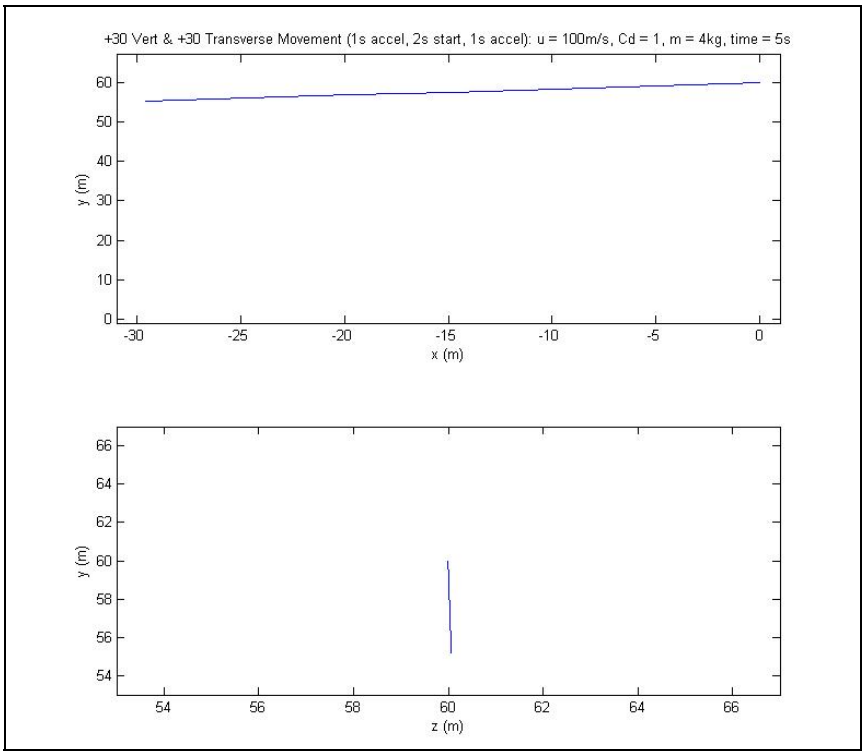

Figure 4.4-9 Multiaxial Perturbation t=5s

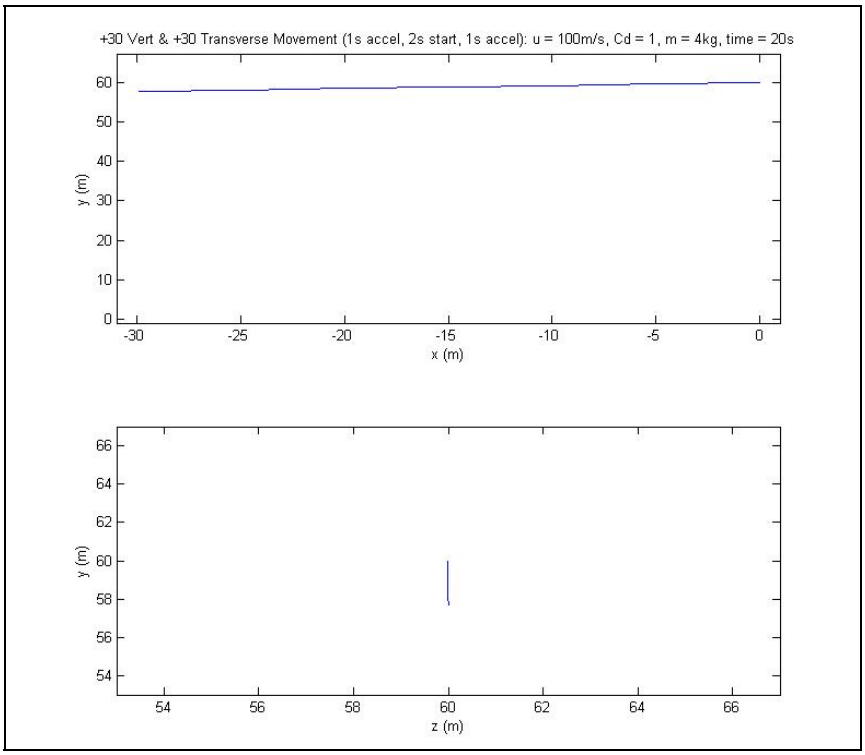

Figure 4.4-10 Multiaxial Perturbation t=20s

The towline overshoots when the aircraft returns to its steady state value (note the aircraft's final position at z = 60m and y = 60m with the body overshooting these values). It appears to cross right behind the aircraft. Applying this to the concern of heat transfer to the towline, this case is potentially worse than the purely vertical perturbation. The towline crosses behind the aircraft in both the *y* and *z* axes, which could put it right in the engine plume if the engine is off center from the towline attachment.

4.5. Heat Transfer

All the previous analyses were assumed to be in standard atmosphere and pressure, thus keeping a constant air density with constant line temperature. To analyze the change in towline temperature and air density about the towline, a routine was written (*Tempset.m*) to calculate these values at every point in space and time and is included in

Appendix C. The code was written with the intention of given data being placed into an ambient temperature array as global or otherwise referenced values.

In the analysis here, however, it was assumed that the ambient temperature was held constant at 1000 K, and although the array is a function of time and three dimensional space (relative to the initial positions of the system), all of its values are the same. This can be easily changed by adding known data. Both the heat transfer to the towline, and the air density about the towline, were analyzed under this constant ambient temperature.

The vertical velocity perturbation in Section 4.3 was run in the same manner as before over a period of 150 seconds. A 1 kg mass was used for this analysis, however, since a lower mass will produce more curvature in the towline (body weight works to damp any curvature). The vertical maneuver was used in order to model how heat transfer is affected by a change in perpendicular velocity over the towline. The aircraft was started at a 100 m/s horizontal velocity and was given an initial vertical acceleration over a period of 1 second to a final vertical velocity of 30 m/s. This was held for 1 second. At the 2 second mark, the same procedure is done in reverse to slow the aircraft down to 0 m/s vertical velocity. As mentioned, however, this time it was placed in an ambient temperature field of 1000 K. The towline temperature was given an initial temperature of 288.2 K (value for standard atmosphere and pressure).

The first plot (Figure 4.5-1) shows the temperature in the towline as a function of time.

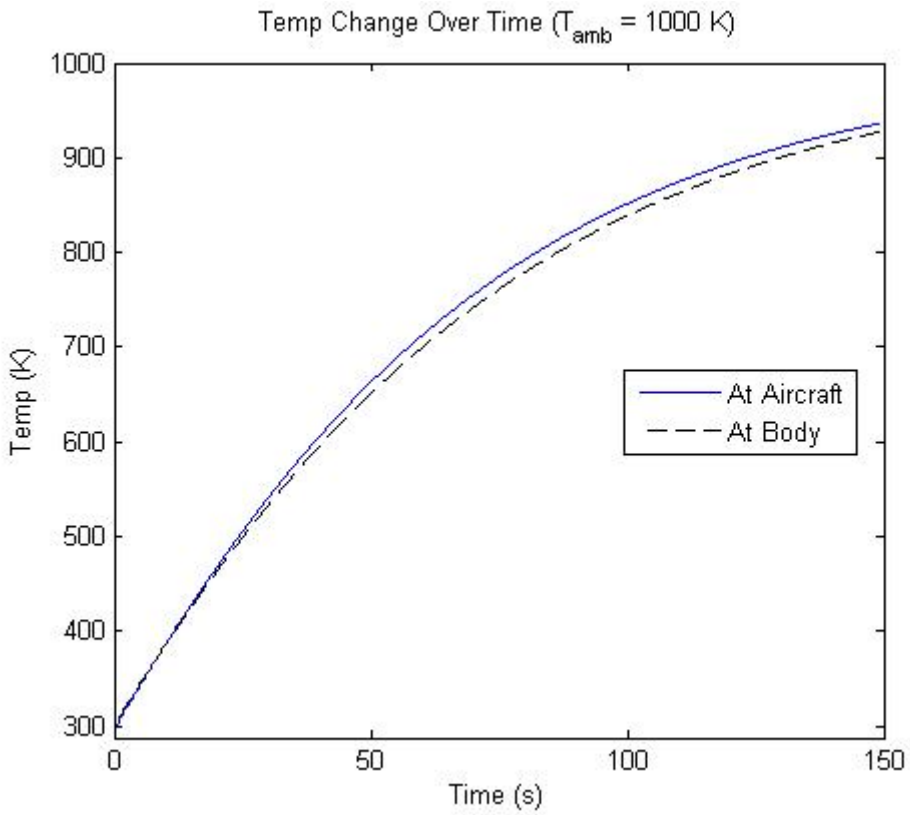

Figure 4.5-1 Temp Change Over Time

Note that the line temperature asymptotically approaches the ambient temperature value of 1000 K. This creates a near linear change initially and a much more gradual change as time goes on. The reason that the line temperature at the aircraft increases faster is due to the towline shape in its steady state value. This is shown in Figure 4.5-2.

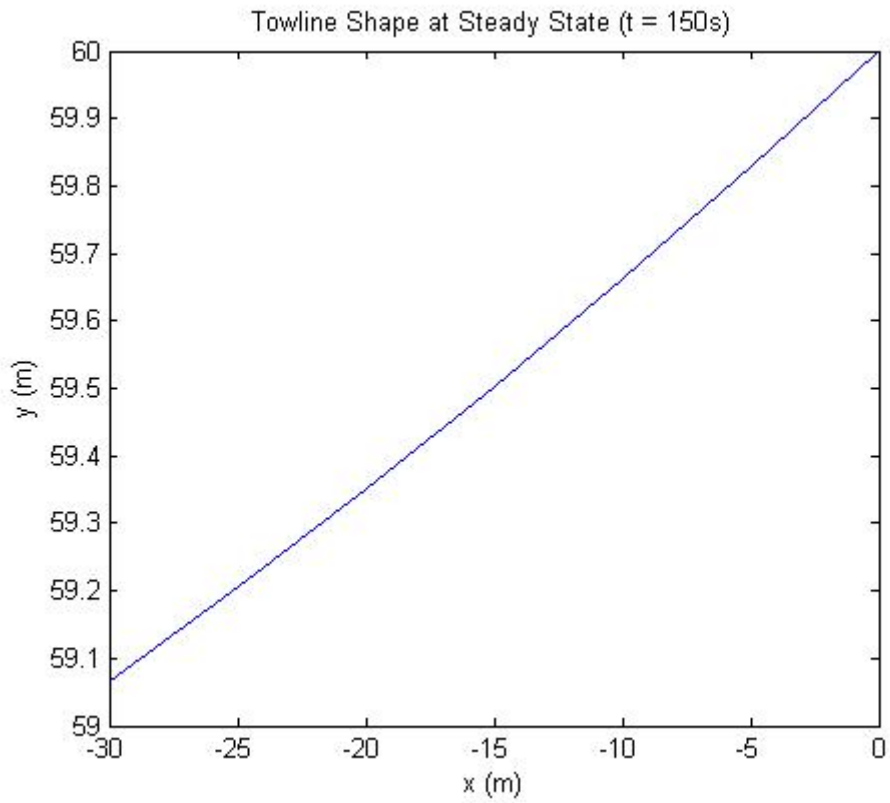

Figure 4.5-2 Towline Shape at Final Steady State

Note the shape of the towline, which allows for a greater perpendicular velocity over the line near the aircraft (right side of plot) versus near the body (left side of plot) since the system is traveling at 100 m/s to the right.

Also of note is the increased droop in the towline. The final droop is about 0.93 meters, whereas the initial droop is about 0.64 meters. The initial position of the towline before the maneuver is shown in Figure 4.5-3.

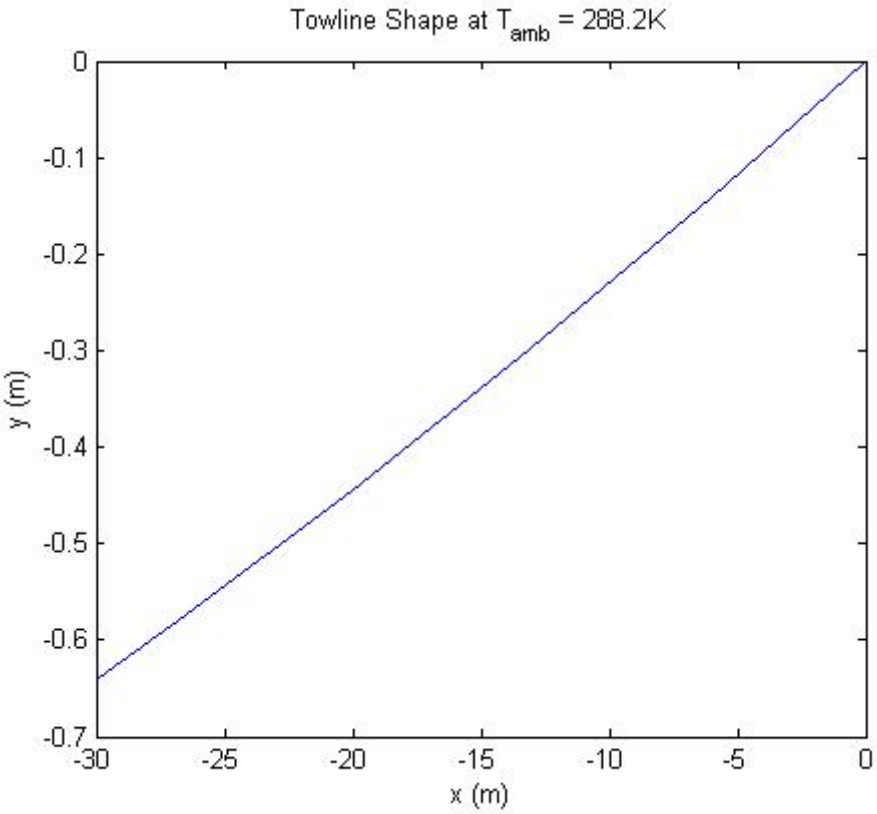

Figure 4.5-3 Towline Shape at Initial Steady State

This increased droop is due to the reduction in drag forces as a result of reduced air density. The air density is shown in Figure 4.5-4.

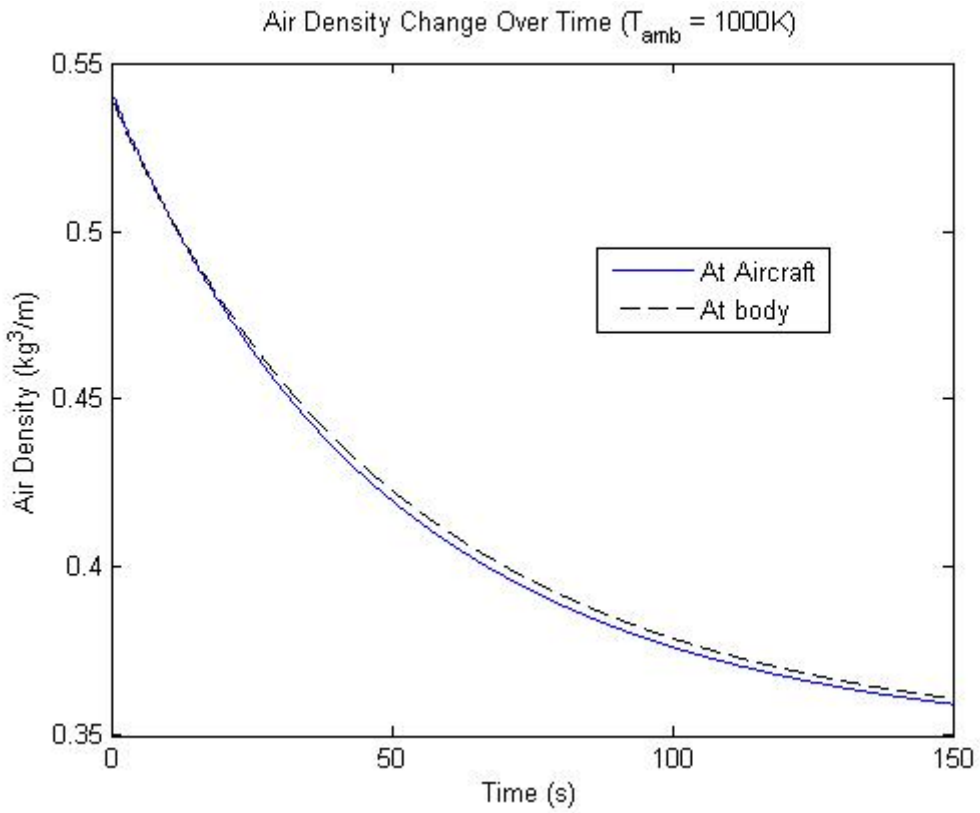

Figure 4.5-4 Air Density Change Over Time

Note how the density changes as a function of temperature. A greater temperature causes a lower air density under constant pressure.

To illustrate the initial rate of heat transfer, the towline temperature is plotted for the first 5 seconds in Figure 4.5-5. The towline shape can be seen over this time period in Figure 4.3-8 through Figure 4.3-15. Note that, over this time period, the towline is traveling faster near the body than near the aircraft. Thus, there is greater heat transfer near the body than near the aircraft. The two values cross around 10 seconds, due to a slightly different slope in the steady state position. It should be noted that the slope is the heat transfer rate.

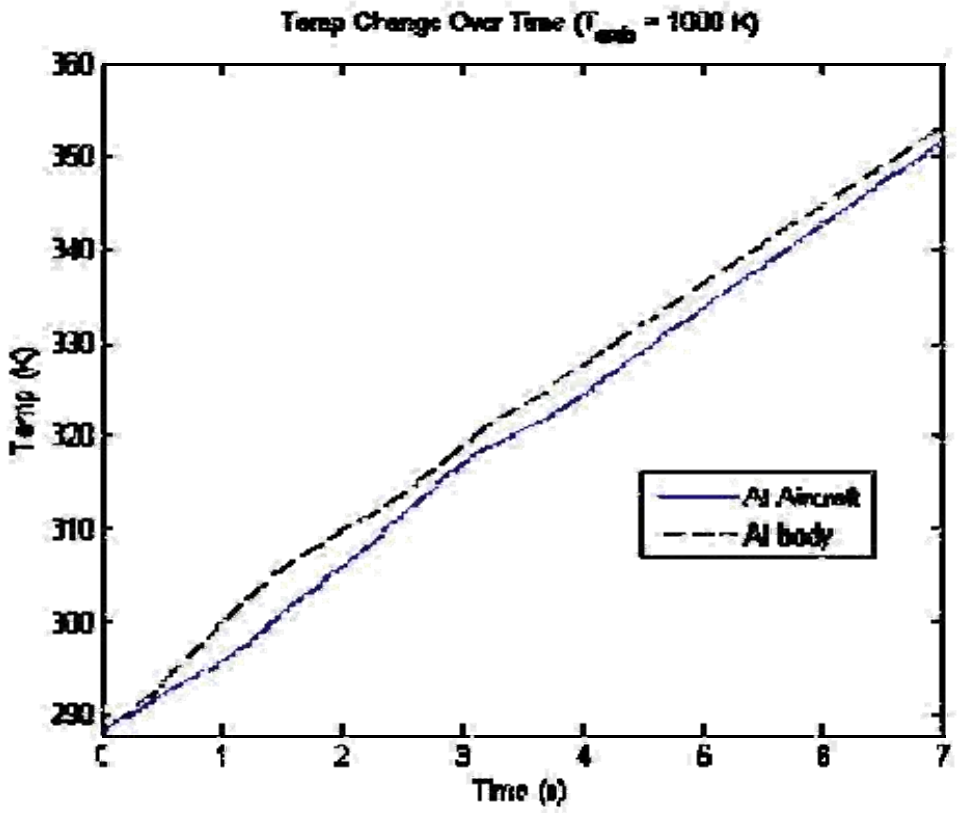

Figure 4.5-5 Temp Change Over 7 Seconds

The change in the heat transfer rate at the aircraft is noticeable at the three inflection points for acceleration (1 second, 2 seconds, and 3 seconds). The first second has the aircraft increasing in velocity (curved heat transfer slope). The second second has the aircraft at a constant velocity, but higher than its initial and final velocities (linear heat transfer). The third second has the aircraft slowing down to its final velocity (curved heat transfer). After this final acceleration is complete and the system approaches steady state again, the heat transfer near the aircraft settles to an essentially linear behavior. The curvature between 3 and 4 seconds is due to the system approaching its steady state. The heat transfer at the body becomes a little more complex due to its oscillations about the steady state value, but follows expected behavior. Note the slightly higher heat transfer rate at the body on the right side of the plot.

V: Conclusions and Recommendations

This paper utilized a variety of research to develop a reliable code to model towline behavior under transient conditions. When compared to past work, it has been shown to accurately predict the position of the towline under any transient maneuvers. This code can also accurately model the heat transfer to the line based on given initial data within the assumptions given (i.e., not heat transfer due to parallel airflow). The theory is presented clearly and the code works effectively.

5.1. Conclusions

A few conclusions can be drawn from the results shown here. The first conclusion is that the method of characteristics gives a good approximation for the towline behavior in both transient and steady state analysis. This was shown in comparison with past work, as well as the modeling of expected behaviors such as the pendulum test.

The second conclusion is that this method cannot analyze slack conditions. Since most towed decoys, which are the focus of this research, are designed to prevent slack, this method should be able to analyze most cases of concern. Although the slack conditions cannot be analyzed, the towline acts as it should when compared to previous work. As a result, special consideration needs to be made regarding the towed body's drag and mass, which must be adjusted in order to prevent slack.

The third conclusion regards the coupling of motion. Previous research has indicated that disturbances in one plane generate disturbances in another (Schram and

Reyle, 1968:219). This is seen in the results here as well except for the case of a straight towline undergoing maneuvers purely in the plane in which it starts (i.e., a purely vertical maneuver from straight, steady state flight). Previous work indicated this exception as well (Schram and Reyle, 1968:219), so the effect is not unexpected. This coupling of motion is due to the change in drag being put on the line and body due to the change in total velocity, which affects the towline's behavior in multiple axes.

The fourth conclusion is that the heat transfer to the towline appears linear over short periods of time. A gradual leveling off over longer periods of time happens, but for shorter periods, the change appears linear. This is expected for large differences in temperature, since Newton's law of cooling says that the rate of heat transfer is dependent on the difference in temperatures. Thus, a smaller difference produces a smaller change.

5.2. Future Work

Future work entails the development of a better way to approximate the Nusselt number, analyzing the boundary layer on the towline, modeling the effects of wake from the aircraft, modeling slack conditions in the line, the use of different mesh schemes, analyzing the towed body's forces, and comparing to real results for specific applications (i.e., specific maneuvers). In addition, in order to analyze heat transfer, a temperature field as a function of time and space must be referenced from known data.

As alluded to in previous sections, the method derived is limited in its ability to model heat transfer to the towline due to the Nusselt number. Future research should entail a manner in which to find the Nusselt number at differing geometries, such that the

heat transfer to the line can be approximated for both parallel and perpendicular flow. This may require boundary layer analysis on the towline.

The drag and heat transfer from airflow parallel to the towline were both assumed to be negligible for this work. One of the primary causes of this assumption is the formation of a boundary layer, which increases in thickness along the towline. There is no sure way to analyze the boundary layer, however, because flow separation will start to occur along different points of the line. Even though flow separation occurs, it was assumed still that the length size of the turbulence was much greater than that of each incremental length of the towline. Due to this, all the airflow becomes, essentially, perpendicular, and thus a perpendicular airflow analysis may be sufficient. More work should be done, however, to model the formation of the boundary layer, its effects on drag and heat transfer, and the result of turbulent effects due to flow separation.

All flow was considered to be laminar at every local point along the towline. This is not necessarily true, especially since this system is being towed behind an aircraft. An analysis of the turbulent wake from the aircraft would determine if this would affect any of the data.

Slack conditions cannot be analyzed with this model. That is because the characteristics used to step data from one timestep to the next are functions of tension. A zero tension value prevents the transfer of data by this method. Thus, another method, or some alteration of the one used here, is necessary to allow for slack in the line. This method could be added to the current code as an *if* statement, called up only during slack conditions.

Although the first order scheme of Courant, Isaacson, and Rees (Ames, 1965:447) used here for the method of characteristics provides a very simple mesh setup, their's is only first order accurate. A better setup for the method of characteristics involves a second order solution based on Hartree's hybrid method, as outlined by Ames (Ames, 1965:445-448). The technique used in this paper is essentially an approximation of this hybrid method. Although probably not necessary, the alternate method Ames lays out would provide a more accurate approximation, especially at larger step sizes. A larger step size would reduce computing time. Unfortunately, it also requires iterative procedures for solutions, which increases computing time. The payoffs or advantages of using this scheme are unknown. However, if computing time becomes an issue, more should be looked into using the second order scheme instead. Also, as was shown in the steady state analysis of Section 4.2, there is a slight discrepancy between the 1^{st} order method used here, and the 4^{th} order method used by Richardson. Using this second order method from Ames should reduce the discrepancy. These errors are small, however, and the work necessary to rewrite all the code may not be worth the slightly increased accuracy.

One assumption that was made involved the orientation of the body being always facing directly into the freestream. This is not a bad assumption, but future work should involve a better modeling of the forces on the body. Depending on the body's weight and drag, it can have a very significant effect on the towline behavior. Since the body shape was unknown and only assumptions were made for this work, future analyses using actual body properties will help produce very useful data.

As an all theoretical work, data from this code should be compared to real life data. There are many real life simulations available. A lot of these (including other methods used to analyze this type of problem) can be found referenced in Kang and Latorre (Kang and Latorre, 1991:5-6). Future work should entail comparing the results from this code to specific scenarios from experiment in order to predict behavior under the known conditions.

Other possible work involves some small additions to the code, both of which would be quite simple. These include utilizing a ramp function for acceleration to reduce the "jerk" in the tension, and adding more possible maneuvers for each simulation (currently only 2 are allowed).

These conclusions and recommendations can be further substantiated with more research. For now, however, the attached code is sufficient for modeling transient maneuvers in aircraft behavior, as well as heat transfer to the towline in a known temperature field.

Bibliography

Ames, William F. *Nonlinear Partial Differential Equations in Engineering*. New York: Academic Press, 1965.

Ball, Robert E. *The Fundamentals of Aircraft Combat Survivability Analysis and Design, Second Edition.* Reston: American Institute of Aeronautics and Astronautics Inc., 2003.

Chapman, D.A. "Towed Cable Behaviour During Ship Turning Manoeuvres," *Ocean Engineering*, 11:327-361 (1984).

Crist, S.A. "Analysis of the Motion of a Long Wire Towed from an Orbiting Aircraft," *Shock/Vibration Bulletin*, Volume unknown:61-73 (1970).

Dowling, A.P. "The dynamics of towed flexible cylinders: Part 1. Neutrally buoyant elements," *Journal of Fluid Mechanics*, 187:507-532 (1988).

Kang, S.W. and V.R. Latorre. *Aerodynamics Modeling of Towed-Cable Dynamics.* Contract W-7405-Eng-48. Livermore CA: Lawrence Livermore National Laboratory, January 1991 (UCRL-ID-106509).

The Raytheon Company. "Raytheon Company: Products & Services: AN ALE-50 Towed Decoy System." Figure taken from website. http://www.raytheon.com/newsroom/ photogal/ale50_h.html. 13 March 2006.

Richardson, Tyler L. *Parametric Study of the Towline Shape of an Aircraft Decoy*. MS thesis, AFIT/GAE/ENY/05-J08. School of Engineering, Air Force Institute of Technology (AU), Wright-Patterson AFB OH, June 2005.

Schram, Jeffrey W. *A Three-Dimensional Analysis of a Towed System*. PhD thesis. Rutgers University, New Brunswick NJ, January 1968.

Schram, Jeffrey W. and Stanley P. Reyle. "A Three-Dimensional Dynamic Analysis of a Towed System," *Journal of Hydronautics,* 2:213-220 (October 1968).

Tannehill, John C., Anderson, Dale A., and Pletcher, Richard H. *Computational Fluid Mechanics and Heat Transfer, Second Edition.* Philadelphia: Hemisphere Publishing Corporation, 1997.

White, F.M. *Viscous Fluid Flow, Second Edition.* Boston: McGraw Hill, 1991.

Appendix A: Development of Angular Acceleration Term

Schram (Schram, 1968: Appendix B) developed a manner in which to calculate the three-dimensional rotational equations of motion of the body. A simplified version of a manner in which to find angular acceleration can be based off of Equation 3.27, where it is noted that the angular terms become

$$\frac{Mb}{dt}\left[W_L(\theta_L-\theta_b)+U_L\cos\theta_L(\phi_L-\phi_b)\right]$$

for the lower boundary. This can be added to the tension at the body to account for angular acceleration at the body.

Appendix B: MATLAB® Code – Primary Code

```
%Theoretical Modeling of the Transient Effects of a Towline
%Using the method of characteristics (June 2006)
%Created by Ensign Christopher A. Hill, USN
%Under the advice of Dr. Ralph Anthenien
%Master Thesis work, Air Force Institute of Technology
%For more information contact Christopher Hill at 612-532-6068
%or Ralph Anthenien at 937-255-3636 x4643

%Primary Code

%all arrays of form f(position,time)

clear all
clc

%Amatrix is a function of the form Amatrix(phi,theta), which forms the
%transformation matrix [A] to convert from space to towline coordinates
and
%vice versa.

set = set_values; %sets variables for maneuvers
params = line_params; %brings in initial conditions

%Set all initial values:
    t=0; %sets initial time
    ds = set.ds; %change in length (meters)
    dt = set.dt; %change in time (sec)
    time = set.time; %sec (total time)
    L = params.LL;
    mu = params.mu; %mass of towline per meter
    g = params.g;
    Wt = params.Wt; %Weight of towline per meter [N]
    Mb = params.mD;
    WB = params.WB;
    Vol = set.ds*pi*params.dL^2/4; %total volume of towline
    Area = set.ds*pi*params.dL; %total surface area of towline
    C = params.Vx; %m/s - constants (velocity) of a/c
    D = params.Vy;
    E = params.Vz;
    upert = set.upert; %perturbations in velocity of a/c
    vpert = set.vpert;
    wpert = set.wpert; %limits in these values
    tpert = set.tpert; %constant acceleration until reaches final
perturbation value at tpert
    tstart2 = set.tstart2; %time to start second perturbation
    upert2 = set.upert2;
    vpert2 = set.vpert2;
    wpert2 = set.wpert2;
    tpert2 = set.tpert2;
```

```
    %Set values for finding heat transfer:
        Cp = 450; %approx value for most steels at 300K - can be
changed to a fnct of temp
        Pr = 0.7; %Prandtl number
        Temp_set = set.CT*ones(15,15,2,set.time/set.dt+1); %Ambient
temp field: Temp_set(x,y,z,t) - currently uses const. temp value
'set.CT' - value of 1 is initial position/time
        GS = .1; %Spacial grid size spacing for Temp_set is 1/GS
meters.  Thus GS = 10 means grid size for Temp_set is .1 meters
        %Set the offset from the a/c at initial conditions for where
the
        %values begin for Temp_set matrix (+ is up and - is down):
            xoffset = -30;
            yoffset = -30;
            zoffset = 0;

% Setup Initial Conditions (this is to find steady state)
% +1 is to account for the zero point on the line (i.e. a '1'
position/time
% refers to a position/time of 0, etc.)
% note: we'll say that t=1 is initial given values, and t=2 is upper
limit
% conditions
% note: everything is oriented about the b position in fig. 3.3-1 of
paper
% ('i' position in code refers to b position in paper)

%Initialize arrays for data:
    Phi = set.Phi*ones(L/ds+1,time/dt+1); %set an initial value for Phi
for t0 - affects possible negative tension at initial values
    Theta = set.Theta*ones(L/ds+1,time/dt+1);
    U = zeros(L/ds+1,time/dt+1);
    W = zeros(L/ds+1,time/dt+1);
    V = zeros(L/ds+1,time/dt+1);
    FX = zeros(L/ds+1,time/dt+1); %note: per meter!
    FY = zeros(L/ds+1,time/dt+1);
    FZ = zeros(L/ds+1,time/dt+1);
    T = zeros(L/ds+1,time/dt+1);
    u = zeros(L/ds+1,time/dt+1);
    v = zeros(L/ds+1,time/dt+1);
    w = zeros(L/ds+1,time/dt+1);
    x = zeros(L/ds+1,time/dt+1);
    y = zeros(L/ds+1,time/dt+1);
    z = zeros(L/ds+1,time/dt+1);
    %These two arrays are all set to the same value, with the
understanding
    %that the non t=1 array positions will be changed later
    Temp = set.LTemp*ones(L/ds+1,time/dt+1); %sets entire line temp to
be initial line temp
    rho = 357.88*((set.LTemp+set.CT)/2)^(-
1.0041)*ones(L/ds+1,time/dt+1); %sets air density along line based on
initial air and line temps

%Set velocities down entire line = constant vel. values of a/c
(spatial)
```

```
    u(:,1) = C;
    v(:,1) = D;
    w(:,1) = E;

%The code between the lines takes in previous steady state data.
%One can comment out this code if they would rather start from
%non-steady state cases.
%-------------------------------------------------------------%
%%The following sets up initial conditions by interpolation from
%%previous tension data (since we have more data pts here).  It should
%%be noted that the previous data plots the towed body at the zero
position
%%and follows the towline shape in the positive x-y direction up to the
%%aircraft.  We need to shift everything down and to the left so that
the
%%aircraft is at zero and the towline hangs down and to the left.

    % Create matrices to store values:
        dx = zeros(L/ds+1,time/dt+1);
        dy = zeros(L/ds+1,time/dt+1);
        dz = zeros(L/ds+1,time/dt+1);

    % Find steady state values:
        [y1 y2] = towlinecomp;
        x_init = y2(:,1); %spatial x pos of steady state line wrt arc
length
        y_init = -y2(:,2); %spatial y pos of ss line wrt arc length...
negative due to sine convention
        z_init = y2(:,3); %spatial z pos of ss line wrt arc length
        dx_init = -y2(:,4); %spatial dx/ds of ss line... negative due
to sine convention
        dy_init = -y2(:,5); %spatial dy/ds of ss line... negative due
to sine convention
        dz_init = y2(:,6); %spatial dz/ds of ss line
        T_init = y2(:,7)*params.T0; %tension in ss line... originally
non-dim, thus multiplied by T0

Last = length(x_init); %references last pt in initial data (same for
all initial matrices)
e = (Last-1)/(length(x(:,1))-1); %ratio for interpolation (same for all
matrices) ... -1 used b/c 1st point is really at 0 (no 0 index)

%The following puts the initial values into the initial matrices
(swapped
%for the convention in this program):
for i=1:1:L/ds+1
    %This sets up the indices for conversion from previous coordinates
for
    %this program using interpolation (A is previous point, B is next
point
    %...these values are subtracted from the 'Last' position in order
to
    %reverse the index):
        A = round((i-1)*e);
        if (i-1)*e > A
            B = A+1;
```

```
        elseif A == 0
            B = A+1;
        else
            B = A;
            A = A-1;
        end
    %These are all in spatial coordinates:
        x(i,1) = [(x_init(Last-B)*((i-1)*e-A) + x_init(Last-A)*(B-(i-
1)*e))*L - x_init(length(x_init))*L];
        y(i,1) = -[(y_init(Last-B)*((i-1)*e-A) + y_init(Last-A)*(B-(i-
1)*e))*L - y_init(length(y_init))*L];
        z(i,1) = -[(z_init(Last-B)*((i-1)*e-A) + z_init(Last-A)*(B-(i-
1)*e))*L - z_init(length(z_init))*L];
        dx(i,1) = dx_init(Last-B)*((i-1)*e-A) + dx_init(Last-A)*(B-(i-
1)*e);
        dy(i,1) = dy_init(Last-B)*((i-1)*e-A) + dy_init(Last-A)*(B-(i-
1)*e);
        dz(i,1) = dz_init(Last-B)*((i-1)*e-A) + dz_init(Last-A)*(B-(i-
1)*e);

    %This finds the initial angles:
        Phi(i,1) = atan(dy(i,1)/dx(i,1));
        Theta(i,1) = -asin(dz(i,1));

%-------------------------------------------------------------%

% for i=0:1:L/ds %comment out this line if using above for loop,
otherwise
% uncomment
%
%     %This sets up the values for a non-steady state case, setting the
%     %towline positions to be directly backward from the aircraft.
These
%     %lines should be commented out if using the steady state values
above:
%         if i ~= 0
%             x(i,1) = x(i,1) - ds*cos(Theta(i,1))*cos(Phi(i,1));
%             y(i,1) = y(i,1) - ds*cos(Theta(i,1))*sin(Phi(i,1));
%             z(i,1) = z(i,1) - ds*sin(Theta(i,1));
%         end
%-------------------------------------------------------------%

    %This converts velocity to towline coordinates:
        Spatial_vel = [u(i,1); v(i,1); w(i,1)];
        Tow_vel = Amatrix(Phi(i,1),Theta(i,1))*Spatial_vel;
        U(i,1) = Tow_vel(1);
        V(i,1) = Tow_vel(2);
        W(i,1) = Tow_vel(3);

    %The following is used to find heat transfer and density in ambient
temp at next timestep.
    %Due to computing power, it can be commented out when not analyzing
heat transfer.
        Tempset;

    if i ~= L/ds
```

```
    %This sets up the aerodynamic forces on the line
        F = Towforce(U(i,1),V(i,1),W(i,1),rho(i,1));
        FX(i,1) = -F(1); %note: per meter
        FY(i,1) = -F(2); %notation is in positive X,Y,Z axes
        FZ(i,1) = -F(3);
    end
end

    %Find drag forces on the body and tension at lower end:
        %No acceleration terms are included since it is assumed this is
        %starting from rest.
        F =
Bodyforce(u(L/ds+1,1),v(L/ds+1,1),w(L/ds+1,1),rho(L/ds+1,1)); %Set
forces on body in spatial axes
        Fx = -F(1);
        Fy = -F(2)-WB;
        Fz = -F(3);
        FTL =
Amatrix(Phi(L/ds+1,1),Theta(L/ds+1,1))*[Fx;Fy;Fz];%Convert to towline
coordinates
        T(L/ds+1,1) = -FTL(2);%Tension is directed only along the
towline Y-axis

    %Set aerodynamic forces on line at lower end:
        F = Amatrix(Phi(L/ds+1,1),Theta(L/ds+1,1))*[F(1);F(2);F(3)];
%Change to towline coordinates
        FX(L/ds+1,1) = -F(1); %negative sign due to drag being in same
direction as velocity
        FY(L/ds+1,1) = -F(2);
        FZ(L/ds+1,1) = -F(3);

    %Set tension one step up line
        T(L/ds,1) = T(L/ds+1,1)+ds*(-
FY(L/ds,1)+Wt*sin(Phi(L/ds,1))*cos(Theta(L/ds,1)));

    %Set tension up rest of line
        for i=L/ds-1:-1:1
            T(i,1) = T(i+2,1)+2*ds*(-
FY(i+1,1)+Wt*sin(Phi(i+1,1))*cos(Theta(i+1,1)));
        end

for t=1:1:time/dt; %t=1 represents t0 (1st timestep) - we're finding
values for next timestep based on this timestep value

    %This sets up the perturbation velocities over time based on
constant
    %acceleration... t is used because we're concerned with the
behavior
    %at time t+1 (i.e., assume all perturbation velocities are 0 at
t0),
    %thus the total change in time up to that point will be t*dt:

        %First perturbation (u/v/wstar values set twice since u/v/wstar
        %values are changed in the second perturbation, but are based
on
```

```
        %constant values of u/v/wstar - the '1' values - since the
second
        %perturbation happens after the first one):
            if t*dt <= tpert
                 ustar1 = upert*t*dt/tpert;
                 vstar1 = vpert*t*dt/tpert;
                 wstar1 = wpert*t*dt/tpert;
                 ustar = ustar1;
                 vstar = vstar1;
                 wstar = wstar1;
            end

        %Second perturbation:
            if t*dt >= tstart2 & t*dt <= tstart2+tpert2
                t0 = t-tstart2/dt; %timestep that this starts at
                ustar = ustar1 + t0*upert2*dt/tpert2;
                vstar = vstar1 + t0*vpert2*dt/tpert2;
                wstar = wstar1 + t0*wpert2*dt/tpert2;
            end

    for i=1:1:L/ds+1

        %Characteristic directions:
            Fa = sqrt(T(i,t)/mu);
            Fb = -sqrt(T(i,t)/mu);
            if i==L/ds+1
                Fb=-sqrt(T(i,t)/Mb); %sets different characteristic
value for lower bdry
            end

        %This checks for stability of mesh:
            if (abs(Fa)*dt/ds) >= 1
                fprintf('Out of boundary!\nTry changing ds & dt (set
ds/dt to at least >= 1000).\nHit ctrl-c to quit\ni = %f\nt = %f\nFa =
%f\n',i,t,Fa)
                pause
            end

        %This checks for negative tension:
            if T(i,t) < 0
                if i == 1
                    Told = T(i,t-1);
                else
                    Told = T(i-1,t);
                end
                fprintf('Tension is negative!\nTry making less drastic
perturbations.\nNote: the code cannot analyze slack
conditions.\ni=%f\nt=%f\nT=%f\nT(previous)=%f\nHit ctrl-c to
quit\n',i,t,T(i,t),Told)
                pause
            end

        %This sets values for the characteristic equations:
            Ga = W(i,t)*sin(Theta(i,t)) - V(i,t)*cos(Theta(i,t)) +
Fa*cos(Theta(i,t));
```

```
            Gb = W(i,t)*sin(Theta(i,t)) - V(i,t)*cos(Theta(i,t)) +
Fb*cos(Theta(i,t));
            if i == L/ds+1 %Sets values at body - based on body mass -
this is currently not being used
                Hb = (1/Mb)*(-FX(i,t) - WB*cos(Phi(i,t)));
                Lb = (1/Mb)*(-FZ(i,t) -
WB*sin(Phi(i,t))*sin(Theta(i,t)));
            else %Sets values along towline - based on towline mass
                Hb = (1/mu)*(-FX(i,t) - Wt*cos(Phi(i,t)));
                Lb = (1/mu)*(-FZ(i,t) -
Wt*sin(Phi(i,t))*sin(Theta(i,t)));
            end
            Ha = Hb;
            Hatrack(i,t)=Ha;
            La = Lb;
            Ja = (V(i,t)-Fa);
            Jb = (V(i,t)-Fb);
            Ka = -U(i,t)*sin(Theta(i,t));
            Kb = Ka;

        %This uses interpolation to find values along the alpha
characteristic:
            if i ~= L/ds+1 %these values don't exist for i=L/ds+1
                b = i*ds; %b position is the next position along the
line
                a = (i-1)*ds; %a position is the current position along
the line (note: line STARTS at i=1, thus subtract 1)
                p = a + dt*Fa; %comes from |r-p| = dt*Fa and the fact
that r = a (position along line)
                % This defines values for interpolation:
                Ua = U(i,t); %Ua is value at same position along line
w/ previous timestep
                Ub = U(i+1,t); %Ub similarly corresponds to the next
position along the line
                Wa = W(i,t);
                Wb = W(i+1,t);
                Phia = Phi(i,t);
                Phib = Phi(i+1,t);
                Thetaa = Theta(i,t);
                Thetab = Theta(i+1,t);
                % The following uses straight line interpolation to
find values
                Up = (1/ds)*((b-p)*Ua + (p-a)*Ub);
                Wp = (1/ds)*((b-p)*Wa + (p-a)*Wb);
                Phip = (1/ds)*((b-p)*Phia + (p-a)*Phib);
                Thetap = (1/ds)*((b-p)*Thetaa + (p-a)*Thetab);
            end

        %This uses interpolation to find values along the beta
characteristic:
            if i ~= 1 %these values don't exist for i=1
                d = (i-2)*ds; %d position is the previous position
along the line
                a = (i-1)*ds; %a position is the current position along
the line
```

```
                q = a + dt*Fb; %comes from |r-q| = dt*Fb and the fact
that r = a (position along line)
                % This defines values for interpolation:
                Ua = U(i,t); %Ua is value at same position along line
w/ previous timestep
                Ud = U(i-1,t); %Ub similarly corresponds to the
previous position along the line
                Wa = W(i,t);
                Wd = W(i-1,t);
                Phia = Phi(i,t);
                Phid = Phi(i-1,t);
                Thetaa = Theta(i,t);
                Thetad = Theta(i-1,t);
                % The following uses straight line interpolation to
find values
                Uq = (1/ds)*((q-d)*Ua + (a-q)*Ud);
                Wq = (1/ds)*((q-d)*Wa + (a-q)*Wd);
                Phiq = (1/ds)*((q-d)*Phia + (a-q)*Phid);
                Thetaq = (1/ds)*((q-d)*Thetaa + (a-q)*Thetad);
            end

        % This finds the upper limit values of U,V,W,Phi,& Theta:
            if i == 1
                % The following finds phi by finding a zero value for
the fnct:
                    phi = fzero(@(phi) phi - (Up + Ga*Phip - Ha*dt - (C
+ ustar)*sin(phi) + (D + vstar)*cos(phi))/Ga, .001);
                % The following finds theta by finding a zero value for
the fnct:
                    theta = fzero(@(theta) theta - (Wp + (C +
ustar)*sin(theta)*cos(phi) - (E + wstar)*cos(theta) + (D +
vstar)*sin(phi)*sin(theta) + Ja*Thetap - Ka*(phi - Phip) - La*dt)/Ja,
.001);
                    if theta < 1e-10 %due to round off, this sets to
correct zero value
                        theta = 0;
                    end
                Phi(i,t+1) = phi;
                Theta(i,t+1) = theta;
                U(i,t+1) = (C + ustar)*sin(phi) - (D + vstar)*cos(phi);
                V(i,t+1) = (C + ustar)*cos(theta)*cos(phi) + (D +
vstar)*cos(theta)*sin(phi) + (E + wstar)*sin(theta);
                W(i,t+1) = -(C + ustar)*sin(theta)*cos(phi) - (D +
vstar)*sin(phi)*sin(theta) + (E + wstar)*cos(theta);
            end

        %This finds the values down the entire line using the
characteristic equations:
            if i ~= 1 & i ~= L/ds+1
               Phi(i,t+1) = (Up - Uq - Gb*Phiq + Ga*Phip)/(Ga - Gb);
               U(i,t+1) = (Up*Gb - Uq*Ga + Gb*Ga*(Phip - Phiq) +
Ha*dt*(Ga - Gb))/(Gb - Ga);
               W(i,t+1) = (Jb*Wp - Ja*Wq + Ja*Jb*(Thetap - Thetaq) +
Jb*Ka*(Phip - Phi(i,t+1)) + Ja*Kb*(Phi(i,t+1) - Phiq) + La*dt*(Jb -
Ja))/(Jb - Ja);
```

```
                Theta(i,t+1) = (Thetap*Ja - Thetaq*Jb + Wp - Wq -
Phi(i,t+1)*(Ka - Kb) + Phip*Ka - Phiq*Kb)/(Ja - Jb);
                V(i,t+1) = V(i-1,t+1) + .5*(U(i-1,t+1) +
U(i,t+1))*cos(.5*(Theta(i-1,t+1) + Theta(i,t+1)))*(Phi(i-1,t+1) -
Phi(i,t+1)) - .5*(W(i-1,t+1) + W(i,t+1))*(Theta(i-1,t+1) -
Theta(i,t+1));
            end

        %This sets up the aerodynamic forces on the line:
            if i ~= L/ds+1 %Last value to be added later
                F = Towforce(U(i,t+1),V(i,t+1),W(i,t+1),rho(i,t+1));
                FX(i,t+1) = -F(1);
                FY(i,t+1) = -F(2);
                FZ(i,t+1) = -F(3);
            end
    end

    %This finds the values at lower boundary conditions:

        %Use combination of equations to step values to lower boundary:
            C1 = Gb+V(L/ds,t+1)*cos(Theta(L/ds,t+1))-
W(L/ds,t+1)*sin(Theta(L/ds,t+1))+(2*ds/dt)*cos(Theta(L/ds,t+1));
%constant for PhiL denominator
            PhiL =
((2*ds/dt)*Phi(L/ds+1,t)*cos(Theta(L/ds,t+1))+(V(L/ds,t+1)*cos(Theta(L/
ds,t+1))-W(L/ds,t+1)*sin(Theta(L/ds,t+1)))*(Phi(L/ds-1,t+1))-U(L/ds-
1,t+1)-Hb*dt+Uq+Gb*Phiq)/C1;
            ThetaL = ((2*ds/dt)*Theta(L/ds+1,t)+V(L/ds,t+1)*Theta(L/ds-
1,t+1)-U(L/ds,t+1)*(PhiL-Phi(L/ds-1,t+1))*sin(Theta(L/ds,t+1))-Wq-
Jb*Thetaq+Lb*dt+W(L/ds-1,t+1)-Kb*(PhiL-Phiq))/(2*ds/dt+V(L/ds,t+1)-Jb);
            UL = Uq-Gb*(PhiL-Phiq)-Hb*dt;
            WL = Wq-Jb*(ThetaL-Thetaq)-Kb*(PhiL-Phiq)-Lb*dt;
            VL = V(L/ds-1,t+1)+W(L/ds,t+1)*(ThetaL-Theta(L/ds-1,t+1))-
U(L/ds,t+1)*cos(Theta(L/ds,t+1))*(PhiL-Phi(L/ds-1,t+1));

        %Set values:
            U(L/ds+1,t+1) = UL;
            V(L/ds+1,t+1) = VL;
            W(L/ds+1,t+1) = WL;
            Theta(L/ds+1,t+1) = ThetaL;
            Phi(L/ds+1,t+1) = PhiL;

        %Convert to Spatial:
            Spatial_vel = [UL VL WL]*Amatrix(PhiL,ThetaL);
            uL = Spatial_vel(1);
            vL = Spatial_vel(2);
            wL = Spatial_vel(3);
            u(L/ds+1,t+1) = uL;
            v(L/ds+1,t+1) = vL;
            w(L/ds+1,t+1) = wL;

        %Find drag forces on the body and tension at lower end:
            F = Bodyforce(uL,vL,wL,rho(L/ds+1,t+1)); %Set forces on
body in spatial axes
            if t == 1 %Solving for t=2:
                au = (u(L/ds+1,t+1)-u(L/ds+1,t))/dt;
```

```
                au = (v(L/ds+1,t+1)-v(L/ds+1,t))/dt;
                aw = (w(L/ds+1,t+1)-w(L/ds+1,t))/dt;
            else
                au = (3*u(L/ds+1,t+1)-4*u(L/ds+1,t)+u(L/ds+1,t-
1))/(2*dt);
                av = (3*v(L/ds+1,t+1)-4*v(L/ds+1,t)+v(L/ds+1,t-
1))/(2*dt);
                aw = (3*w(L/ds+1,t+1)-4*w(L/ds+1,t)+w(L/ds+1,t-
1))/(2*dt);
            end

            Fx = -F(1)-Mb*au; %negative sign on force is due to drag
force orientation being same direction as velocity
            Fy = -F(2)-WB-Mb*av;
            Fz = -F(3)-Mb*aw;
            FTL = Amatrix(PhiL,ThetaL)*[Fx;Fy;Fz];
            T(L/ds+1,t+1) = -FTL(2);

        %Set aerodynamic forces on line at lower end:
            F = Amatrix(PhiL,ThetaL)*[F(1);F(2);F(3)]; %Change to
towline coordinates
            FX(L/ds+1,t+1) = -F(1);
            FY(L/ds+1,t+1) = -F(2);
            FZ(L/ds+1,t+1) = -F(3);

    %Set tension one step up line:
        T(L/ds,t+1) = T(L/ds+1,t+1)+ds*((mu/dt)*(V(L/ds,t+1)-V(L/ds,t)-
W(L/ds,t+1)*(Theta(L/ds,t+1)-Theta(L/ds,t))+U(L/ds,t+1)
*cos(Theta(L/ds,t+1))*(Phi(L/ds,t+1)-Phi(L/ds,t)))-
FY(L/ds,t+1)+Wt*sin(Phi(L/ds,t+1))*cos(Theta(L/ds,t+1)));

    %Set tension up rest of line:
        for i=L/ds-1:-1:1
            T(i,t+1) = T(i+2,t+1)+2*ds*((mu/dt)*(V(i+1,t+1)-V(i+1,t)-
W(i+1,t+1)*(Theta(i+1,t+1)-Theta(i+1,t))+U(i+1,t+1)
*cos(Theta(i+1,t+1))*(Phi(i+1,t+1)-Phi(i+1,t)))-
FY(i+1,t+1)+Wt*sin(Phi(i+1,t+1))*cos(Theta(i+1,t+1)));
        end

    for i=1:1:L/ds+1
        %Find spatial velocity values:
            Spatial_vel = [U(i,t+1) V(i,t+1)
W(i,t+1)]*Amatrix(Phi(i,t+1),Theta(i,t+1));
            u(i,t+1) = Spatial_vel(1);
            v(i,t+1) = Spatial_vel(2);
            w(i,t+1) = Spatial_vel(3);

        %Find spatial position values:
            if i == 1  %Sets the value at the a/c - subtracing the
initial velocities keeps system about these velocities
                x(i,t+1) = x(i,t) + (u(i,t+1)-C)*dt;
                y(i,t+1) = y(i,t) + (v(i,t+1)-D)*dt;
                z(i,t+1) = z(i,t) + (w(i,t+1)-E)*dt;
            else
                x(i,t+1) = x(i-1,t+1) -
ds*cos(Theta(i,t+1))*cos(Phi(i,t+1));
```

```
                y(i,t+1) = y(i-1,t+1) -
ds*cos(Theta(i,t+1))*sin(Phi(i,t+1));
                z(i,t+1) = z(i-1,t+1) - ds*sin(Theta(i,t+1));
            end

        %The following is used to find heat transfer and density in
ambient temp.
        %Due to computing power, it can be commented out when not
analyzing heat transfer.
            Tempset;

    end
end
```

Appendix C: MATLAB® Code – Tempset Code

```
%This takes in values of x, y, and z in meters, U, V, and W as m/s,
%Told in K, and t as timestep and outputs the temperature and air
%density at the current position for the next timestep.  This method
%can be applied to the entire towline.  It is not applied to the towed
%body, but values are calculated at the point of attachment between the
%line and body, and these values are assumed to be the density values
%for the body.  The body should be sufficiently far from a heat source,
%thus this method should give accurate data.
%
%Time spacing in Temp_set is same as dt, thus 't' is timestep value.
%
%x,y,z values are relative to the initial aircraft position (this can
be
%altered by setting x,y,z values in other code to be dependent on a
%different position).

%Set up coordinates for interpolation:
    %The +1 value is due to the first grid position being at zero
    xpos = x(i,t+1)*GS+1-xoffset*GS; %sets true x position within grid
points
    ypos = y(i,t+1)*GS+1-yoffset*GS; %sets true y position within grid
points
    zpos = z(i,t+1)*GS+1-zoffset*GS; %sets true z position within grid
points
    x1 = floor(xpos); %finds the lower position for x for Temp_set
    x2 = ceil(xpos); %finds the upper position for x for Temp_set
    y1 = floor(ypos); %finds the lower position for y for Temp_set
    y2 = ceil(ypos); %finds the upper position for y for Temp_set
    z1 = floor(zpos); %finds the lower position for z for Temp_set
    z2 = ceil(zpos); %finds the upper position for z for Temp_set

    %The 'if' statements prevent an output of a zero value later due to
x1=x2, y1=y2, or z1=z2.
    if x1==x2
        x2=x1+1;
    end
    if y1==y2;
        y2=y1+1;
    end
    if z1==z2;
        z2=z1+1;
    end

%Set up four values for interpolation at eight points:
    T1 = Temp_set(x1,y1,z1,t+1);
    T2 = Temp_set(x2,y1,z1,t+1);
    T3 = Temp_set(x1,y2,z1,t+1);
    T4 = Temp_set(x2,y2,z1,t+1);
    T5 = Temp_set(x1,y1,z2,t+1);
    T6 = Temp_set(x2,y1,z2,t+1);
```

```
    T7 = Temp_set(x1,y2,z2,t+1);
    T8 = Temp_set(x2,y2,z2,t+1);

%Set values at current position through interpolation:
    %Since everything is in terms of grid position (i.e., not real
position), no need to divide by grid size.
    Tx1 = (x2-xpos)*T1 + (xpos-x1)*T2; %value along x-axis at y1,z1
    Tx2 = (x2-xpos)*T3 + (xpos-x1)*T4; %value along x-axis at y2,z1
    Tx3 = (x2-xpos)*T5 + (xpos-x1)*T6; %value alone x-axis at y1,z2
    Tx4 = (x2-xpos)*T7 + (xpos-x1)*T8; %value alone x-axis at y2,z2
    Txy1 = (y2-ypos)*Tx1 + (ypos-y1)*Tx2; %value in x-y plane at z1
    Txy2 = (y2-ypos)*Tx3 + (ypos-y1)*Tx4; %value in x-y plane at z2
    Txyz = (z2-zpos)*Txy1 + (zpos-z1)*Txy2; %final air temp
interpolated at the position

%This should be commented out for now since the Nusselt number in
%currently only for perpendicular velocity (i.e., heat transfer only
%happens in perpendicular direction):
%-----------------------------%
%Set the diameter to calculate values (we only use perpendicular
velocity due to Nusselt number calculations - this is left for future
work):
%     Vperp = sqrt(U(i,t+1)^2 + W(i,t+1)^2); %perpendicular velocity
%     Vpar = abs(V(i,t+1)); %parallel velocity - make positiv
%     if Vpar ~= 0; %divide by zero error if it does
%         Angle = atan(Vperp/Vpar); %angle at which airflow acts
%         if Vperp/Vpar > params.dL/set.ds %if the air completely
crosses the perpendicular component of line over the interval ds
%             DL = params.dL/sin(Angle); %diameter over which airflow
acts
%         else %if the air completely crosses the parallel component of
line over the interval ds
%             DL = set.ds/cos(Angle); %diameter over which airflow acts
%         end
%     else
%         DL = set.ds; %diameter over which airflow acts
%     end
%-----------------------------%
      DL = params.dL; %diameter over which airflow acts - perpendicular
diameter

%Calculate values to find temp and rho:
    %Old values:
        Tf=(Temp(i,t+1)+set.CT)/2; %film temp based on old line temp
        nu = 8e-10*(Tf)^1.7235; %kinematic viscosity based on old temp
    %Calculate values based on old temp:
        Re = abs(U(i,t+1))*DL/nu; %Reynolds number - this would change
for a different Nu number calculation
        Nu = 0.42*Pr^0.2 + .057*Pr^(1/3)*sqrt(Re); %Nusselt number
        k = 0.0002235*(Tf)^0.8302; %thermal conductivity of air
        h = Nu*k/params.dL; %convection coefficient
    %Calculate new values:
        Temp(i,t+2) = Temp(i,t+1) + Area*h*dt*(Tf-
Temp(i,t+1))/(Vol*params.rhoL*Cp); %new temp on line
        Tf = (Temp(i,t+2)+set.CT)/2; %new film temp
        rho(i,t+2) = 357.88*(Tf)^(-1.0041); %new air density in film
```

Appendix D: MATLAB® Code – Other Functions

The first function is used to set the initial values for the entire simulation, and is called up in multiple other functions. It is currently set to model a 1 second vertical acceleration to 30 m/s, with an immediate acceleration back to zero over 1 second.

```
function set=set_values()
%Set initial conditions:
    set.u = 100; %intial vel in x-dir
    set.v = 0; %initial vel in y-dir
    set.w = 0; %initial vel in z-dir
    set.Phi = 0.01; %initial angle of towline (constant down line) -
nonzero prevents negative tension
    set.Theta = 0; %initial angle of towline (constant down line)

%Set mesh spacing:
    set.ds = 5; %change in length (meters)
    set.dt = .01; %change in time (sec)
    set.time = 10; %sec (total time)

%First perturbation:
    set.upert = 0.0; %perturbations in velocity of a/c
    set.vpert = 30.0;
    set.wpert = 0.0; %limits in these values
    set.tpert = 1; %constant acceleration until reaches final
perturbation value at tpert

%Second perturbnation:
    set.tstart2 = 1; %time to start second perturbation
    set.upert2 = 0.0;
    set.vpert2 = -30.0;
    set.wpert2 = 0.0;
    set.tpert2 = 1;

%Set constant temp value [K] for air for Tempset.m (to be changed for
temp field later)
    set.CT = 288.2; %Sea level St. Atm. and Press. value is 288.2 K

%Set value for initial line temp [K]:
    set.LTemp = 288.2;
```

The second function was modified from Richardson and sets the initial parameters along the line. These values were set somewhat arbitrarily (although some values, such

as the density of steel, were set specifically) to analyze different towline behaviors. This function is also called into Richardson's work for steady state analysis:

```
function params=line_params()
%Original program written by Ralph Anthenien and Tyler Richardson,
AFIT/ENY
%Modified by Ralph Anthenien and Christopher Hill, AFIT/ENY
%function line_params
%return parameters about towline and decoy

set=set_values;

params.g=9.8; %gravitational acceleration [m/s^2]
params.dB=0.496; %decoy diam
params.Ad=pi*params.dB^2/4; %frontal area [m^2]
params.CdD=1; %Decoy drag coeff
params.mD=4; %decoy mass [kg]
params.WB=params.mD*params.g; %decoy weight [N]
params.LD=1; %Decoy length [m]
params.CdL=1.1; %Perpendicular line drag coeff
params.CdLSF=0.04; %Skin friction line drag coeff (for Y-axis)
params.rhoL=7600; %line density [kg/m^3] - approx. value for most
steels
params.dL=0.00127; %Line Diam [m]
params.mu=params.rhoL*pi*params.dL^2/4; %Mass of towline per meter
length [kg/m]
params.Wt=params.mu*params.g; %Weight of towline per meter [N]
params.Vx=set.u; %velocity (lookup to be used later) [m/s]
params.Vy=set.v; %upward vel [m/s]
params.Vz=set.w; %transverse vel [m/s]
params.V=sqrt(params.Vx^2+params.Vy^2+params.Vz^2); %relative vel
params.vchar=params.V; %characteristic velocity to calc char drag
tension - assumed to be same as total velocity
params.rhoa=357.88*((set.LTemp+set.CT)/2)^(-1.0041); %air density
[kg/m^3]
params.LL=30; %line length [m]
params.tc=1; %time constant (for transient only)
params.T0=params.LL*params.g*pi*params.rhoL*params.dL^2/4;
```

The third function is the transformation matrix to convert from towline to space coordinates and vice versa:

```
function A = Amatrix(phi,theta)
% This transforms from space to towline coordinate systems as follows:
% Towline(3x1) = [A]*Space(3x1)
% Space(3x1) = (Towline(1x3)*[A])'
% note: phi and theta are angles btwn current and old line positions
A11 = sin(phi);
A12 = -cos(phi);
A13 = 0;
A21 = cos(phi)*cos(theta);
```

```
A22 = cos(theta)*sin(phi);
A23 = sin(theta);
A31 = -cos(phi)*sin(theta);
A32 = -sin(theta)*sin(phi);
A33 = cos(theta);
A = [A11 A12 A13; A21 A22 A23; A31 A32 A33];
```

The fourth function calculates the forces on the body in spatial coordinates:

```
function F = Bodyforce(u,v,w,rho)
% This calculates the total aerodynamic forces on the body
params=line_params;
Tot_vel = sqrt(u^2 + v^2 + w^2);
Dx = .5*rho*u*Tot_vel*params.CdD*params.Ad; %Drag in x-direction
Dy = .5*rho*v*Tot_vel*params.CdD*params.Ad; %Drag in y-direction
Dz = .5*rho*w*Tot_vel*params.CdD*params.Ad; %Drag in z-direction
F=[Dx Dy Dz];
```

The fifth function calculates the forces on the towline in towline coordinates:

```
function F = Towforce(U,V,W,rho)
% This calculates the aerodynamic forces on the towline per meter
params=line_params;
V_perp = sqrt(U^2 + W^2); %total velocity in the perpendicular
direction
DX = .5*rho*params.dL*U*V_perp*(params.CdL+params.CdLSF); %Drag in X-
direction
DY = 0; %Drag in Y-direction
DZ = .5*rho*params.dL*W*V_perp*(params.CdL+params.CdLSF); %Drag in Z-
direction
F=[DX DY DZ];
```

Vita

Ensign Christopher A. Hill graduated from Southwest Christian High School in Eden Prairie, Minnesota. He entered undergraduate studies at the University of Minnesota where he graduated with a Bachelor of Aerospace Engineering and Mechanics degree in May 2005. He was commissioned through NROTCU, University of Minnesota, receiving the Distinguished Midshipman Graduate Award. His first assignment was the Graduate School of Engineering and Management, Air Force Institute of Technology, which he entered in June 2005. Upon graduation in June 2006, he will be assigned to NAS Pensacola, FL with his newly married wife to begin flight training as a student naval aviator.

REPORT DOCUMENTATION PAGE

Form Approved
OMB No. 074-0188

The public reporting burden for this collection of information is estimated to average 1 hour per response, including the time for reviewing instructions, searching existing data sources, gathering and maintaining the data needed, and completing and reviewing the collection of information. Send comments regarding this burden estimate or any other aspect of the collection of information, including suggestions for reducing this burden to Department of Defense, Washington Headquarters Services, Directorate for Information Operations and Reports (0704-0188), 1215 Jefferson Davis Highway, Suite 1204, Arlington, VA 22202-4302. Respondents should be aware that notwithstanding any other provision of law, no person shall be subject to an penalty for failing to comply with a collection of information if it does not display a currently valid OMB control number.
PLEASE DO NOT RETURN YOUR FORM TO THE ABOVE ADDRESS.

1. REPORT DATE *(DD-MM-YYYY)*	**2. REPORT TYPE**	**3. DATES COVERED** *(From – To)*
05-06-2006	**Master's Thesis**	Jun 2005 – Jun 2006

4. TITLE AND SUBTITLE

Theoretical Modeling of the Transient Effects of a Towline Using the Method of Characteristics

5a. CONTRACT NUMBER

5b. GRANT NUMBER

5c. PROGRAM ELEMENT NUMBER

6. AUTHOR(S)

Hill, Christopher A., Ensign, USN

5d. PROJECT NUMBER

5e. TASK NUMBER

5f. WORK UNIT NUMBER

7. PERFORMING ORGANIZATION NAMES(S) AND ADDRESS(S)
Air Force Institute of Technology
Graduate School of Engineering and Management (AFIT/EN)
2950 Hobson Way
WPAFB OH 45433-7765

8. PERFORMING ORGANIZATION REPORT NUMBER

AFIT/GAE/ENY/06-J06

9. SPONSORING/MONITORING AGENCY NAME(S) AND ADDRESS(ES)

10. SPONSOR/MONITOR'S ACRONYM(S)

11. SPONSOR/MONITOR'S REPORT NUMBER(S)

12. DISTRIBUTION/AVAILABILITY STATEMENT
APPROVED FOR PUBLIC RELEASE; DISTRIBUTION UNLIMITED.

13. SUPPLEMENTARY NOTES

14. ABSTRACT

The use of decoys in combat has become more advanced in recent years. Some of the newest military aircraft, such as the US Navy's F/A-18E/F Superhornet, have the capability to deploy a towline with an attached decoy when entering hostile territory as a defense mechanism against enemy threats. In steady state, the towline extends behind and below the aircraft. A major concern is the position of the towline, as aircraft maneuvers can cause the line to enter the engine plume. The high exhaust heat can cause problems, such as damaging electrical equipment and severing the line. In order to better understand the behavior of the towline, as well as setting up a method to analyze the heat transfer to the towline, computer modeling has been utilized using numerical integration with the method of characteristics.

The method of characteristics has been applied to 4 hyperbolic equations of motion, leaving 2 parabolic equations of motion to be calculated at each timestep. The energy equation for heat transfer to the towline was also derived, which provides a means to find local air density and towline temperature. From these a model was created to observe towline behavior and temperature, which is shown to be consistent with past research. This model is applicable to any towed body in any medium with zero slack conditions.

The effects of transient aircraft maneuvers on towline behavior in a predetermined temperature field were analyzed under different conditions using a code developed in MATLAB®. This code is included such that aircraft maneuvers in unique temperature fields can be analyzed for future research.

15. SUBJECT TERMS
Towline, Towed Decoy, Towed Cable, Method of Characteristics, Aircraft Survivability, Heat Transfer

16. SECURITY CLASSIFICATION OF:			**17. LIMITATION OF ABSTRACT**	**18. NUMBER OF PAGES**	**19a. NAME OF RESPONSIBLE PERSON**
REPORT	**ABSTRACT**	**c. THIS PAGE**			Ralph A. Anthenien Jr., PhD, PE, AFIT/ENY
U	**U**	**U**	**UU**	136	**19b. TELEPHONE NUMBER** *(Include area code)* 937-255-3636 x4643; e-mail: Ralph.Anthenien@afit.edu

Standard Form 298 (Rev: 8-98)
Prescribed by ANSI Std. Z39-18